

TESI DI DOTTORATO

UNIVERSITÀ DEGLI STUDI DI NAPOLI “FEDERICO II”

DIPARTIMENTO DI INGEGNERIA ELETTRICA
E DELLE TECNOLOGIE DELL’INFORMAZIONE

DOTTORATO DI RICERCA IN
ELECTRICAL ENGINEERING AND INFORMATION TECHNOLOGY

**FAST AND ULTRAFAST NONLINEAR
MAGNETIZATION DYNAMICS IN
MAGNETIC STORAGE TECHNOLOGIES**

VALENTINO SCALERA

Relatore

Prof. Claudio SERPICO

Co-relatore

Prof. Massimiliano D’AQUINO

A. A. 2019–2020

Contents

1	Micromagnetics and LLG	17
1.1	Magnetostatic Equations	17
1.2	Principles of thermodynamics	19
1.3	Free Energy Contributions	22
1.3.1	Exchange energy	22
1.3.2	Anisotropy energy	27
1.3.3	Magnetostatic energy	29
1.3.4	Zeeman energy	30
1.4	Brown Equation	30
1.5	Magnetization Dynamics	33
1.5.1	Gyromagnetic precession	33
1.5.2	Landau-Lifshitz equation	34
1.5.3	Gilbert equation	35
1.5.4	Normalized equation	38
1.6	Spin Injection	39
2	Magnetization Dynamics in Nanosystems	45
2.1	Stoner-Wohlfarth Asteroid	46
2.2	Conservative Dynamics	49
2.3	Ferromagnetic Resonance: Kittel Frequency	53
2.4	Bifurcation map for axially symmetric system	56
2.5	Analysis of non-symmetric systems	63
2.6	Hysteresis in ferromagnetic resonance	65
3	Noise in Nanosystems	69
3.1	Probability density function at equilibrium	71
3.2	Data persistence in magnetic memories	72
3.3	Pseudospectral methods	75

3.4	Switching time distribution for a magnetic memory	80
4	Ultrafast Magnetization Dynamics	87
4.1	Experimental techniques for ultrafast dynamics	88
4.2	Inertial magnetization dynamics	91
4.3	Derivation of the inertial LLG equation	92
4.4	Analysis of the iLLG equation	96
4.5	Experimental evidence of inertial dynamics in a ferromagnet .	103
4.6	Spin waves in thin films	106
A	Helmholtz and Tellegen Theorems	119
A.1	Helmholtz Theorem	120
A.2	Tellegen theorem	121
B	Poynting Theorem	123
C	Nonlinear Dynamics	125
C.1	Saddle node bifurcation	125
C.2	Hopf bifurcation	126
C.3	Homoclinic bifurcation	127
D	Magnetostatic field in thin films	131
D.1	Field Generated by Surface Charges	132
D.2	Field Generated by Volume Charges	133
E	Formal definition of the noise	135

Abstract

Ferromagnetic materials play an important role in data recording technologies. Several types of memories in the past relied on magnetic materials, such as magnetic core memories and magnetic tapes, and even in modern hard disks ferromagnetic media are used to store information. Hard disk devices are nowadays the preferred type of digital memories for large databases thanks to their low price per GB and their high data density. In the recent years, two new types of technologies for hard disks became object of intense research and brought significant improvements in the hard disk data density. Such technologies are the Heat Assisted Magnetic Recording and the Microwave Assisted Magnetic Recording.

The realization of these devices requires a deep understanding of the magnetization processes. The physical theory employed to study these technologies is the micromagnetic theory, which is presented in the first chapter.

The second chapter is entirely dedicated to the magnetization dynamics of uniformly magnetized bodies. This is typically the case of magnetic memories, where the small size of the memory cell forces the magnetization to be uniform. One of the main points of this chapter is the study of the ferromagnetic resonance, which is an important tool for the measurement of material parameters and plays also an important role in the Microwave Assisted Magnetic Switching. In this context my contribution is the description of the bifurcation diagram of axial symmetric systems. Such diagram was already studied in literature for small values of the AC excitation, but a description for intense AC field is still missing.

The third and fourth chapters deal with the magnetization dynamics when the dimension and the time scale involved, respectively, are very small.

The magnetization process in small particles highlights the main problems related to the enhancement of data density in magnetic storage technologies, such as thermal instability or the reliability of the writing process. My work on this topic mostly concerns numerical methods (Pseudospectral) for the

solution of the Fokker-Planck equation and the analysis of the switching time statistical distribution for magnetic memories. The pseudospectral method turns out to be a useful tool for the study of systems with strong noise whereas it does not perform well in systems where the energy barriers are high. The analysis of the switching time statistical distribution is a relevant result for the optimization of the switching process in both hard disks and Magnetic Random Access Memories (MRAM).

Both ferromagnetic resonance and switching can be considered as fast magnetization dynamics since the time resolution of interest is generally a fraction of nanosecond. Phenomena that occur on a timescale of picoseconds or less are instead considered ultrafast. In the last chapter of the thesis the ultrafast magnetization dynamics is considered. This is a relatively recent topic not entirely explored yet, but it is of interest for the development of future magnetic storage technologies with high speed. According to theory, in the ultrafast regime the effects of magnetization inertia become relevant and the equation governing the magnetization dynamics must be properly adjusted. The first direct experimental observation of one of these effects was done by the Neeraj et al. [81] of the Stockholm University in a experimental facility in Dresden. My contribution in this work was providing theoretical support, and it is presented in the last chapter of the thesis.

Introduction

Ferromagnetic materials are one of the most important class of materials for applications in electrical engineering. They are crucial components in electrical machines, transformers, actuators, etc. Beside these traditional applications, magnetic materials have had a central importance in information technology. In this thesis we are mainly concerned with this latter class of applications.

The spontaneous magnetization of ferromagnetic materials can be exploited to store information in nonvolatile forms, which can be used for the realization of data recording technologies.

A widespread technology that relies on ferromagnetic materials is the hard disk, which is the main type of memory used for large databases.

The working principle of hard disks is rather simple: data are stored into ferromagnetic media with a strong anisotropy such that only two possible orientations of the magnetization are stable, one corresponds to the bit "0" and the other corresponds to the bit "1". The device and the media are shown in Figure 1.

What made hard disks one of the top products for data storage is their high data density and their low price per GB (figure 2). The achievement of such a high density was a technological challenge that required a deep knowledge of the magnetization dynamics and other related phenomena like the Giant Magneto Resistive effect.

While the writing process on hard disks is simply achieved by applying an intense magnetic field in the area of interest, the reading process is somehow more complex and it employs spin valves. An illustration of the hard disk's head is on figure 3.

Spin valves are three layer structures, consisting of two ferromagnetic layers separated by a nonferromagnetic spacer (see figure 4).

One magnetic layer, called "pinned" layer has a fixed magnetization. The other one, called "free" layer, can change its magnetization when subject to

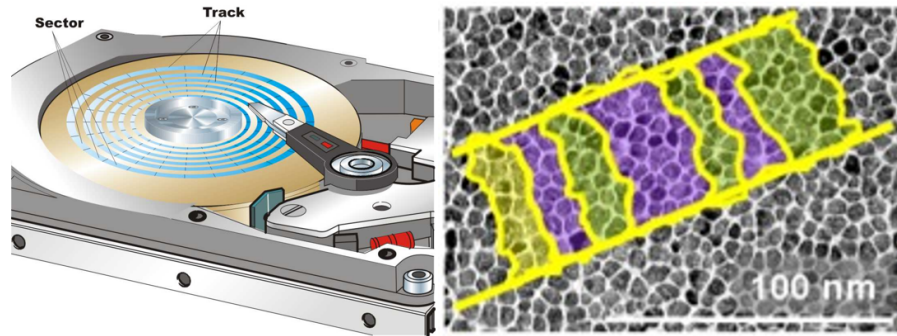


Figure 1: Schematic representation of hard disk structure (left) and the magnetic media used for the recording (right). The orientation of the magnetic grains magnetization defines the stored data.

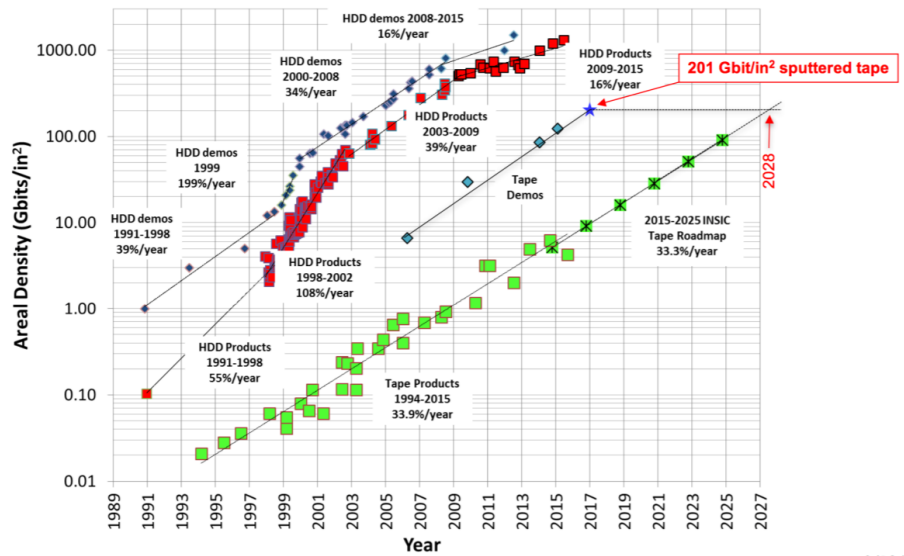


Figure 2: Increase of the areal density of data in the years for different types of memories

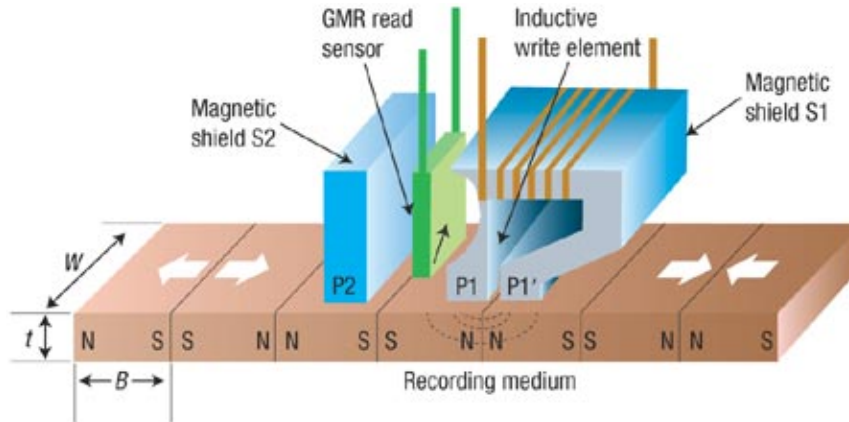


Figure 3: Representation of the HDD Write/Read head. P1 and P1' are used for the writing process to locally enhance the magnetic field generated by the coils. P1 and P2 are used in the reading process to enhance the magnetic field generated by the recording media. The green element (GMR read sensor or spin valve) is sensitive to the magnetic field.

polarized currents or, in the case of hard disks, external magnetic fields.

Because of the GMR effect the electrical resistance of a ferromagnetic material to a polarized current depends on whether the polarization of the current is parallel or antiparallel to the magnetization.

The reading process is done by injecting current into the spin valve and measuring the electrical resistance, which depends on the magnetization of the free layer and, hence, on the magnetic field generated by the memory cell of interest.

For what concerns the future of magnetic recording, in order to reach an even higher data density, three important problems are to be faced, i.e. the thermal stability, the power consumption and the low signal to noise ratio. It turns out that solving one of these problems can worsen the others. This is elegantly represented by the magnetic trilemma [9]. For example a reduction of the memory cell dimension will eventually cause thermal instability. Data can become more stable if a high energy barrier is set, for example by using materials with strong anisotropy, but resistance to thermal noise also implies resistance to the fields used in the writing process, hence higher fields are required and more energy losses occur, which raise the temperature and lower

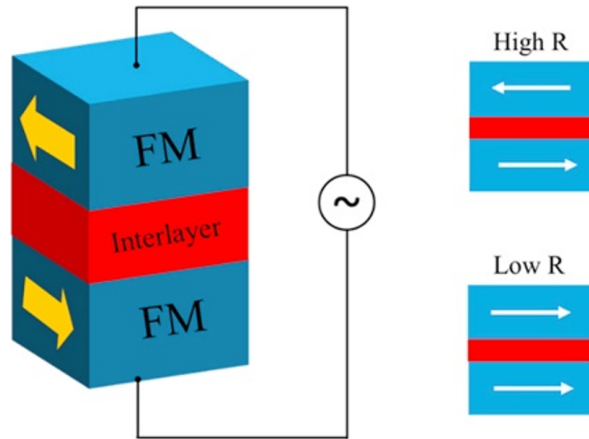


Figure 4: Representation of a spin valve device, blue layers are made of ferromagnetic materials, the red layer is nonmagnetic. On the right there are the configurations which achieve the highest and the lowest electrical resistance.

the maximum density.

An ingenious possible solution to partially overcome this problem is the Energy Assisted Magnetic Recording (EAMR). The basic idea is to “prepare” the memory cell to be overwritten by lowering the energy barrier, so that a weaker magnetic field is sufficient to switch the magnetization. The energy barrier is restored after the switching so that the data are thermally stable. Two different methods are included in this category: Heat Assisted Magnetic Recording (HAMR) and Microwave Assisted Magnetic Recording (MAMR). The two methods are illustrated in figure 5.

HAMR technology is based on positioning a laser diode directly in front of the write head assembly, and very rapidly heating the high coercivity media that cannot be written unless it is heated during the writing process. As the media cools down from the intense laser heat, the coercivity of the media increases, holding the bits in state, and making it difficult for the magnetization to inadvertently change.

Seagate has been investing on HAMR technology [5, 6, 7] and succeeded in manufacturing 20TB hard disks that will probably be available on market in 2020. Figure 6 shows the trend predicted by Seagate for such technology. MAMR technology uses a microwave field generated from a spin torque

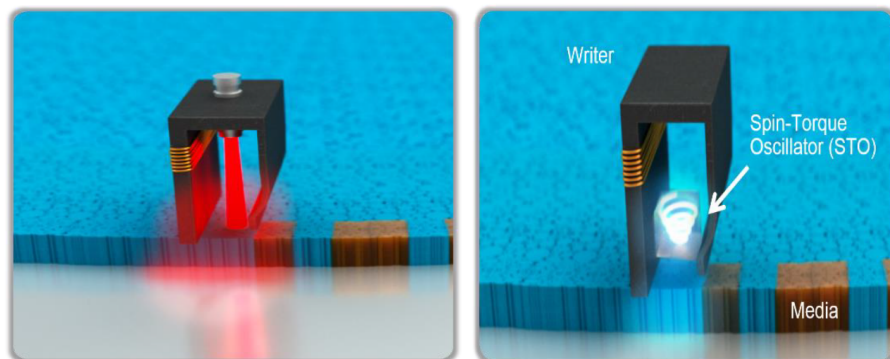


Figure 5: Working principle of the Heat Assisted Magnetic Recording (left): a laser heats the magnetic recording media at the beginning of the write process. Working principle of the Microwave Assisted Magnetic Recording (right): a microwave frequency magnetic field is used to move the magnetization away from the stable equilibrium point and make the writing process easier.

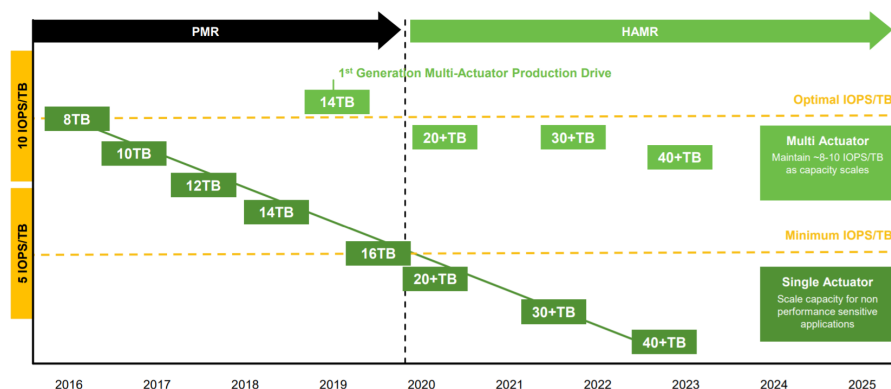


Figure 6: Seagate previsions for the speed and capacity of magnetic HDD. Perpendicular Magnetic Recording (PMR) is the HDD technology currently employed, a remarkable boost in performance is expected from the development of the Heat Assisted Magnetic Recording (HAMR) technology.

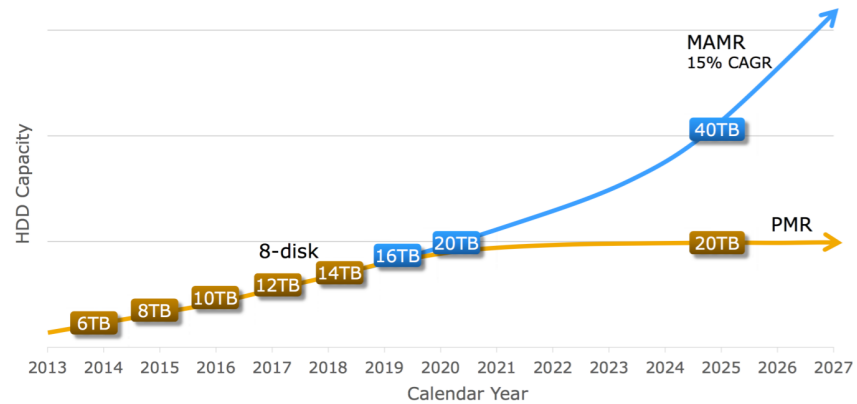


Figure 7: Western Digital previsions for the HDD capacity, Microwave Assisted Magnetic Recording (MAMR) technology is expected to give a significant enhancement of HDD capacity compared to Perpendicular Magnetic Recording (PMR) technology.

oscillator (STO) [1, 2, 3]. In this method, the STO located near the writing pole of the head generates an electromagnetic field that allows data to be written on the perpendicular magnetic media at a lower magnetic field. Western Digital has been working on MAMR [8] and commercial hard disks with this technology will probably be available in the 2020. Figure 7 shows the trend predicted by Western Digital for such technology.

Magnetic recordings do not only compete on the high density. Magnetic Random Access Memories (MRAM) are non-volatile memories with high speed and endurance. Their structure is displayed in figure 9. Information are stored in arrays of spin valves, each device contains a single bit of information. The bit is read by injecting current into the cell of interest. A measure of the electrical resistance gives the state of the cell analogously to the reading process in hard disks. The writing process is achieved by injecting a stronger current into the cell, this causes a rotation of the magnetization in the free layer according to the Spin Transfer Torque effect. A representation of the electrical circuit is in figure 10.

Typical values of switching time, endurance and other features of interest for the most widespread types of memories are reported in figure 8.

An important physical aspect of magnetic storage technologies is the speed at which magnetization can be switched and the repeatability of the switching.


Characteristics	STT-MRAM	DRAM	3D Xpoint	Resistive RAM	Low Power CBRAM	NAND
Supplier	 EVERSPIN TECHNOLOGIES	Multiple	Intel/Micron	Crossbar	Adesto	Multiple
Latency R/W	70ns/70ns	40-180ns ¹	100ns/500ns	100ns/100μs	1μs/25-100μs	25μs - 1500μs
Endurance	10 ¹⁰ - 10 ¹²	10 ¹⁵	10 ⁶ -10 ⁷	10 ⁵ -10 ⁶	10 ⁵	10 ² -10 ³
Persistent	Yes	No	Yes	Yes	Yes	Yes
Interface	ST-DDR3/ST-DDR4	DDR3/DDR4	Proprietary	Flash-like	SPI	NAND
Status	Shipping	Shipping	Shipping Optane	R&D	Production	Shipping
Density Path	Gigabit+	Gigabit+	64Gb+	Terabit	64Mb	Gigabit+

Figure 8: Summary of the main feature of the recent competitive types of memories.

Hence to obtain fast and reliable memories it is important to study fast magnetization switching.

Another interesting technology based of ferromagnetic materials are the magnetic nano-oscillators. It is indeed possible to induce oscillations of the magnetization in a small magnet by injecting a constant current. This type of oscillators is not ready yet for commercial use because of the low power of the output signal.

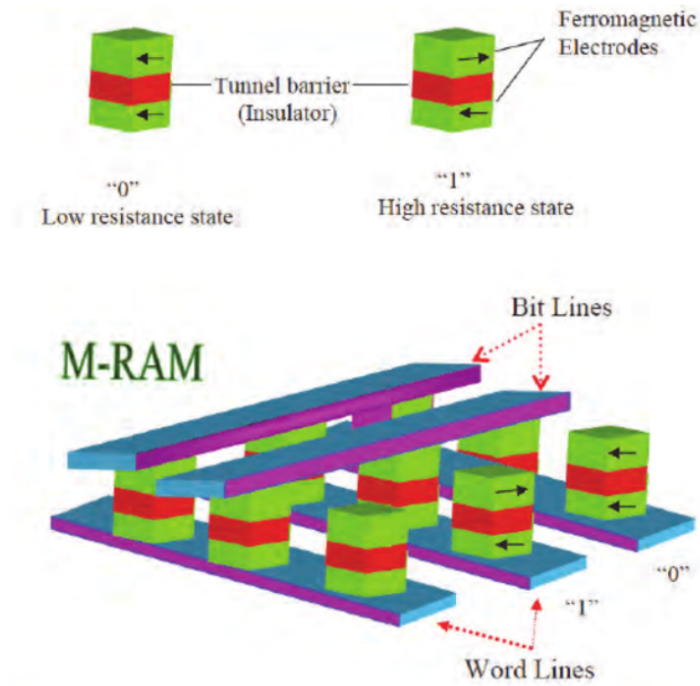


Figure 9: Scheme of a Magnetic Random Access Memory (MRAM), the green and red blocks are spin valves and they are used as memory cells, the blue bars are conductors.

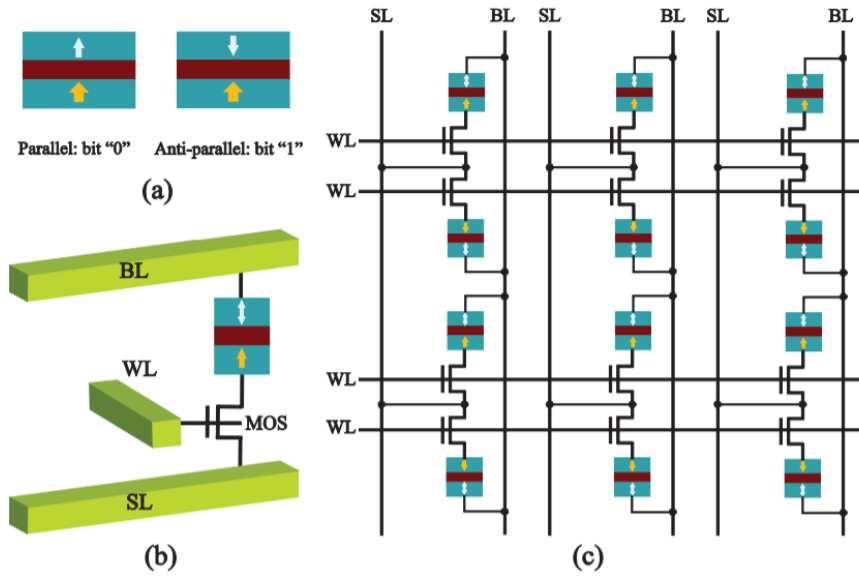


Figure 10: Scheme of the one transistor architecture [4] used to select a memory cell and read the data stored in it. Spin valves are organized into arrays, one word line (WL) is set to high such that one line of cells are electrically connected to the source line (SL) and the bit line (BL). Injection of current can be either used to read the data or to modify the cell status.

Chapter 1

Micromagnetics and LLG

In this chapter, the micromagnetic theory [10], [12], [13] is presented. The discussion starts from the equation of magnetostatic and the principles of thermodynamics in order to formulate an equilibrium condition for ferromagnetic systems in terms of an appropriate thermodynamic potential.

Once the equilibrium condition is defined, the dynamic equation is introduced using a phenomenological approach and its main properties are discussed.

1.1 Magnetostatic Equations

Let us consider a magnetic field \mathbf{H} generated by assigned current density \mathbf{J}_0 and magnetization \mathbf{M} of a body occupying the volume V as in the situation schematically represented in figure 1.1. The magnetostatic equation reads

$$\nabla \times \mathbf{H} = \mathbf{J}_0, \quad \nabla \cdot (\mu_0 \mathbf{H} + \mu_0 \mathbf{M}) = 0, \quad (1.1)$$

where μ_0 is the magnetic permeability of the void.

The magnetization itself is a function of the magnetic field. Consequently equation (1.1) must be complemented with a constitutive relation $\mathbf{M} = \mathcal{M}(\mathbf{H})$ and the magnetostatic problem must be solved consistently.

In order to separate the contribution of the current density \mathbf{J}_0 and the one of the magnetization \mathbf{M} to the magnetic field \mathbf{H} , we consider Helmholtz decomposition of the field

$$\begin{cases} \nabla \times \mathbf{H}_a = \mathbf{J}_0 \\ \nabla \cdot \mathbf{H}_a = 0 \end{cases}, \quad \begin{cases} \nabla \times \mathbf{H}_M = 0 \\ \nabla \cdot \mathbf{H}_M = -\nabla \cdot \mathbf{M} \end{cases}, \quad (1.2)$$

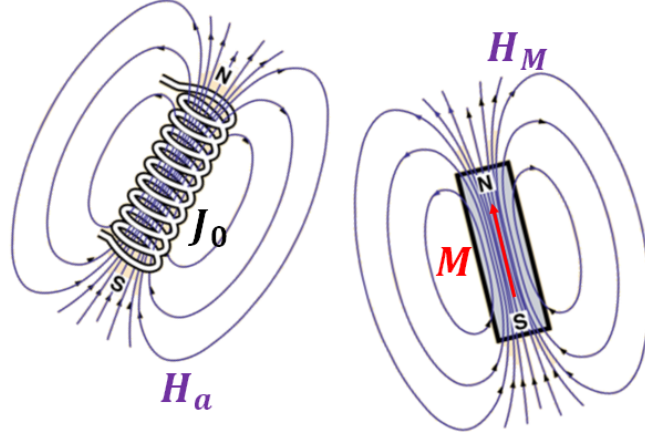


Figure 1.1: Magnetic field generated by a magnetized body and by a coil with an electric current, the first (on the right) is the field \mathbf{H}_M , the second (on the left) is the field \mathbf{H}_a .

where $\mathbf{H} = \mathbf{H}_a + \mathbf{H}_M$. The analytical solutions for the two fields are respectively

$$\mathbf{H}_a(\mathbf{x}) = \frac{1}{4\pi} \int_{\mathbb{R}^3} \frac{\mathbf{J}_0(\mathbf{y}) \times (\mathbf{x} - \mathbf{y})}{|\mathbf{x} - \mathbf{y}|^3} dV_{\mathbf{y}}, \quad (1.3)$$

and

$$\mathbf{H}_M(\mathbf{x}) = \frac{1}{4\pi} \nabla \left(\int_V \frac{\nabla \cdot \mathbf{M}(\mathbf{y})}{|\mathbf{x} - \mathbf{y}|} dV_{\mathbf{y}} - \int_{\partial V} \frac{\mathbf{M}(\mathbf{y}) \cdot \hat{\mathbf{n}}(\mathbf{y})}{|\mathbf{x} - \mathbf{y}|} dS_{\mathbf{y}} \right). \quad (1.4)$$

According to Poynting theorem (see appendix B) the power required to modify the magnetic flux density is given by

$$P = \int_{\mathbb{R}^3} \mathbf{H} \cdot \frac{d\mathbf{B}}{dt} d\mathbf{x}. \quad (1.5)$$

However not all the energy spent is stored in the material, indeed some energy is required even when there is no material.

By using the Helmholtz decomposition in equation (1.2), given $\mathbf{B} = \mu_0(\mathbf{H}_a + \mathbf{H}_M + \mathbf{M})$, we can write

$$P = \int_{\mathbb{R}^3} \left(\mu_0 \mathbf{H}_a \cdot \frac{d\mathbf{H}_a}{dt} + \mu_0 \mathbf{H}_a \cdot \frac{d\mathbf{H}_M}{dt} + \mu_0 \mathbf{H}_a \cdot \frac{d\mathbf{M}}{dt} + \mu_0 \mathbf{H}_M \cdot \frac{d\mathbf{H}_a}{dt} + \mu_0 \mathbf{H}_M \cdot \frac{d\mathbf{H}_M}{dt} + \mu_0 \mathbf{H}_M \cdot \frac{d\mathbf{M}}{dt} \right) d\mathbf{x}. \quad (1.6)$$

The second and fourth addend in the sum give zero contribution when integrated in the whole space. This happens because \mathbf{H}_a and its time derivative are conservative, while \mathbf{H}_M and its time derivative are solenoidal. Consequently the Tellegen theorem (see appendix A) gives

$$\int_{\mathbb{R}^3} \mathbf{H}_a \cdot \frac{d\mathbf{H}_M}{dt} dV = 0, \quad (1.7)$$

and

$$\int_{\mathbb{R}^3} \mathbf{H}_M \cdot \frac{d\mathbf{H}_a}{dt} dV = 0. \quad (1.8)$$

By using again the Tellegen theorem it can also be proved that the last two terms cancel out exactly. Indeed applying Helmholtz decomposition to \mathbf{M} yields

$$\mathbf{M} = \frac{\mathbf{B}_M}{\mu_0} - \mathbf{H}_M. \quad (1.9)$$

Consequently we have

$$\begin{aligned} \int_{\mathbb{R}^3} \mathbf{H}_M \cdot \frac{d\mathbf{M}}{dt} dV &= \int_{\mathbb{R}^3} \mathbf{H}_M \cdot \frac{d}{dt} \left(\frac{\mathbf{B}_M}{\mu_0} - \mathbf{H}_M \right) dV \\ &= - \int_{\mathbb{R}^3} \mathbf{H}_M \cdot \frac{d\mathbf{H}_M}{dt} dV. \end{aligned} \quad (1.10)$$

where we used the fact that \mathbf{B}_M is solenoidal and the Tellegen theorem. Eventually the power required to modify the magnetic field is

$$P = \int_{\mathbb{R}^3} \mu_0 \mathbf{H}_a \cdot \frac{d\mathbf{H}_a}{dt} d\mathbf{x} + \int_V \mu_0 \mathbf{H}_a \cdot \frac{d\mathbf{M}}{dt} d\mathbf{x}. \quad (1.11)$$

The first term can be interpreted as the power required to create \mathbf{H}_a in absence of material. Accordingly the second term gives the energy stored in the magnetic material, i.e.

$$\frac{dL_M}{dt} = \int_V \mu_0 \mathbf{H}_a \cdot \frac{d\mathbf{M}}{dt} d\mathbf{x}. \quad (1.12)$$

1.2 Principles of thermodynamics

Let us consider a small volume ΔV of magnetic material which is subject to a fixed magnetic field \mathbf{H} and is in contact with a thermal bath at a constant temperature T . Let us also assume that the volume is small enough to be

considered at the thermodynamic equilibrium, given the internal energy ΔU and the entropy ΔS of the volume ΔV . We define the density of energy and entropy respectively as

$$u = \frac{U}{\Delta V}, \quad s = \frac{S}{\Delta V}. \quad (1.13)$$

The first principle of thermodynamics states

$$\frac{dU}{dt} = \frac{dL}{dt} + \frac{dQ}{dt}, \quad (1.14)$$

where L is the work done on the system and Q is the heat injected. If no work can be done by deforming the volume and there is no generated heat, according to (1.12) the first principle becomes, after dividing by ΔV ,

$$\frac{\partial u}{\partial t} = \mathbf{H} \cdot \frac{\partial \mathbf{M}}{\partial t} - \nabla \cdot \mathbf{q} \quad (1.15)$$

where \mathbf{q} is the density of the heat flux.

The second law of thermodynamics states that for any isolated system the entropy s cannot decrease in time, i.e.

$$\frac{\partial s}{\partial t} \geq 0. \quad (1.16)$$

This principle can be extended to a non isolated system. It reads

$$\frac{\partial s}{\partial t} \geq -\frac{1}{T} \nabla \cdot \mathbf{q} \quad \text{or} \quad \frac{\partial s}{\partial t} = -\frac{1}{T} \nabla \cdot \mathbf{q} + \frac{\partial s^*}{\partial t}, \quad (1.17)$$

where T is the temperature and s^* is the entropy generated by irreversible processes and is non negative

$$\frac{\partial s^*}{\partial t} \geq 0. \quad (1.18)$$

By substituting (1.14) into (1.17) and multiplying by the temperature, after some algebra, it yields

$$\frac{\partial u}{\partial t} - T \frac{\partial s}{\partial t} - \mathbf{H} \cdot \frac{\partial \mathbf{M}}{\partial t} = -T \frac{\partial s^*}{\partial t}. \quad (1.19)$$

By introducing the Helmholtz free energy

$$f = u - Ts \quad (1.20)$$

we get

$$\frac{df}{dt} + s \frac{dT}{dt} - \mathbf{H} \cdot \frac{\partial \mathbf{M}}{\partial t} = -T \frac{ds^*}{dt}. \quad (1.21)$$

In experiments or applications the controlled variable is the applied field \mathbf{H}_a . Hence using the Leibenitz formula the equation (1.21) is reformulated as

$$\frac{df}{dt} - \frac{d}{dt}(\mu_0 \mathbf{H} \cdot \mathbf{M}) + s \frac{dT}{dt} + \mu_0 \mathbf{M} \cdot \frac{d\mathbf{H}_a}{dt} = -T \frac{ds^*}{dt}. \quad (1.22)$$

By recalling the hypothesis of constant temperature and applied field, equation (1.22) becomes

$$\frac{df}{dt} - \frac{d}{dt}(\mu_0 \mathbf{H} \cdot \mathbf{M}) = -T \frac{ds^*}{dt}. \quad (1.23)$$

We finally define the density of Gibbs-Landau free energy as

$$g = f - \mu_0 \mathbf{H} \cdot \mathbf{M}. \quad (1.24)$$

The state variable just defined is a thermodynamic potential when temperature and applied field are fixed. Indeed it holds

$$\frac{dg}{dt} = -T \frac{ds^*}{dt}, \quad (1.25)$$

which implies that equilibrium is reached when g is minimized.

In the general case the systems considered here are not small enough to assume homogeneity of every thermodynamic property. In these circumstances we can integrate equations from (1.21) to (1.25) over the volume occupied by the body and define the total Helmholtz free energy, the Gibbs-Landau free energy, the total entropy and the entropy generated

$$F = \int_V f \, dV, \quad G = \int_V g \, dV, \quad S = \int_V s \, dV, \quad S^* = \int_V s^* \, dV. \quad (1.26)$$

Equation (1.25) becomes

$$\frac{dG}{dt} = -T \frac{dS^*}{dt}, \quad (1.27)$$

since the global quantities are now well defined thanks to equations (1.26). This is called principle of minimization of free energy.

1.3 Free Energy Contributions

So far it was highlighted the role of the free energy in the determination of the magnetization. What is still missing is an explicit expression of the Helmholtz free energy.

A precise derivation of F from fundamental principles would require a detailed knowledge of the microscopic structure of the material, which is in general not available.

In micromagnetics the expression of the free energy is postulated according to some phenomenological considerations. In particular four contributions to the free energy are considered: the exchange energy, the anisotropy energy, the magnetostatic energy and Zeeman energy.

1.3.1 Exchange energy

Exchange free energy is the main feature of ferromagnetic materials and it is the one which causes spontaneous magnetization.

Weiss Mean Field Theory

Microscopically the media can be modeled as a large ensemble of magnetic dipoles $\{\boldsymbol{\mu}_i\}$. When an external field \mathbf{H} is applied, dipoles rotate to align with the field, on the other hand thermal agitation prevents the realization of a fully ordered structure.

Magnetic dipoles have random orientation with a preference for the direction pointed by the external field. If the temperature is kept fixed, the probability density function of any configuration is provided by the Boltzmann distribution [14]

$$P(\boldsymbol{\mu}_1, \boldsymbol{\mu}_2, \dots) \propto \exp\left(-\frac{\mathcal{H}(\boldsymbol{\mu}_1, \boldsymbol{\mu}_2, \dots)}{k_B T}\right) \quad (1.28)$$

where \mathcal{H} is the Hamiltonian, k_B is Boltzmann constant and T is the temperature.

For sake of simplicity, let us consider as Hamiltonian

$$\mathcal{H}(\boldsymbol{\mu}_1, \boldsymbol{\mu}_2, \dots) = - \sum_i \mu_0 \boldsymbol{\mu}_i \cdot \mathbf{H} \quad (1.29)$$

where μ_0 is the magnetic permeability of void. Magnetization is given by the vector sum of all magnetic dipoles. Note that in the Hamiltonian (1.29) there

is no interaction between different dipoles, they only interact with the external magnetic field.

The magnetization is given by the average of the sum of all the moments, i.e.

$$\mathbf{M} = \left\langle \sum_i \boldsymbol{\mu}_i \right\rangle. \quad (1.30)$$

Because of the rotational symmetry of the system we expect \mathbf{M} to be aligned with the external field and the whole derivation can be developed by using the scalar quantities. Moreover we assume, according to quantum mechanics, that dipoles can only exhibit two orientations. Hence

$$M = \frac{1}{Z} \frac{N}{V} \mu \left[\exp\left(\frac{\mu_0 \mu H}{k_B T}\right) - \exp\left(-\frac{\mu_0 \mu H}{k_B T}\right) \right], \quad (1.31)$$

where $\mu = |\boldsymbol{\mu}|$, $H = |\mathbf{H}|$, N is the number of magnetic dipoles, V is the volume occupied by the dipoles and

$$Z = \exp\left(\frac{\mu_0 \mu H}{k_B T}\right) + \exp\left(-\frac{\mu_0 \mu H}{k_B T}\right) \quad (1.32)$$

is the normalization constant which grants that probability is well defined. Z is also called partition function.

Equation (1.31) gives

$$M = M_0 \tanh(y) \quad (1.33)$$

where $y = \frac{\mu_0 H \mu}{k_B T}$ and $M_0 = \frac{N}{V} \mu$.

The Hamiltonian in equation (1.29) can not allow spontaneous magnetization, the fundamental missing feature is the interaction between magnetic dipoles.

A simple but still effective way to introduce interaction consists in substituting the applied field H with an effective field

$$H_{\text{eff}} = H + \lambda M, \quad (1.34)$$

where λM is called molecular field and the parameter λ is determined experimentally.

The magnetization is still given by equation (1.33) with $y = \frac{\mu_0 H_{\text{eff}} \mu}{k_B T}$ and, although it can not be expressed explicitly, the model can be easily analyzed by using graphical methods. From equations (1.33) and (1.34), we have

$$\begin{cases} M = M_0 \tanh(y), \\ M = \lambda^{-1} \frac{k_B T}{\mu_0 \mu} y - \lambda^{-1} H. \end{cases} \quad (1.35)$$

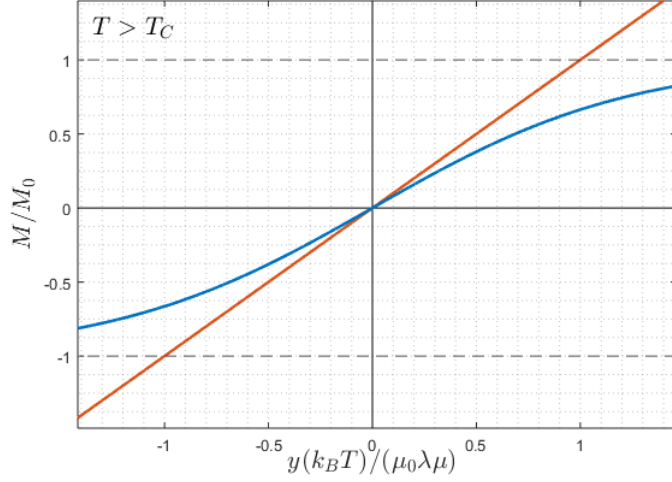


Figure 1.2: Equations of system (1.35) for temperature higher than the Curie temperature (T_C). The only intersection is at zero and no spontaneous magnetization can occur.

M is a linear function of y , hence the value of the magnetization is given by the intersection of (1.33) and (1.34) in the plane y - M .

Let us consider $H = 0$. Qualitatively two possible scenarios can manifest: if the slope of (1.35) is greater than the slope of (1.33) in $y = 0$ there is only one intersection for $M = 0$ as sketched in figure 1.2; otherwise there are three intersections and for two of them we have $|M| > 0$, which means that spontaneous magnetization occurs as illustrated in figure 1.3.

Spontaneous magnetization is a function of temperature. In particular magnetization vanishes in correspondence of the Curie temperature, which can be obtained by imposing the derivative of (1.33) in 0 to be equal to the angular coefficient of (1.35). It yields

$$M_0 = \frac{k_B T_C}{\mu_0 \mu \lambda} \implies T_c = \frac{\mu_0 \mu M_0 \lambda}{k_B}. \quad (1.36)$$

The plot of the spontaneous magnetization as a function of the temperature is in figure 1.4.

We can finally estimate the free energy due to the exchange interaction by

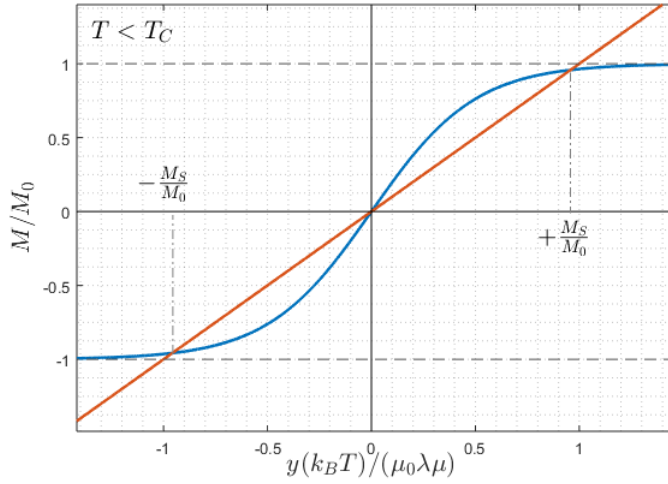


Figure 1.3: Equations of system (1.35) for temperature lower than the Curie temperature (T_C). There are three intersections: two of them correspond to a spontaneous magnetization, while the third one, in $M = 0$, has no spontaneous magnetization and is unstable.

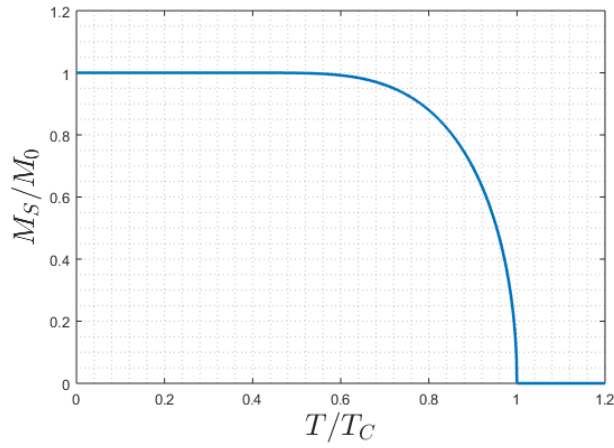


Figure 1.4: Magnitude of the spontaneous magnetization as a function of the temperature.

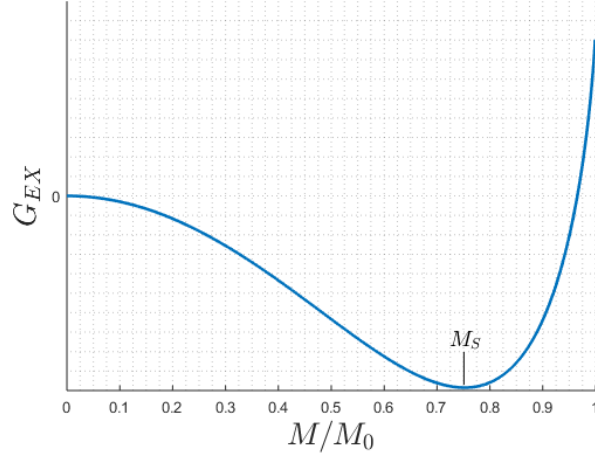


Figure 1.5: Gibbs free energy calculated by the Weiss model. The deep minimum in $M = M_S$ justifies the assumption of considering $|\mathbf{M}|$ a given constant of the material.

calculating the magnetic field from (1.35)

$$H = \frac{k_B T}{\mu_0 \mu} \tanh^{-1} \frac{M}{M_0} - \lambda M. \quad (1.37)$$

Integrating H in dM gives

$$G_{EX} = \frac{k_B T}{\mu \mu_0} \left[(M_0 + M) \log \left(1 + \frac{M}{M_0} \right) + (M_0 - M) \log \left(1 - \frac{M}{M_0} \right) \right] - \frac{\lambda}{2} M^2. \quad (1.38)$$

The plot of the free energy as function of M/M_0 is displayed in figure 1.5.

Effect of exchange interaction

The main result of Weiss theory is the existence of a spontaneous magnetization due to exchange interaction. This means that free energy must have a minimum for some module of the magnetization $M_S > 0$, also called saturation magnetization. The energy minimum is in fact so deep that even small

variations of the magnetization module are hard to observe. For this reason the module is generally considered fixed

$$|\mathbf{M}| = M_S . \quad (1.39)$$

The exchange interaction affects also the variation of the magnetization. The orientation of neighboring electrons spin is forced to be almost the same, but after a long enough chain of neighboring electrons some significant change in the spin orientation can arise. Its contribution to the free energy is given by

$$G_{EX} = \int_V A (|\nabla m_x|^2 + |\nabla m_y|^2 + |\nabla m_z|^2) d\mathbf{x} , \quad (1.40)$$

where $m_i = M_i/M_S$ is the normalized i -th component of the magnetization and A is called exchange constant. It is measured in J/m and depends on the material considered.

1.3.2 Anisotropy energy

Anisotropy energy depends on the relative orientation of the magnetization with respect to some preferred directions, this is a frequent occurrence in ferromagnetic materials because of their crystalline structure.

Microscopically this is due to the interaction of electron spins angular momenta, which are responsible for the magnetization, and electrons orbital angular momenta, which are constrained by the crystal structure.

The free energy contribution is given by

$$G_{AN} = \int f_{AN}(\mathbf{m}) d\mathbf{x} . \quad (1.41)$$

The explicit expression of f_{AN} depends on the material considered.

Uniaxial Anisotropy

The simplest type of anisotropy is the uniaxial one, the function $g(\mathbf{m})$ has a rotational symmetry around some direction $\hat{\mathbf{e}}_z$.

Let us call θ the angle between \mathbf{m} and $\hat{\mathbf{e}}_z$ as sketched in figure 1.6. The expression of the free energy density can be expanded in series of powers of $\sin^2 \theta$ as

$$f_{AN}(\theta) = K_0 + K_1 \sin^2 \theta + K_2 \sin^4 \theta + \dots \quad (1.42)$$

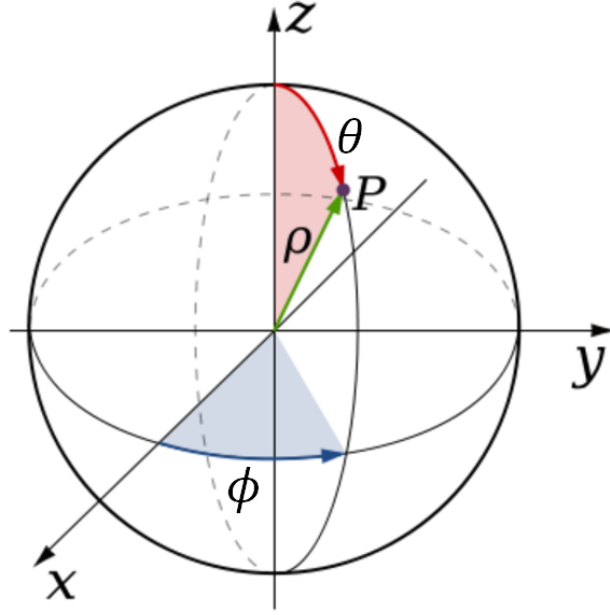


Figure 1.6: Reference frame of the section 1.3.2

where K_i are anisotropy constants measured in J/m^3 .

The first constant K_0 is not relevant and can be set to zero. If $g_{AN}(0) < g_{AN}(\pi/2)$ the axis of $\hat{\mathbf{e}}_\perp$ is called easy axis, if instead $g_{AN}(0) > g_{AN}(\pi/2)$ it is called hard axis.

For the applications of the following chapters, it is generally sufficient only the first term of the expansion, i.e.

$$f_{AN}(\theta) = K_1 \sin^2 \theta, \quad (1.43)$$

and the free energy can be expressed as follows

$$G_{AN} = \int_V K_1 [1 - (\mathbf{m} \cdot \hat{\mathbf{e}}_z)^2] d\mathbf{x}. \quad (1.44)$$

A representation of g_{AN} as function of the direction is illustrated in figure 1.7 for negative and positive values of K_1 .

Cubic anisotropy

Cubic anisotropy is usually observed in materials with cubic crystalline structures. In this case there are three privileged directions, say $\hat{\mathbf{e}}_x$, $\hat{\mathbf{e}}_y$ and $\hat{\mathbf{e}}_z$.

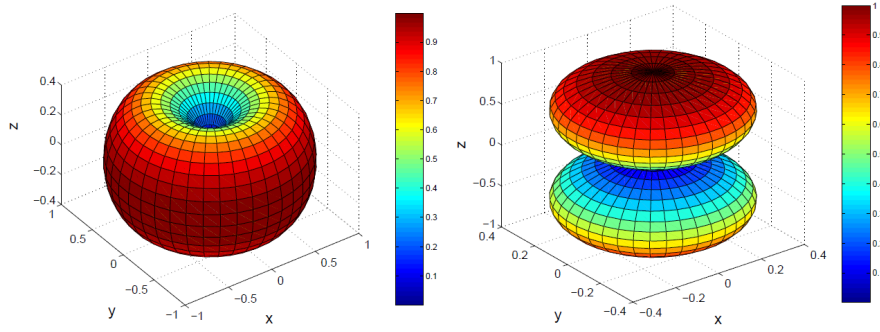


Figure 1.7: Free energy as function of the magnetization orientation for a media with uniaxial anisotropy. The easy axis case ($K_1 > 0$) is in the left panel and the hard axis case ($K_1 < 0$) in the right panel

A typical expression for the free energy contribution is

$$f_{AN}(\mathbf{m}) = K_0 + K_1(m_x^2 m_y^2 + m_y^2 m_z^2 + m_z^2 m_x^2) + K_2 m_x^2 m_y^2 m_z^2 + \dots, \quad (1.45)$$

as before, the term K_0 is irrelevant.

If the terms of order greater than four are neglected, free energy density in equation (1.45) has six minima when $K_1 < 0$ or six maxima when $K_1 > 0$. The total free energy is given by

$$f_{AN} = \int_V K_1(m_x^2 m_y^2 + m_y^2 m_z^2 + m_z^2 m_x^2) d\mathbf{x}. \quad (1.46)$$

A plot of g_{AN} as function of the direction is illustrated in figure 1.8 for negative and positive values of K_1 .

1.3.3 Magnetostatic energy

We have to take into account the dipole-dipole interaction, since magnetization itself creates a magnetic field as shown in equation (1.4). The resulting free energy is then given by

$$G_{MS} = - \int_V \frac{\mu_0}{2} \mathbf{H}_M \cdot \mathbf{M} d\mathbf{x}. \quad (1.47)$$

By using Helmholtz decomposition and Tellegen theorem (see appendix A), equation (1.47) can be reformulated as

$$G_{MS} = \int_{\mathbb{R}^3} \frac{1}{2} \mu_0 \mathbf{H}_M^2 d\mathbf{x}. \quad (1.48)$$

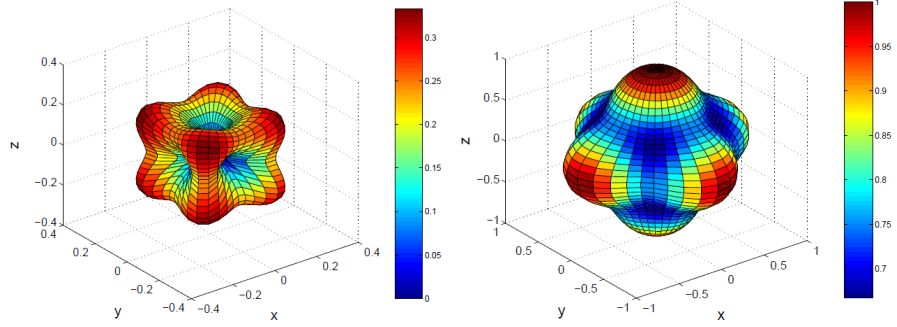


Figure 1.8: Free energy as function of the magnetization orientation for a media with cubic anisotropy. On the left the case $K_1 > 0$ where lattice directions are energetically convenient, on the right the case $K_1 < 0$ where the lattice directions are energetically not convenient.

We observe that magnetostatic energy expresses a nonlocal interaction, since the magnetostatic field depends on the whole magnetization vector field.

A criterion to guess the configuration that minimizes the magnetostatic energy is the pole avoidance principle, i.e. the configurations with low magnetostatic energy have divergenceless magnetization and possibly no discontinuities on the normal component of \mathbf{M} .

1.3.4 Zeeman energy

Zeeman energy is not a contribution to Helmholtz free energy, it is instead included in Gibbs free energy as illustrated in equation (1.24), i.e.

$$G_{ZE} = -\mu_0 \int_V \mathbf{H}_a \cdot \mathbf{M} \, d\mathbf{x} . \quad (1.49)$$

This energy tends to align magnetization with external applied fields.

1.4 Brown Equation

So far the micromagnetic formulation is presented in term of a minimization problem. By using mathematical tools of functional analysis it is possible to express the same model in terms of equations.

Since the module of \mathbf{M} is fixed, we can consider the unit vector $\mathbf{m} = \mathbf{M}/M_S$

and the normalized magnetic fields $\mathbf{h}_a = \mathbf{H}_a/M_S$ and $\mathbf{h}_M = \mathbf{h}_M/M_S$. If the magnetization field $\mathbf{m}(\mathbf{x})$ is an equilibrium, and hence gives a minimum of G , for any sufficiently small perturbation $\varepsilon\delta\mathbf{m}$ we have

$$G(\mathbf{m} + \varepsilon\delta\mathbf{m}) > G(\mathbf{m}) , \quad (1.50)$$

and this is possible if and only if

$$\frac{dG(\mathbf{m} + \varepsilon\delta\mathbf{m})}{d\varepsilon} = 0 , \quad (1.51)$$

for any perturbation $\delta\mathbf{m}$.

By summing all the contribution to G given in equations (1.40), (1.41), (1.47) and (1.49) we obtain

$$G = \int_V \left(A \nabla \mathbf{m} : \nabla \mathbf{m} + f_{AN}(\mathbf{m}) - \frac{1}{2} \mu_0 M_S^2 \mathbf{h}_M \cdot \mathbf{m} - \mu_0 M_S^2 \mathbf{h}_a \cdot \mathbf{m} \right) dV_{\mathbf{x}} , \quad (1.52)$$

where $:$ indicates the double dot product.

Let us consider a variation of the magnetization field $\delta\mathbf{M}(\mathbf{x})$. The first order variation in $\delta\mathbf{M}$ of Zeeman energy and anisotropy energy are given by

$$\delta G_{ZE} = - \int_V \mu_0 M_S^2 \mathbf{h}_a \cdot \delta\mathbf{m} dV_{\mathbf{x}} , \quad (1.53)$$

and

$$\delta G_{AN} = \int_V \frac{\partial f_{AN}}{\partial \mathbf{m}} \cdot \delta\mathbf{m} dV_{\mathbf{x}} . \quad (1.54)$$

In order to have the first order variation of exchange energy we develop the double dot product of the gradient $\nabla(\mathbf{m} + \delta\mathbf{m})$ and keep only terms of first order in $\delta\mathbf{m}$

$$\delta G_{EX} = \int_V 2A \nabla \mathbf{m} : \nabla \delta\mathbf{m} d\mathbf{x} . \quad (1.55)$$

Integrating by parts and applying the divergence theorem yields

$$\delta G_{EX} = \int_{\partial V} 2A \frac{\partial \mathbf{m}}{\partial \hat{\mathbf{n}}} \cdot \delta\mathbf{m} dS_{\mathbf{x}} - \int_V 2A \nabla^2 \mathbf{m} \cdot \delta\mathbf{m} dV_{\mathbf{x}} \quad (1.56)$$

where $\hat{\mathbf{n}}$ is the unit vector normal to ∂V and pointing outward.

Finally we consider the variation of the magnetostatic free energy. For this contribution it has to be kept in mind that \mathbf{h}_M is an integrodifferential operator

acting on \mathbf{m} , hence a variation $\delta\mathbf{m}$ corresponds also to a variation $\delta\mathbf{h}_M$. The variation is then given by

$$\delta G_{MS} = - \int_V \frac{1}{2} \mu_0 M_S^2 (\mathbf{h}_M \cdot \delta\mathbf{m} + \delta\mathbf{h}_M \cdot \mathbf{m}) \, dV_{\mathbf{x}} . \quad (1.57)$$

The two addends in the integral give the same contribution due to the reciprocity theorem, hence we can write

$$\delta G_{MS} = - \int_V \mu_0 M_S^2 \mathbf{h}_M \cdot \delta\mathbf{m} \, dV_{\mathbf{x}} . \quad (1.58)$$

We have the total free energy variation by summing the contributions from (1.53), (1.54), (1.56) and (1.58)

$$\begin{aligned} \delta G = \int_V \left(-2A \nabla^2 \mathbf{m} + \frac{\partial f_{AN}}{\partial \mathbf{m}} - \mu_0 M_S^2 \mathbf{h}_a - \mu_0 M_S^2 \mathbf{h}_M \right) \cdot \delta\mathbf{m} \, dV_{\mathbf{x}} + \\ + \int_{\partial V} 2A \frac{\partial \mathbf{m}}{\partial \hat{\mathbf{n}}} \cdot \delta\mathbf{m} \, dS_{\mathbf{x}} . \end{aligned} \quad (1.59)$$

The variation $\delta\mathbf{m}$ has to satisfy a constraint due to the fixed module of \mathbf{M} , indeed it must hold

$$\mathbf{m} \cdot \delta\mathbf{m} = 0 \quad (1.60)$$

to keep the module unchanged. This constraint can be automatically satisfied by imposing

$$\delta\mathbf{m} = \mathbf{m} \times \delta\boldsymbol{\theta} . \quad (1.61)$$

Inserting (1.61) into (1.59) yields

$$\begin{aligned} \delta G = \int_V \left(-2A \nabla^2 \mathbf{m} + \frac{\partial f_{AN}}{\partial \mathbf{m}} - \mu_0 M_S^2 \mathbf{h}_a - \mu_0 M_S^2 \mathbf{h}_M \right) \cdot \mathbf{m} \times \delta\boldsymbol{\theta} \, dV_{\mathbf{x}} + \\ + \int_{\partial V} 2A \frac{\partial \mathbf{m}}{\partial \hat{\mathbf{n}}} \cdot \mathbf{m} \times \delta\boldsymbol{\theta} \, dS_{\mathbf{x}} . \end{aligned} \quad (1.62)$$

We now define the effective magnetic field as

$$\mathbf{h}_{\text{eff}} = \frac{2A}{\mu_0 M_S^2} \nabla^2 \mathbf{m} - \frac{1}{\mu_0 M_S^2} \frac{\partial f_{AN}}{\partial \mathbf{m}} + \mathbf{h}_a + \mathbf{h}_M . \quad (1.63)$$

This field is the sum of two maxwellian terms, \mathbf{h}_a and \mathbf{h}_M , which are the actual magnetic fields and two extra terms which arise from the microscopic structure of the material.

By applying the mixed product properties and substituting (1.63) into (1.62) we have

$$\delta G = - \int_V \mu_0 M_S^2 (\mathbf{h}_{\text{eff}} \times \mathbf{m}) \cdot \delta \boldsymbol{\theta} \, dV_{\mathbf{x}} + \int_{\partial V} 2A \left(\frac{\partial \mathbf{m}}{\partial \hat{\mathbf{n}}} \times \mathbf{m} \right) \cdot \delta \boldsymbol{\theta} \, dS_{\mathbf{x}} . \quad (1.64)$$

At equilibrium $\delta G = 0$ for every $\delta \boldsymbol{\theta}$, hence a magnetization field $\mathbf{m}(\mathbf{x})$ is an equilibrium if and only if it holds

$$\begin{cases} \mathbf{m} \times \mathbf{h}_{\text{eff}} = 0 & \forall \mathbf{x} \in V , \\ \frac{\partial \mathbf{m}}{\partial \hat{\mathbf{n}}} \times \mathbf{m} = 0 & \forall \mathbf{x} \in \partial V . \end{cases} \quad (1.65)$$

The boundary condition can be further simplified if we note that \mathbf{m} is perpendicular to its derivatives because of the module constraint. We eventually obtain Browns equation for the equilibrium

$$\begin{cases} \mathbf{m} \times \mathbf{h}_{\text{eff}} = 0 & \forall \mathbf{x} \in V , \\ \frac{\partial \mathbf{m}}{\partial \hat{\mathbf{n}}} = 0 & \forall \mathbf{x} \in \partial V . \end{cases} \quad (1.66)$$

1.5 Magnetization Dynamics

Up to now, we have presented a variational method based on the minimization of the free energy of a ferromagnetic body. This method allows one to find the equilibrium configurations for a magnetized body, regardless of how magnetization reaches the equilibrium during time.

This section illustrates the equation describing the magnetization dynamics and how it approaches the equilibrium.

1.5.1 Gyromagnetic precession

As previously stated, magnetization in ferromagnets originates from the electrons spin magnetic moments $\boldsymbol{\mu}$. This is proportional to the spin angular momentum \mathbf{S}

$$\boldsymbol{\mu} = \frac{q_e}{m_e c} \mathbf{S} = -\gamma \mathbf{S} , \quad (1.67)$$

where q_e is the electron charge, m_e is the electron mass and c is the speed of light. γ is called gyromagnetic ratio [26].

When an external magnetic field \mathbf{H} is applied, the angular momentum changes and its derivative is given by the applied torque

$$\frac{d\mathbf{S}}{dt} = \boldsymbol{\mu} \times \mathbf{H} . \quad (1.68)$$

Substituting (1.67) into the latter equation yields

$$\frac{d\mathbf{S}}{dt} = \gamma \mathbf{S} \times \mathbf{H} . \quad (1.69)$$

Equation (1.69) describes the precession of the electron magnetic spin around the applied magnetic field. This is also called Larmor precession and the frequency

$$f_L = \frac{\gamma |\mathbf{H}|}{2\pi} \quad (1.70)$$

is also called Larmor frequency.

1.5.2 Landau-Lifshitz equation

The equation (1.69) holds for a single spin, magnetization arises from the collective orientation of a large number of spins and it may have different dynamics. The dynamic of magnetization was described for the first time by Landau and Lifshitz [25], who postulated the so called Landau-Lifshitz equation starting from some phenomenological aspects. A starting point for a feasible equation is the conservation of the module. With this aim the following equation is defined

$$\frac{\partial \mathbf{M}}{\partial t} = \boldsymbol{\Omega} \times \mathbf{M} . \quad (1.71)$$

It can be immediately verified that (1.71) preserves the module. Indeed a scalar multiplication by \mathbf{M} gives

$$\mathbf{M} \cdot \frac{\partial \mathbf{M}}{\partial t} = \frac{1}{2} \frac{\partial |\mathbf{M}|^2}{\partial t} = \mathbf{M} \times (\boldsymbol{\Omega} \times \mathbf{M}) = 0 . \quad (1.72)$$

To determine $\boldsymbol{\Omega}$ it is assumed that at low temperatures and low wavelengths dissipation can be neglected [26], this implies

$$\frac{dG}{dt} = \frac{\delta G}{\delta \mathbf{m}} \frac{\partial \mathbf{m}}{\partial t} = 0 . \quad (1.73)$$

By replacing $\delta G/\delta \mathbf{M} = -\mathbf{H}_{\text{eff}}$ we have

$$\int_V \mathbf{H}_{\text{eff}} \cdot (\boldsymbol{\Omega} \times \mathbf{M}) dV_{\mathbf{x}} = 0. \quad (1.74)$$

The latter condition is satisfied if $\boldsymbol{\Omega} \propto \mathbf{H}_{\text{eff}}$, which is also compatible with the equilibrium condition provided by Brown equations. Finally the constant of proportionality is determined by observing that, when no anisotropy occurs and the magnetization is uniform, the magnetization is expected to behave like a freely precessing moment

$$\frac{\partial \mathbf{M}}{\partial t} = -\gamma \mathbf{M} \times \mathbf{H}_{\text{eff}}. \quad (1.75)$$

This is called Landau-Lifshitz equation and it is the fundamental equation of micromagnetic dynamics, nonetheless the equation is still unsatisfactory since it does not allow magnetization to reach the equilibrium condition.

In order to approach the equilibrium it is necessary to add a phenomenological damping term into (1.75), which leads to the Landau-Lifshitz equation with damping

$$\frac{\partial \mathbf{M}}{\partial t} = -\gamma_L \mathbf{M} \times \mathbf{H}_{\text{eff}} - \frac{\alpha_L \gamma_L}{M_S} \mathbf{M} \times (\mathbf{M} \times \mathbf{H}_{\text{eff}}), \quad (1.76)$$

where $\alpha_L > 0$ is an adimensional damping constant and the subscript L is introduced for convenience.

The qualitative behavior of equation (1.76) and (1.76) is illustrated in figure 1.9

1.5.3 Gilbert equation

A different approach to take into account the damping was proposed by Gilbert in [27], where he derived equation (1.76) from a Lagrangian formulation with generalized coordinates M_x , M_y and M_z . To this end we define the Lagrangian function

$$\mathcal{L}(\mathbf{M}, \dot{\mathbf{M}}) = \mathcal{T}(\mathbf{M}, \dot{\mathbf{M}}) - G(\mathbf{M}), \quad (1.77)$$

where G is the Gibbs Landau free energy and \mathcal{T} is the kinetic energy and has yet to be defined. Conservative Landau-Lifshitz equation can be obtained starting from the Euler-Lagrange equations, namely

$$\frac{d}{dt} \frac{\partial \mathcal{L}(\mathbf{M}, \dot{\mathbf{M}})}{\partial \dot{\mathbf{M}}} - \frac{\partial \mathcal{L}(\mathbf{M}, \dot{\mathbf{M}})}{\partial \mathbf{M}} = 0. \quad (1.78)$$

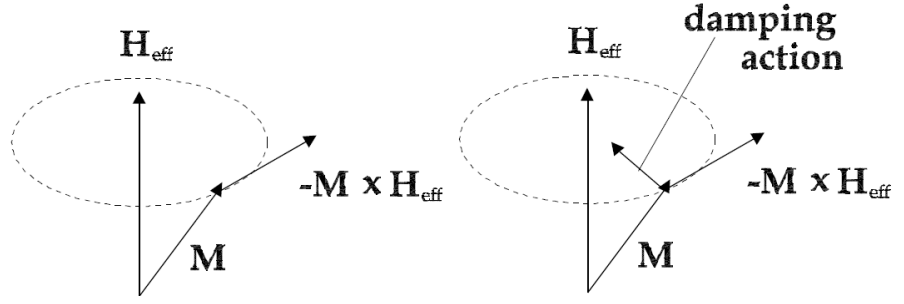


Figure 1.9: Representation of the precession motion of the magnetization (left) and the effect of the phenomenological damping term (right).

In this framework, damping is usually introduced by the Rayleigh term $\mathcal{R}(\dot{\mathbf{M}})$. A typical expression of such term is

$$\mathcal{R}(\dot{\mathbf{M}}) = \frac{\eta}{2} \int \dot{\mathbf{M}} \cdot \dot{\mathbf{M}} dV, \quad (1.79)$$

so that equation (1.78) is restated as

$$\frac{d}{dt} \frac{\partial \mathcal{L}(\mathbf{M}, \dot{\mathbf{M}})}{\partial \dot{\mathbf{M}}} - \frac{\partial \mathcal{L}(\mathbf{M}, \dot{\mathbf{M}})}{\partial \mathbf{M}} + \frac{\partial \mathcal{R}(\dot{\mathbf{M}})}{\partial \dot{\mathbf{M}}} = 0. \quad (1.80)$$

Replacing equation (1.77) into the last equation, and recalling the definition of the effective field \mathbf{H}_{eff} , yields

$$\frac{d}{dt} \frac{\partial \mathcal{T}(\mathbf{M}, \dot{\mathbf{M}})}{\partial \dot{\mathbf{M}}} - \frac{\partial \mathcal{T}(\mathbf{M}, \dot{\mathbf{M}})}{\partial \mathbf{M}} + [-\mathbf{H}_{\text{eff}} + \eta \dot{\mathbf{M}}] = 0. \quad (1.81)$$

In the paper [27], Gilbert did not find explicitly the expression of \mathcal{T} , but he circumvented the problem by means of the following argument. When $\eta = 0$ the Landau-Lifshitz equation (1.75) must be obtained. The introduction of the damping simply adds an extra term to the effective field, so that we eventually get

$$\frac{\partial \mathbf{M}}{\partial t} = -\gamma_G \mathbf{M} \times \mathbf{H}_{\text{eff}} + \frac{\gamma_G \alpha_G}{M_S} \mathbf{M} \times \frac{\partial \mathbf{M}}{\partial t}, \quad (1.82)$$

where γ_G must be equal to γ_L if the damping is zero and we set $\eta = \alpha_G M_S$. The attempts of Gilbert to obtain an expression for \mathcal{T} required the introduction

of an inertial tensor with two of the three principal components equal to zero, and such object was considered not physically acceptable. Nonetheless this approach was reconsidered later by Wegrowe in [55] and it is illustrated in the section 4.3 of the thesis.

Although they are formally different, equation (1.76) and equation (1.82) describe exactly the same dynamic if the gyromagnetic ratio and the damping coefficient are appropriately adjusted. In order to see the equivalence of Landau-Lifshitz equation and Gilbert equation let us vector multiply equation (1.82) by \mathbf{M} , we have

$$\mathbf{M} \times \frac{\partial \mathbf{M}}{\partial t} = -\gamma_G \mathbf{M} \times (\mathbf{M} \times \mathbf{H}_{\text{eff}}) - \gamma_G \alpha_G M_S \frac{\partial \mathbf{M}}{\partial t}, \quad (1.83)$$

where we used

$$\frac{\partial \mathbf{M}}{\partial t} \cdot \mathbf{M} = 0 \quad \text{and} \quad \mathbf{M} \times \left(\mathbf{M} \times \frac{\partial \mathbf{M}}{\partial t} \right) = -M_S^2 \frac{\partial \mathbf{M}}{\partial t}. \quad (1.84)$$

By substituting the expression of $\mathbf{M} \times \frac{\partial \mathbf{M}}{\partial t}$ from (1.82) into (1.83), after some algebra, we have

$$\frac{\partial \mathbf{M}}{\partial t} = -\frac{\gamma_G}{1 + \gamma_G^2 \alpha_G^2} \mathbf{M} \times \mathbf{H}_{\text{eff}} + \gamma_G \frac{\gamma_G \alpha_G}{M_S (1 + \gamma_G^2 \alpha_G^2)} \mathbf{M} \times (\mathbf{M} \times \mathbf{H}_{\text{eff}}). \quad (1.85)$$

This equation is exactly the Landau-Lifshitz equation if we set

$$\gamma_L = \frac{\gamma_G}{1 + \gamma_G^2 \alpha_G^2} \quad \text{and} \quad \alpha_L = \gamma_G \alpha_G. \quad (1.86)$$

The opposite transformation is instead given by

$$\gamma_G = \gamma_L (1 + \alpha_L^2) \quad \text{and} \quad \alpha_G = \frac{\alpha_L}{\gamma_L (1 + \alpha_L^2)}. \quad (1.87)$$

It is worthy to remark that Gilbert equation has a Lyapunov structure [23] for a fixed applied field, i.e. there exists a function of the magnetization which always decreases in time. The Lyapunov function is the free energy G

$$\begin{aligned} \frac{dG}{dt} = & \int \left(\frac{\delta G}{\delta \mathbf{M}} \cdot \frac{\partial \mathbf{M}}{\partial t} + \frac{\delta G}{\delta \mathbf{H}_a} \cdot \frac{\partial \mathbf{H}_a}{\partial t} \right) dV_{\mathbf{x}} = \\ & - \int \mathbf{H}_{\text{eff}} \cdot \frac{\partial \mathbf{M}}{\partial t} dV_{\mathbf{x}} + \int \mathbf{M} \cdot \frac{\partial \mathbf{H}_a}{\partial t} dV_{\mathbf{x}}. \end{aligned} \quad (1.88)$$

Substituting the expression of the effective field from the Gilbert equation yields

$$\frac{dG}{dt} = - \int \alpha_G \left| \frac{\partial \mathbf{M}}{\partial t} \right|^2 dV_{\mathbf{x}} + \int \mathbf{M} \cdot \frac{\partial \mathbf{H}_a}{\partial t} dV_{\mathbf{x}}, \quad (1.89)$$

which proves the Lyapunov structure of the equation.

1.5.4 Normalized equation

For the analysis of magnetization dynamics, the use of normalized dimensionless equations is often preferred. Let us define

$$g = \frac{G}{\mu_0 M_S^2 V}, \quad \mathbf{m} = \frac{\mathbf{M}}{M_S}, \quad \mathbf{h}_a = \frac{\mathbf{H}_a}{M_S}, \quad \mathbf{h}_M = \frac{\mathbf{H}_M}{M_S}, \quad (1.90)$$

and introduce the dimensionless anisotropy function

$$f(\mathbf{m}) = \frac{1}{2K_1} f_{AN}(\mathbf{m}). \quad (1.91)$$

The normalized Gibbs-Landau free energy is then given by

$$g = \frac{1}{V} \int \left(\frac{\ell_{EX}^2}{2} (\nabla \mathbf{m})^2 + \kappa f(\mathbf{m}) + \frac{1}{2} \mathbf{h}_M \cdot \mathbf{m} + \mathbf{h}_a \cdot \mathbf{m} \right) dV_{\mathbf{x}}, \quad (1.92)$$

where we defined the exchange length ℓ_{EX} as

$$\ell_{EX} = \sqrt{\frac{2A}{\mu_0 M_S^2}}, \quad (1.93)$$

and the dimensionless parameter κ as

$$\kappa = \frac{2K_1}{\mu_0 M_S^2}. \quad (1.94)$$

The demagnetizing field satisfies the equations

$$\nabla \times \mathbf{h}_M = 0, \quad \nabla \cdot \mathbf{h}_M = -\nabla \cdot \mathbf{m}. \quad (1.95)$$

The effective field is now provided by the expression

$$\mathbf{h}_{\text{eff}} = \ell_{\text{ex}}^2 \nabla^2 \mathbf{m} - \kappa \frac{\partial f}{\partial \mathbf{m}} + \mathbf{h}_a + \mathbf{h}_M = \frac{\mathbf{H}_{\text{eff}}}{M_S} = -\frac{\delta g}{\delta \mathbf{m}}. \quad (1.96)$$

When the normalization is applied inside the Gilbert equation it gives

$$M_S \frac{\partial \mathbf{m}}{\partial t} = -\gamma_G M_S^2 \mathbf{m} \times \mathbf{h}_{\text{eff}} + \alpha_G \gamma_G M_S \mathbf{m} \times \frac{\partial \mathbf{m}}{\partial t}, \quad (1.97)$$

dividing by $\gamma_G M_S^2$ yields

$$\frac{1}{\gamma_G M_S} \frac{\partial \mathbf{m}}{\partial t} = -\mathbf{m} \times \mathbf{h}_{\text{eff}} + \frac{\alpha_G \gamma_G M_S}{\gamma_G M_S} \mathbf{m} \times \frac{\partial \mathbf{m}}{\partial t}. \quad (1.98)$$

We want to remove the coefficient of the time derivative and make time and damping constant adimensional. To this end we define a normalized time and the adimensional damping constant

$$\tau = \gamma_G M_S t, \quad \alpha = \alpha_G \gamma_G \quad (1.99)$$

and the Gilbert equation becomes

$$\frac{\partial \mathbf{m}}{\partial \tau} = -\mathbf{m} \times \mathbf{h}_{\text{eff}} + \alpha \mathbf{m} \times \frac{\partial \mathbf{m}}{\partial \tau}. \quad (1.100)$$

Typical values of the exchange length and normalized time are respectively 5-10 nm and 5 ps. In the following parts of the thesis the normalized time will be denoted with t instead of τ in order to keep the notation simple.

1.6 Spin Injection

Electrons exert a torque of quantum-mechanical origin when they flow across a ferromagnetic element, this torque is known as spin-transfer torque.

Spin-transfer effects are most often investigated in three-layer structures, also called spin valves, consisting of two ferromagnetic layers separated by a non-magnetic metallic spacer (see Fig. 1.10).

One layer, commonly known as the 'fixed' or the 'pinned' layer, is used as a polarizer for the electron spins, its magnetization is kept fixed by using a large volume or a large anisotropy or pinning by additional underlayers. The second layer, termed the 'free' layer, is the one where various dynamic phenomena occur.

It is worthy to remark that the thickness of the spacer plays a crucial role. The ferromagnetic coupling between the two magnetic layers is described by Rudermann Kittel Kasuya Yosida (RKKY) interaction [30], which gives a contribution to the free energy [31]

$$G_{RKKY} = S J_{RKKY}(x) \mathbf{M}_1 \cdot \mathbf{M}_2, \quad (1.101)$$

where \mathbf{m}_1 and \mathbf{m}_2 are the unit vector of the magnetization of the two magnetic layers, S is the surface of contact and x is the thickness of the spacer. A qualitative plot of $J_{RKKY}(x)$ is reported in figure 1.11. To avoid coupling between magnetic layers, the spacer thickness must be close to the zeros of the RKKY function.

Spin valve devices are used in many technologies. The most remarkable one

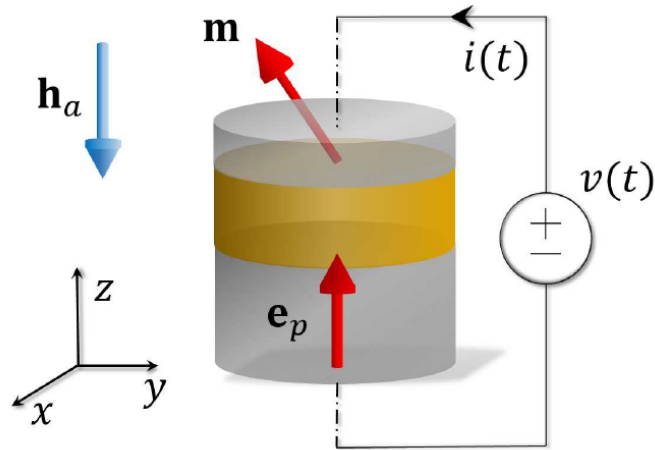


Figure 1.10: Structure of a spin valve device: the layers in grey are made of ferromagnetic material, the layer in yellow is nonmagnetic (it can either be an insulator or a conductor). When a current i is injected, the magnetization of the free layer (the one on the top) is altered by the spin transfer torque. The electrical resistance of the device depend on whether the magnetization of the free layer is parallel or antiparallel with the magnetization of the fixed layer (the one at the bottom).

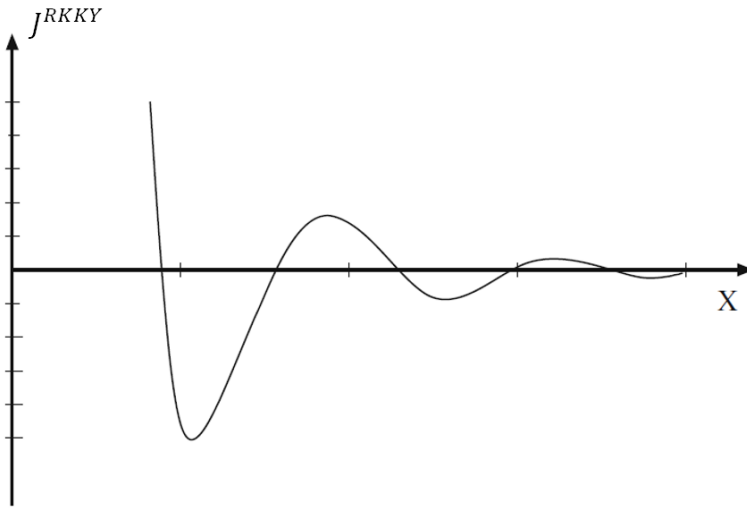


Figure 1.11: Qualitative plot of the RKKY interaction as function of the distance between the two ferromagnetic layers. Usually spin valve separators thickness are close to the zeros of J_{RKKY} , antiferromagnetic coupling can also be achieved by exploiting the fact that J_{RKKY} can be negative.

is the hard disk, where the spin valve devices are employed in the reading process thanks to the Gigantic Magneto Resistive (GMR) effect [29].

Other applications of the spin valves are Magnetic Random Access Memories (MRAM) - where current is used in the writing to switch the magnetization of the free layer - and the nano-oscillator - where DC current generates AC output signal tunable with the intensity of the current.

By applying a semiclassical approach to the analysis of spin transfer between the two ferromagnetic layers, Slonczewski [33] derived the following generalized LLG equation

$$\frac{d\mathbf{S}_2}{dt} = \mathbf{s}_2 \times \left(\gamma H_{AN}(\hat{\mathbf{e}}_x \cdot \mathbf{S}_2)\hat{\mathbf{e}}_x - \alpha \frac{d\mathbf{S}_2}{dt} - \frac{GJ_e}{q_e} \mathbf{s}_1 \times \mathbf{s}_2 \right), \quad (1.102)$$

where \mathbf{S}_1 and \mathbf{S}_2 are the global spin orientation per unit area in the fixed and free layers, \mathbf{s}_1 and \mathbf{s}_2 are the unit vectors along them, H_{AN} is the anisotropy field magnitude, $\hat{\mathbf{e}}_x$ identifies the direction of inplane anisotropy in the free layer, q_e is the absolute value of the electron charge, and J_e is the electric current density, taken as positive when the electrons flow from the free into the fixed layer. The quantity G is given by the expression

$$G = \left[-4 + (1 + P)^3 \frac{3 + \mathbf{s}_1 \cdot \mathbf{s}_2}{4P^{2/3}} \right]^{-1} \quad (1.103)$$

where P is the spin-polarizing factor of the incident current. Typical values in ferromagnetic metals are $P \approx 0.3 - 0.4$.

The total magnetic moment of the free layer is equal to $-\gamma\hbar\mathbf{S}_2A_s/\mu_0$, whereas its volume is equal to A_sd , where d is the free-layer thickness and A_s is the section.

Therefore: $\mathbf{M} = -\gamma\hbar\mathbf{S}_2/\mu_0d$ and $\mathbf{s}_2 = -\mathbf{m}_2$. The correct way to generalize Eq. (1.102) is to replace $H_{AN}(\hat{\mathbf{e}}_x \cdot \mathbf{s}_2)\hat{\mathbf{e}}_x$ with $\mathbf{H}_{\text{eff}} = \mathbf{H}_a + \mathbf{H}_{AN} + \mathbf{H}_M$

$$\frac{d\mathbf{m}}{dt} = -\gamma M_S \left(\mathbf{h}_{\text{eff}} - \frac{\alpha}{\gamma M_S} \frac{d\mathbf{m}}{dt} \frac{J_e G}{J_p} \hat{\mathbf{e}}_p \times \mathbf{m} \right) \quad (1.104)$$

where $\hat{\mathbf{e}}_p = -\mathbf{s}_1$ and $J_p = \mu_0 M_S^2 \frac{q_e d}{\hbar}$. In terms of normalized time equation (1.104) becomes

$$\frac{d\mathbf{m}}{dt} - \alpha \frac{d\mathbf{m}}{dt} = -\mathbf{m} \times \mathbf{h}_{\text{eff}} + \beta \frac{\mathbf{m} \times (\mathbf{m} \times \hat{\mathbf{e}}_p)}{1 + c_p \mathbf{m} \cdot \hat{\mathbf{e}}_p}, \quad (1.105)$$

where

$$\beta = b_p \frac{J_e}{J_p}, \quad b_p = \frac{4P^{3/2}}{3(1+P)^3 - 16P^{2/3}}, \quad c_p = \frac{(1+P)^3}{3(1+P)^3 - 16P^{2/3}}.$$

In equation (1.104) it is possible to separate the conservative part of the dynamics by using a Helmholtz decomposition. In such a case the equation is reformulated as

$$\frac{d\mathbf{m}}{dt} = \mathbf{m} \times \frac{\partial g}{\partial \mathbf{m}} + \alpha \mathbf{m} \times \left(\mathbf{m} \times \frac{\partial \Phi}{\partial \mathbf{m}} \right), \quad (1.106)$$

where g is the normalized Gibbs-Landau free energy and

$$\Phi = g + \frac{\beta}{\alpha} \frac{\log(1 + c_p \mathbf{m} \cdot \hat{\mathbf{e}}_p)}{c_p}. \quad (1.107)$$

Chapter 2

Magnetization Dynamics in Nanosystems

In this section the magnetization dynamics in nanosystems is analyzed. When the system considered is sufficiently small, such as the case of nanomagnets, exchange energy becomes the prevalent energy and all nonuniform configurations are strongly penalized. The typical assumption for nanosystems is to consider uniform magnetization. Gilbert equation for nanosystems reads

$$\frac{d\mathbf{m}}{d\tau} = -\mathbf{m} \times \mathbf{h}_{\text{eff}} + \alpha \mathbf{m} \times \frac{d\mathbf{m}}{d\tau} . \quad (2.1)$$

Despite its simplicity, uniform magnetized systems have static hysteresis and, when subject to a time dependent magnetic field, they may exhibit complex magnetization dynamics, including quasiperiodic motion and chaos.

The exchange energy is no longer present and the effective magnetic field is now given by

$$\mathbf{h}_{\text{eff}} = -\kappa \frac{\partial f}{\partial \mathbf{m}} + \mathbf{h}_M + \mathbf{h}_a . \quad (2.2)$$

The demagnetizing magnetic field \mathbf{h}_M generally is a function of space, nonetheless only its mean value affects either the energy or the dynamics and we can safely use the replacement

$$\mathbf{h}_M \rightarrow \int \mathbf{h}_M(\mathbf{x}) dv .$$

Since the relationship between magnetization and demagnetizing field is linear, it is represented by a 3×3 matrix

$$\mathbf{h}_M = -N\mathbf{m} . \quad (2.3)$$

A special case is given by the ellipsoidal particle because the demagnetizing field is exactly constant [18], [19] inside the particle and no substitution with the average field is needed.

Finally we assume that anisotropy is uniaxial and, if not specified otherwise, f is

$$f = -\frac{1}{2}(\mathbf{m} \cdot \hat{\mathbf{e}}_{AN})^2 \implies \frac{\delta f}{\delta \mathbf{m}} = \hat{\mathbf{e}}_{AN} [\mathbf{m} \cdot \hat{\mathbf{e}}_{AN}]. \quad (2.4)$$

The effective field due to anisotropy and demagnetizing field can be combined in a single matrix. Since both contributions are represented by symmetric matrices, there exist a reference frame where the resulting matrix D is diagonal

$$\mathbf{h}_{\text{eff}} = -D\mathbf{m} + \mathbf{h}_a \quad (2.5)$$

where $D = N - \kappa \hat{\mathbf{e}}_{AN} \otimes \hat{\mathbf{e}}_{AN}$.

2.1 Stoner-Wohlfarth Asteroid

Stoner Wohlfarth model applies to spheroidal particles with rotational symmetry. Let us consider a nanomagnet with symmetry axis and anisotropy axis both aligned with the z axis, this implies $D_x = D_y = D_\perp$.

By using $|\mathbf{m}| = 1$, the free energy can be recasted as

$$g = \frac{1}{2}D_z + \frac{1}{2}\kappa_{\text{eff}}\sin^2\theta - h_{az}\cos\theta - h_{a\perp}\sin\theta \quad (2.6)$$

where $\kappa_{\text{eff}} = D_z - D_\perp$ and θ is the angle with the z axis as in figure 1.6.

The equilibria can be found by setting to zero the derivative of the free energy

$$\begin{aligned} \frac{dg}{d\theta} &= \kappa_{\text{eff}}\sin\theta\cos\theta + h_{az}\sin\theta - h_{a\perp}\cos\theta = 0 \\ &\implies \frac{h_{a\perp}}{\sin\theta_0} - \frac{h_{az}}{\cos\theta} = \kappa_{\text{eff}}. \end{aligned} \quad (2.7)$$

Equation (2.7) can be recasted in a polynomial form as

$$h_{a\perp}^2 m_z^2 = (h_{az} + \kappa_{\text{eff}} m_z)^2 (1 - m_z^2). \quad (2.8)$$

This equation has two or four real solutions depending of the values on the parameters h_{az} and $h_{a\perp}$.

Qualitatively speaking, for small values of the applied field the anisotropy energy prevails and the free energy has four extrema, when instead large fields

are applied the Zeeman energy prevails and only two extrema are present. A more systematic study can be carried out by computing the second derivative of the free energy,

$$\frac{d^2 g}{d\theta^2} = \frac{\kappa_{\text{eff}} \cos^3 \theta + h_{az}}{\cos \theta} = \frac{h_{a\perp} - \kappa_{\text{eff}} \sin^3 \theta}{\sin \theta}. \quad (2.9)$$

The boundary between the region with four equilibria and the region with two equilibria is a bifurcation line which can be found by searching equilibria with $\frac{d^2 g}{d\theta^2} = 0$. These points correspond to a critical condition when equilibrium disappears.

This condition yields the parametric representation of the bifurcation line which is referred to as the Stoner-Wolffarth asteroid

$$\begin{cases} h_{az} = -\kappa_{\text{eff}} \cos^3 \theta, \\ h_{a\perp} = \kappa_{\text{eff}} \sin^3 \theta, \end{cases} \quad (2.10)$$

which can be expressed in implicit form by the following equation

$$h_{az}^{\frac{2}{3}} + h_{a\perp}^{\frac{2}{3}} = \kappa_{\text{eff}}^{\frac{2}{3}}. \quad (2.11)$$

The Stoner Wolffarth asteroid is shown in figure 2.1.

From the Stoner Wolffarth asteroid the admissible directions of magnetization equilibria can be identified: given an assigned value of θ , (2.7) is linear in h_{az} and $h_{a\perp}$, hence equilibria with angle θ are represented by a line in the plane $h_{a\perp}$ - h_{az} with angular coefficient $\tan \theta$.

It is easy to check that this line is tangent to the asteroid at the point given by the chosen θ

$$\frac{dh_{a\perp}}{dh_{az}} = \tan \theta. \quad (2.12)$$

This geometrical property suggests the following construction: given a point in the control plane $h_{a\perp}$ - h_{az} , we can draw the lines tangent to the asteroid emanating from this point as illustrated in figure 2.2. Tangent lines to the upper half of the asteroid correspond to magnetization pointing upward, tangent lines to the lower half correspond to magnetization pointing downward.

Figure 2.2 shows that only two tangent lines can be drawn from points external to the asteroids, while four tangent lines can be drawn from points inside it. Stability can be determine using equation (2.9).

The asteroid properties are the bases for the analysis of the magnetization process taking place when the applied field is slowly varied over time. This variation occurs on a time scale much larger than the time scale needed by the

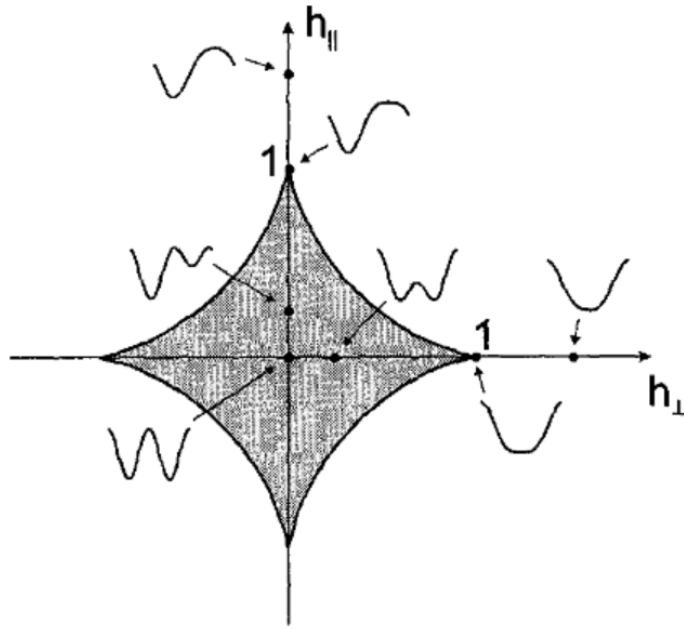


Figure 2.1: Asteroid figure generated by equation (2.11), the grey area corresponds to the values of the field for which there are two minima.

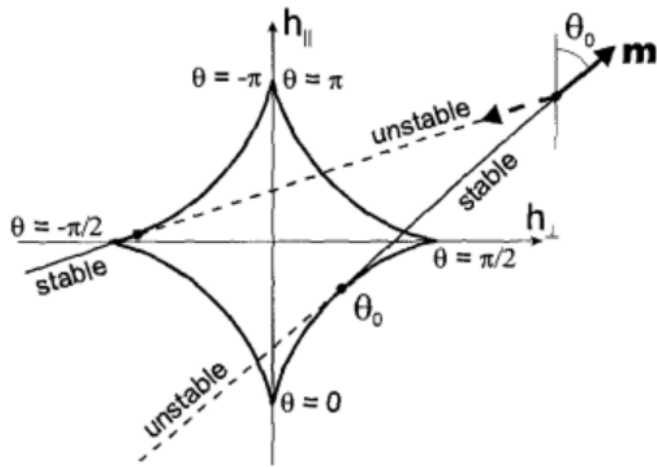


Figure 2.2: Graphical construction of the magnetization for a given applied field.

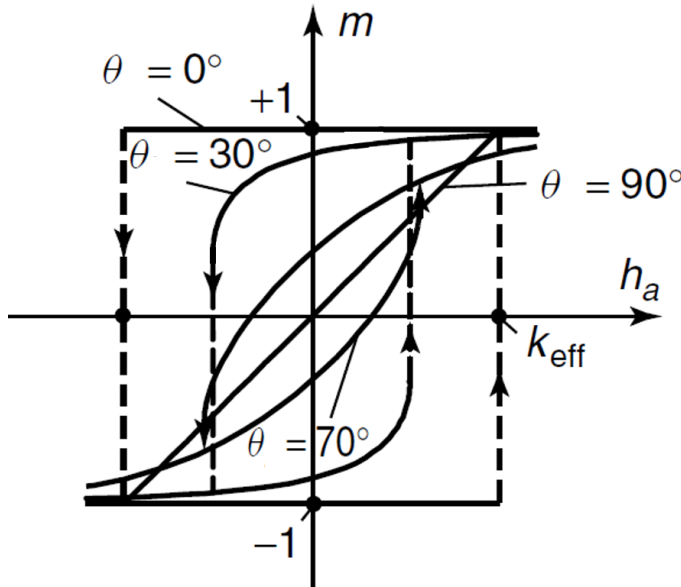


Figure 2.3: Hysteresis loops obtained with the Stoner-Wolfarth model. Different loops are computed for different orientations of the applied field.

transient to let magnetization relax to a stable equilibrium state. This condition corresponds to a static hysteresis process.

Let us consider the case when \mathbf{h}_a oscillates between opposite values along a fixed direction. If the field oscillations are contained inside the asteroid the magnetization oscillates reversibly. If instead the \mathbf{h} crosses the asteroid, the state may lose stability when the field point exits from the asteroid and the magnetization discontinuously jumps to a new equilibrium; these jumps are called Barkhausen jumps. A graphic construction of hysteresis loops is shown in figure 2.3.

2.2 Conservative Dynamics

In many ferromagnetic materials the damping constant α is quite small. This means that, on a relatively short time scale, the magnetization dynamics is expected to be very close to the undamped dynamics.

This suggests that a first fundamental step is analyzing the conservative mag-

netization dynamics, which can be analytically studied by using the techniques developed in this section.

Moreover, due to the smallness of α , the actual dissipative dynamics can be treated as a perturbation of the conservative dynamics. Let us consider the Landau-Lifshitz equation for a uniformly magnetized body without damping, i.e.

$$\frac{d\mathbf{m}}{dt} = -\mathbf{m} \times \mathbf{h}_{\text{eff}} . \quad (2.13)$$

It turns out that (2.13) represents an Hamiltonian system, where G is an integral of motion. Although the most common definition of an Hamiltonian system requires the number of variables to be even, it is possible to define an Hamiltonian system by defining a Poisson bracket, i.e. a binary operation that satisfies

$$\begin{aligned} [f, h] &= -[h, f], & [f, vh] &= [f, v]h + v[f, h] \quad \text{and} \\ [[f, v], h] &+ [[v, h], f] + [[h, f], v] &= 0 . \end{aligned} \quad (2.14)$$

In the system considered the Poisson bracket is given by

$$[f, h] = \mathbf{m} \times \left(\frac{\partial f}{\partial \mathbf{m}} \times \frac{\partial h}{\partial \mathbf{m}} \right) , \quad (2.15)$$

and the time derivative of any scalar quantity f , including the magnetization components, is obtained as

$$\frac{df}{dt} = [g, f] . \quad (2.16)$$

For $f = m_i$, (2.16) gives the Landau-Lifshitz equation.

We now focus on the derivation of the analytical solution of the conservative dynamics. Let us consider an ellipsoidal particle with uniaxial anisotropy, the effective field is

$$\mathbf{h}_{\text{eff}} = -N\mathbf{m} + \kappa(\mathbf{m} \cdot \hat{\mathbf{e}}_{AN})\hat{\mathbf{e}}_{AN} + \mathbf{h}_a . \quad (2.17)$$

We can merge together the contributions of the media anisotropy and the shape anisotropy and rewrite the effective field as

$$\mathbf{h}_{\text{eff}} = -D\mathbf{m} + \mathbf{h}_a , \quad (2.18)$$

where D is a symmetric matrix and hence it is diagonal in some reference frame.

We choose the reference frame such that D is diagonal with $D_x \leq D_y \leq D_z$ and we further assume that $H_z = 0$. The free energy is given by

$$g = \frac{1}{2}(D_x m_x^2 + D_y m_y^2 + D_z m_z^2) - m_x h_x - m_y h_y . \quad (2.19)$$

If we substitute $m_z^2 = 1 - m_x^2 - m_y^2$ and multiply equation (2.19) by 2, after some algebra, we get

$$(m_x - a_x)^2 + k(m_y - a_y) = p , \quad (2.20)$$

where

$$\begin{aligned} a_x &= -\frac{h_x}{D_z - D_x} , & a_y &= -\frac{h_y}{D_z - D_y} , \\ k^2 &= \frac{D_z - D_y}{D_z - D_x} , & p^2 &= a_x^2 + k^2 a_y^2 + \frac{D_z - 2g}{D_z - D_x} . \end{aligned} \quad (2.21)$$

Trajectories are given in the m_x - m_y plane by ellipses centered in (a_x, a_y) . This can produce four different topologies illustrated in figure 2.4. In order to have the time dependence of the magnetization, we consider the following parametrization

$$m_x = a_x - p \cos u , \quad m_y = a_y - \frac{p}{k} \sin u . \quad (2.22)$$

Consequently it holds

$$m_z = \sqrt{1 - (a_x - p \cos u)^2 - \left(a_y - \frac{p}{k} \sin u\right)^2} , \quad (2.23)$$

and the equation governing the dynamics are

$$\frac{dm_x}{d\tau} = (D_z - D_y)m_z(m_y - a_y) , \quad (2.24)$$

$$\frac{dm_y}{d\tau} = -(D_z - D_x)m_z(m_x - a_x) , \quad (2.25)$$

$$\frac{dm_z}{d\tau} = (D_z - D_x)m_y(m_x - a_x) - (D_z - D_y)m_x(m_y - a_y) . \quad (2.26)$$

By substituting the parametrization (2.22) into equation (2.25) we get

$$\int \frac{du}{\sqrt{1 - (a_x - p \cos u)^2 - \left(a_y - \frac{p}{k} \sin u\right)^2}} = \int k(D_z - D_x)dt . \quad (2.27)$$

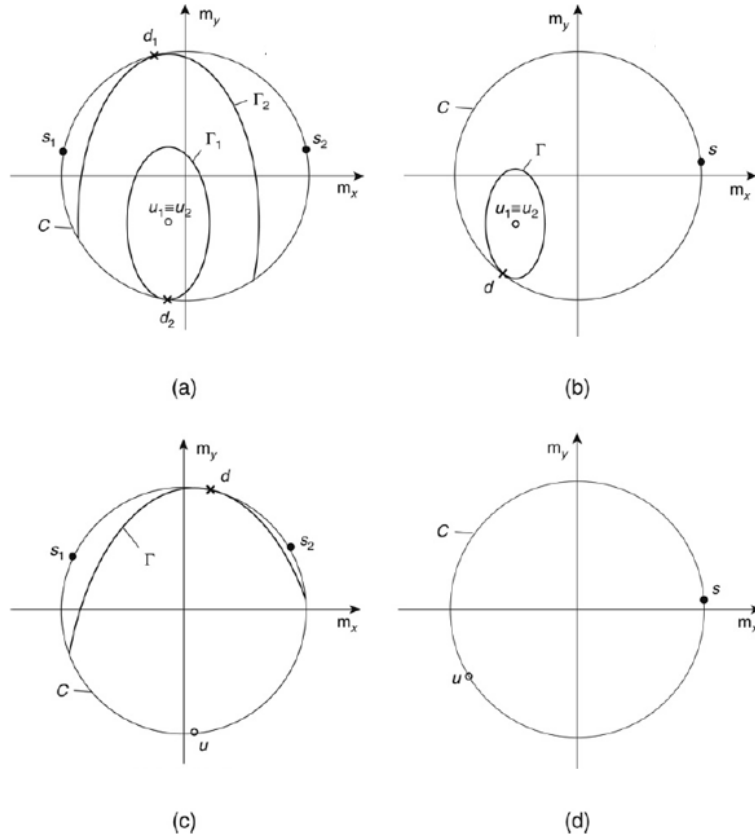


Figure 2.4: Different topologies for the conservative dynamics: (a) two ellipses are tangent to the unit sphere, there are two stable equilibria (s_1 and s_2), two unstable equilibria (u_1 and u_2) and two saddles (d_1 and d_2); (b) two ellipses are tangent to the unit circle, one of them does not enter in the circle, there are two unstable equilibria (u_1 and u_2), one saddle (d) and a stable equilibrium (s); (c) the center of the ellipses is outside the circle, one ellipse is tangent to the unit circle, there are two stable equilibria (s_1 and s_2), one saddle (d) and one unstable equilibrium (u); (d) there is only one ellipse tangent to the unit circle and it is entirely outside the circle, there is one stable point (s) and one unstable equilibrium (u).

On the left hand side of equation (2.27) there is an elliptic integral. Let us take $a_x = a_y = 0$, by using the substitution $w = \sin u$ equation (2.27) becomes

$$\int \frac{dw}{\sqrt{(1-w^2)(1-k_H^2 w^2)}} = \int \Omega_H dt, \quad (2.28)$$

where

$$k_H = \frac{p}{k} \frac{\sqrt{1-k^2}}{\sqrt{1-p^2}}, \quad \Omega_H = k\sqrt{1-p^2}(D_z - D_x). \quad (2.29)$$

The analytical solution in the high energy region is

$$m_x = \mp p \operatorname{cn}(\Omega_H t, k_H), \quad (2.30)$$

$$m_y = \frac{p}{k} \operatorname{sn}(\Omega_H t, k_H), \quad (2.31)$$

$$m_z = \pm \sqrt{1-p^2} \operatorname{dn}(\Omega_H t, k_H), \quad (2.32)$$

where cn , sn and dn are Jacobi elliptic functions [21]. With a similar derivation, the following solutions are obtained for the low energy region

$$m_x = \mp p \operatorname{dn}(\Omega_L t, k_L), \quad (2.33)$$

$$m_y = \frac{\sqrt{1-p^2}}{\sqrt{1-k^2}} \operatorname{sn}(\Omega_L t, k_L), \quad (2.34)$$

$$m_z = \pm \sqrt{1-p^2} \operatorname{cn}(\Omega_L t, k_L). \quad (2.35)$$

with

$$k_L = \frac{k}{p} \frac{\sqrt{1-p^2}}{\sqrt{1-k^2}}, \quad \Omega_L = k_H \Omega_H. \quad (2.36)$$

The trajectories are illustrated in figure 2.5.

2.3 Ferromagnetic Resonance: Kittel Frequency

Let us consider a uniformly magnetized body with the effective field given by (2.18) and the applied field aligned with the z -axis. If $D_z - h_a < D_y, D_z$ the system has a stable equilibrium for $\mathbf{m} = \hat{\mathbf{e}}_z$.

In the present section the behavior of the system for small perturbations around

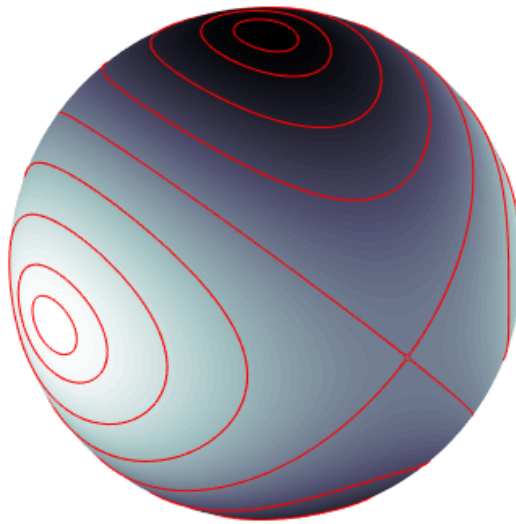


Figure 2.5: Trajectories of the conservative Landau-Lifshitz-Gilbert equation with anisotropy and no applied field.

the stable equilibrium point is analyzed. To this end we consider the applied field

$$\mathbf{h}_a = h_{DC}\hat{\mathbf{e}}_z + h_{AC}(\hat{\mathbf{e}}_x \cos \omega t + \hat{\mathbf{e}}_y \sin \omega t) \quad (2.37)$$

with $h_{AC} \ll h_{DC}$, and we write the magnetization as

$$\mathbf{m} = \hat{\mathbf{e}}_z + \delta m_x \hat{\mathbf{e}}_x + \delta m_y \hat{\mathbf{e}}_y \quad (2.38)$$

where $\delta m_x, \delta m_y \ll 1$.

By substituting (2.38) into the Gilbert equation and neglecting all the higher powers of the perturbative terms we have

$$\begin{aligned} \frac{d}{dt}\delta m_x &= -\delta m_y h_{\text{eff},z} + h_{\text{eff},y} - \alpha \frac{d}{dt}\delta m_y, \\ \frac{d}{dt}\delta m_y &= -h_{\text{eff},x} + \delta m_x h_{\text{eff},z} + \alpha \frac{d}{dt}\delta m_x. \end{aligned} \quad (2.39)$$

Replacing the expression of the effective field yields

$$\begin{aligned} \frac{d}{dt}\delta m_x + \alpha \frac{d}{dt}\delta m_y &= -(h_{DC} - D_z + D_y)\delta m_y + h_{AC} \sin \omega t, \\ \frac{d}{dt}\delta m_y - \alpha \frac{d}{dt}\delta m_x &= (h_{DC} - D_z + D_x)\delta m_x - h_{AC} \cos \omega t. \end{aligned} \quad (2.40)$$

This system of equations can be easily solved using the phasors method. In matrix form it reads

$$\begin{bmatrix} i\omega & i\alpha\omega + h_{DC} - D_z + D_y \\ -i\alpha\omega - h_{DC} + D_z - D_x & i\omega \end{bmatrix} \begin{bmatrix} \overline{\delta m_x} \\ \overline{\delta m_y} \end{bmatrix} = -h_{AC} \begin{bmatrix} i \\ 1 \end{bmatrix}. \quad (2.41)$$

Natural frequencies of the system are given by the zeros of the determinant of the matrix on the left hand side, hence we have

$$\begin{aligned} \omega^2(1 + \alpha^2) - i\alpha\omega(2h_{DC} - 2D_z + D_x + D_y) \\ - (h_{DC} - D_z + D_x)(h_{DC} - D_z + D_y) = 0. \end{aligned} \quad (2.42)$$

If the damping is negligible we obtain the Kittel frequency [39]

$$\omega = \sqrt{(h_{DC} - D_z + D_x)(h_{DC} - D_z + D_y)}. \quad (2.43)$$

2.4 Bifurcation map for axially symmetric system

When damping is present, there is no general analytical solution for magnetization dynamics, although solutions may exist for specific cases [45]. However it is possible to sketch the qualitative features of the trajectories using tools of nonlinear dynamics. Let us consider a magnetic particle with axial symmetry, i.e. $D_x = D_y = D_\perp$, the effective field is

$$\mathbf{h}_{\text{eff}} = -D_\perp m_x \hat{\mathbf{e}}_x - D_\perp m_y \hat{\mathbf{e}}_y - D_z m_z \hat{\mathbf{e}}_z + \mathbf{h}_a . \quad (2.44)$$

We can sum $D_\perp \mathbf{m}$ to the effective field without modifying the dynamics, so that the effective field becomes

$$\mathbf{h}_{\text{eff}} = \kappa_{\text{eff}} m_z \hat{\mathbf{e}}_z + \mathbf{h}_a , \quad (2.45)$$

with $\kappa_{\text{eff}} = D_\perp - D_z$. Moreover we consider as applied magnetic field

$$\mathbf{h}_a = h_{DC} \hat{\mathbf{e}}_z + h_{AC} (\hat{\mathbf{e}}_x \cos \omega t + \hat{\mathbf{e}}_y \sin \omega t) , \quad (2.46)$$

and an injected current polarized along the z axis with $c_p = 0$, so that Gilbert equation reads

$$\begin{aligned} \frac{d\mathbf{m}}{dt} - \alpha \mathbf{m} \times \frac{d\mathbf{m}}{dt} = \\ - \mathbf{m} \times ((h_{DC} + \kappa_{\text{eff}} m_z) \hat{\mathbf{e}}_z + h_{AC} \cos(\omega t) \hat{\mathbf{e}}_x + h_{AC} \sin(\omega t) \hat{\mathbf{e}}_y - \beta \mathbf{m} \times \hat{\mathbf{e}}_z) . \end{aligned} \quad (2.47)$$

Explicit time dependence in equation (2.46) makes the system non-autonomous, hence standard tools of bifurcation theory for a 2D system cannot be applied.

Time dependence can be removed by an appropriate change in the reference frame

$$\begin{aligned} \hat{\mathbf{e}}_{x'} &= \cos \omega t \hat{\mathbf{e}}_x + \sin \omega t \hat{\mathbf{e}}_y , \\ \hat{\mathbf{e}}_{y'} &= -\sin \omega t \hat{\mathbf{e}}_x + \cos \omega t \hat{\mathbf{e}}_y . \end{aligned} \quad (2.48)$$

In the new rotating reference frame the applied field is

$$\mathbf{h}_a = h_{DC} \hat{\mathbf{e}}_z + h_{AC} \hat{\mathbf{e}}_{x'} , \quad (2.49)$$

while the derivative of the magnetization becomes

$$\left[\frac{d\mathbf{m}}{dt} \right]_{\text{lab.frame}} = \left[\frac{d\mathbf{m}}{dt} \right]_{\text{rot.frame}} - \omega \mathbf{m} \times \hat{\mathbf{e}}_z , \quad (2.50)$$

so that Gilbert equation turns into

$$\begin{aligned} \frac{d\mathbf{m}}{dt} - \alpha \mathbf{m} \times \frac{d\mathbf{m}}{dt} = \\ - \mathbf{m} \times ((h_{DC} + \kappa_{\text{eff}} m_z - \omega) \hat{\mathbf{e}}_z + h_{AC} \hat{\mathbf{e}}_{x'} + (\alpha\omega - \beta) \mathbf{m} \times \hat{\mathbf{e}}_z) . \end{aligned} \quad (2.51)$$

In equation (2.51) the effect of β can be included in the other terms by redefining

$$\omega' = \omega - \frac{\beta}{\alpha} \quad \text{and} \quad h'_{DC} = h_{DC} + \frac{\beta}{\alpha} . \quad (2.52)$$

We eventually have

$$\begin{aligned} \frac{d\mathbf{m}}{dt} - \alpha \mathbf{m} \times \frac{d\mathbf{m}}{dt} = \\ - \mathbf{m} \times ((h'_{DC} + \kappa_{\text{eff}} m_z - \omega) \hat{\mathbf{e}}_z + h_{AC} \hat{\mathbf{e}}_{x'} + \alpha\omega' \mathbf{m} \times \hat{\mathbf{e}}_z) . \end{aligned} \quad (2.53)$$

It is convenient to rewrite equation (2.53) in polar coordinates

$$\frac{d\theta}{dt} - \alpha \sin \theta \frac{d\phi}{dt} = h_{AC} \sin \phi - \alpha\omega' \sin \theta , \quad (2.54)$$

$$\alpha \frac{d\theta}{dt} + \sin \theta \frac{d\phi}{dt} = h_{AC} \cos \phi \cos \theta - (h'_{DC} - \omega' + \kappa_{\text{eff}} \cos \theta) \sin \theta . \quad (2.55)$$

Equilibrium conditions are obtained by setting all time derivatives to zero

$$h_{AC} \sin \phi_0 = \alpha\omega' \sin \theta_0 , \quad (2.56)$$

$$h_{AC} \cos \phi_0 \cos \theta_0 = (h'_{DC} - \omega' + \kappa_{\text{eff}} \cos \theta_0) \sin \theta_0 . \quad (2.57)$$

Let us define the variable

$$\nu_0 = \alpha\omega' \cot \phi_0 . \quad (2.58)$$

Equilibrium equations (2.56) and (2.57) are conveniently reformulated as

$$\nu_0 = \frac{h'_{DC} - \omega'}{\cos \theta_0} + \kappa_{\text{eff}} , \quad \nu_0^2 = \frac{h_{AC}^2}{\sin^2 \theta_0} - \alpha^2 \omega'^2 . \quad (2.59)$$

It turns out that equations (2.59) can have two or four solutions, hence no information about the type of equilibrium is available from it. In order to determine stability of the equilibrium we have to consider the linearization of (2.53) in an equilibrium. To this purpose we define the unit vectors

$$\hat{\mathbf{e}}_1 = \frac{(\hat{\mathbf{e}}_z \times \mathbf{m}_0) \times \mathbf{m}_0}{|(\hat{\mathbf{e}}_z \times \mathbf{m}_0) \times \mathbf{m}_0|} , \quad \hat{\mathbf{e}}_2 = \frac{\hat{\mathbf{e}}_z \times \mathbf{m}_0}{|\hat{\mathbf{e}}_z \times \mathbf{m}_0|} . \quad (2.60)$$

Let δm_1 and δm_2 be the projections of $\delta \mathbf{m} = \mathbf{m} - \mathbf{m}_0$ on the unit vectors just defined, the linearized system is given by

$$\frac{d}{dt} \begin{bmatrix} \delta m_1 \\ \delta m_2 \end{bmatrix} = A \begin{bmatrix} \delta m_1 \\ \delta m_2 \end{bmatrix}, \quad (2.61)$$

where

$$A = \frac{1}{1 + \alpha^2} \begin{bmatrix} 1 & -\alpha \\ \alpha & 1 \end{bmatrix} \begin{bmatrix} -\alpha\omega' \cos \theta_0 & -\nu_0 \\ \nu_0 - \kappa_{\text{eff}} \sin^2 \theta_0 & -\alpha\omega' \cos \theta_0 \end{bmatrix}. \quad (2.62)$$

Eigenvalues of A establish the type of equilibrium: eigenvalues with negative real part correspond to stable modes converging to the equilibrium, while eigenvalues with positive real part correspond to unstable modes escaping from the equilibrium.

Since the matrix dimension is two all the information about stability can be obtained by the determinant and the trace, which are respectively the product and the sum of the eigenvalues.

Determinant and trace of A are given by

$$\det(A) = \frac{1}{1 + \alpha^2} (\nu_0^2 - \kappa_{\text{eff}} \sin^2 \theta_0 \nu_0 + \alpha^2 \omega'^2 \cos^2 \theta_0) \quad (2.63)$$

and

$$\text{tr}(A) = \frac{-2\alpha}{1 + \alpha^2} \left(\nu_0 - \frac{\kappa_{\text{eff}} \sin^2 \theta_0}{2} + \omega' \cos \theta_0 \right). \quad (2.64)$$

If the determinant is negative the equilibrium point is a saddle. If instead the determinant is positive, then the equilibrium is stable for negative trace and unstable for positive trace.

Rather than checking directly the sign of trace and determinant in every equilibrium condition, one can efficiently map the types and the number of equilibrium points by analyzing when the trace or the determinant become zero. Whenever one or more eigenvalues change the sign of their real part the system has a qualitative change of its phase portrait, such event are called bifurcations (Appendix C).

Let us consider the trace first. When the trace becomes zero a Hopf bifurcation takes place and a limit cycle collides with an equilibrium point and changes its stability, as sketched in figure 2.6.

Substituting the first expression of (2.59) into (2.64) yields

$$\omega_{\text{Hopf}} = \frac{\kappa_{\text{eff}} \cos \theta_0 (1 + \cos^2 \theta_0) + 2h'_{DC}}{2 \sin^2 \theta_0} + \frac{\beta}{\alpha}. \quad (2.65)$$

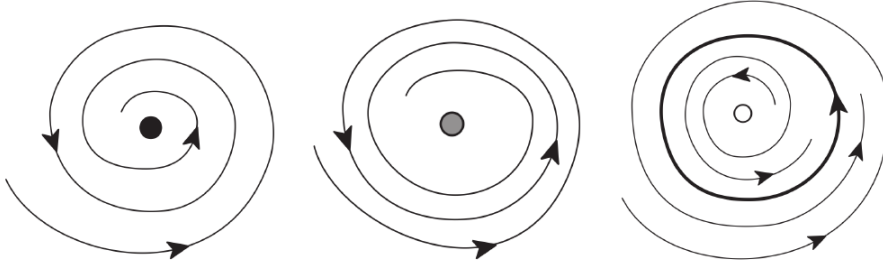


Figure 2.6: Qualitative representation of a Hopf bifurcation: on the left a stable focus, in the middle the focus eigenvalues cross the real axis, on the right a limit cycle appears and the focus becomes unstable

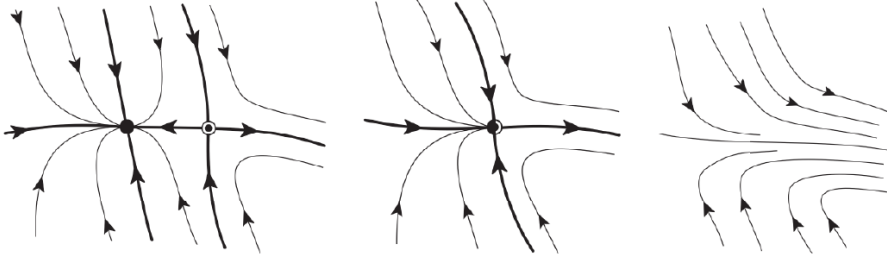


Figure 2.7: Qualitative representation of a saddle node bifurcation: on the left a stable node and a saddle, in the middle the two equilibria collide and they become a semistable node, on the right, after the bifurcation, there are no equilibria

By choosing a value for θ_0 we obtain the angular frequency ω_{Hopf} . The value of h_{AC} can then be obtained by using the second equation of (2.59): After some algebra it yields

$$h_{AC,\text{Hopf}} = \sin \theta_0 \sqrt{\nu_0^2 + \alpha^2 (\omega_{\text{Hopf}} - \beta/\alpha)^2}. \quad (2.66)$$

The same exact procedure can be applied to find the zeros of the determinant (2.63). In this case we are looking for saddle node bifurcations, where a couple of equilibria with different stability collide and disappear, as sketched in figure 2.7.

Angular frequency as a function of θ_0 reads

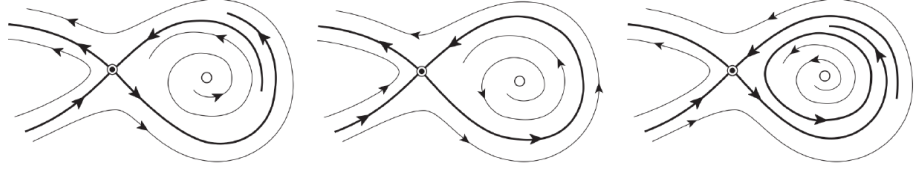


Figure 2.8: Qualitative representation of a homoclinic bifurcation: on the left a trajectory pointing to the saddle starts from the unstable focus; in the middle a trajectory pointing to the saddle matches exactly a trajectory starting from the saddle and a closed trajectory is generated; on the right the closed trajectory leaves the saddle and surrounds the unstable focus.

$$\omega_{\text{SaddleNode}} = \frac{-B \pm \sqrt{B^2 - 4AC}}{2A} + \frac{\beta}{\alpha}, \quad (2.67)$$

with

$$\begin{aligned} A &= 1 + \alpha^2 \cos^4 \theta_0, & B &= -(2h'_{DC} + \kappa_{\text{eff}} \cos \theta_0 (1 + \cos^2 \theta_0)), \\ C &= h'^2_{DC} + h'_{DC} \kappa_{\text{eff}} \cos \theta_0 (1 + \cos^2 \theta_0) + \kappa_{\text{eff}}^2 \cos^4 \theta_0, \end{aligned} \quad (2.68)$$

and the applied field is given by

$$h_{AC, \text{SaddleNode}} = \sin \theta_0 \sqrt{\nu_0^2 + \alpha^2 (\omega_{\text{SaddleNode}} - \beta/\alpha)^2}. \quad (2.69)$$

By sweeping θ_0 one can obtain the bifurcation curves through (2.65), (2.66), (2.67) and (2.69). An example of bifurcation map is in figure 2.9.

There is a third type of bifurcations which can modify the topology of the analyzed system, they are the homoclinic bifurcations.

This type of bifurcations occurs when a trajectory starting from a saddle ends on the saddle itself, this generates a limit cycle as sketched in figure 2.8. Unlike the other bifurcations, this type is not local and it is not detectable from the linearized system. For this reason homoclinic bifurcations have been analyzed using numerical methods [38] to integrate Gilbert equation.

A complete map of bifurcations is shown in figure 2.10. Each area is marked by a letter and the topology of the trajectories is shown in figures 2.11.

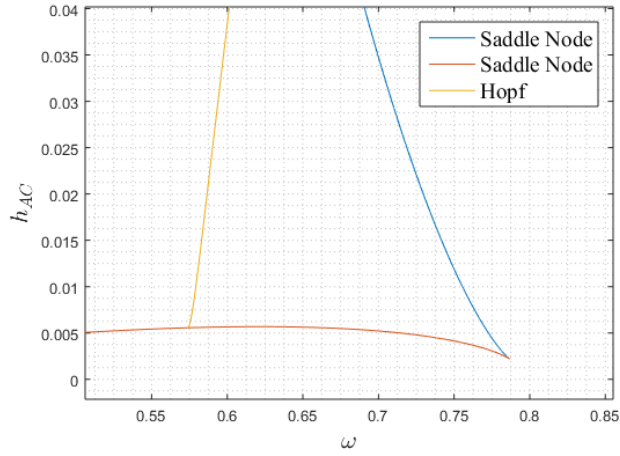


Figure 2.9: A bifurcation diagram for a system with the following parameters: $\alpha = 0.01$, $\kappa_{\text{eff}} = 0.3$, $h_{DC} = 0.5$, $\beta = 0$. Only local bifurcations are shown here.

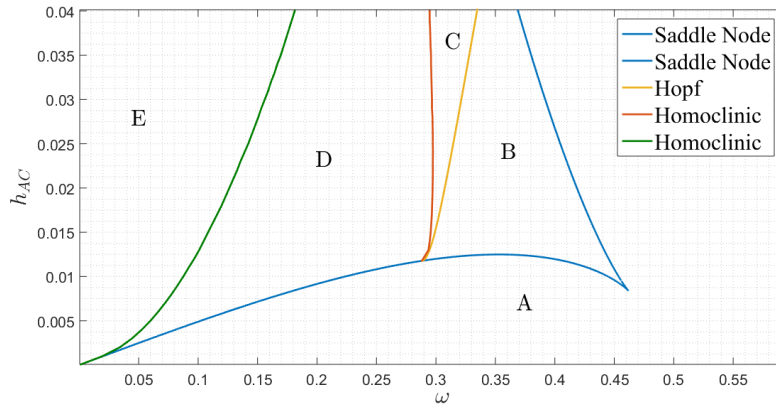


Figure 2.10: A bifurcation map of a system with the following parameters: $\alpha = 0.05$, $\kappa_{\text{eff}} = 0.5$, $h_{DC} = 0$, $\beta = 0$. Five different areas are labeled, the topological configuration of each area is illustrated in figure 2.11.

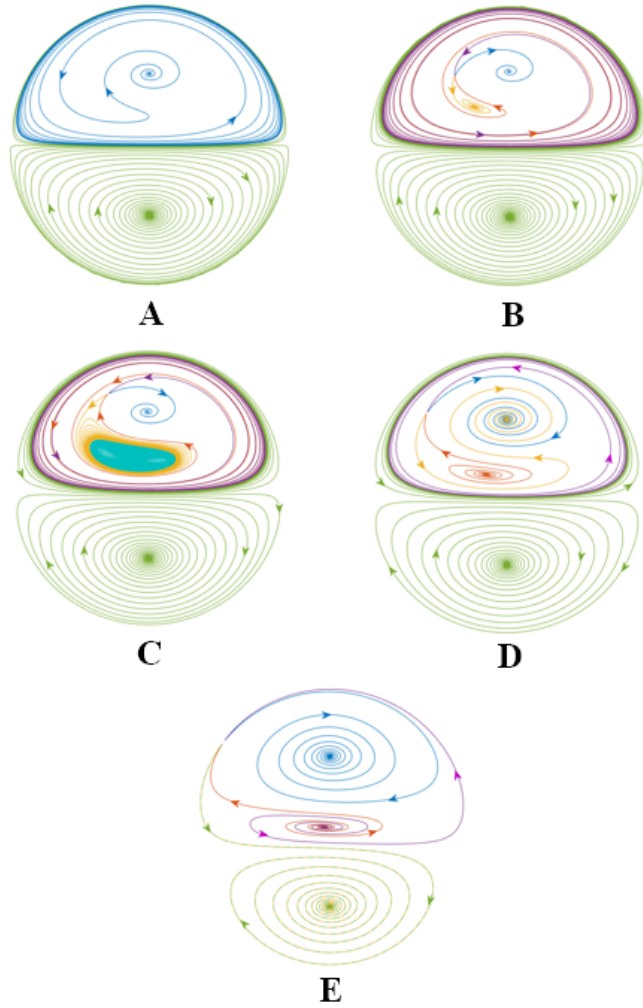


Figure 2.11: Topological configurations of the areas labeled in figure 2.10. (A) Two stable equilibria separated by a limit cycle. (B) A saddle node bifurcation generates a saddle and a third stable equilibrium in the upper half of the sphere. (C) A Hopf bifurcation generates a new limit cycle and the equilibrium generated by the saddle node bifurcation becomes unstable. (D) The limit cycle created by the Hopf bifurcation collides with the saddle during the homoclinic bifurcation, equilibrium points do not change but the connections are different. (E) The saddle collides with the limit cycle (homoclinic bifurcation), only the four equilibria remain with no limit cycle.

2.5 Analysis of non-symmetric systems

Let us consider again a uniformly magnetized particle with effective field

$$\mathbf{h}_{\text{eff}} = -D\mathbf{m} + \mathbf{h}_a(t), \quad (2.70)$$

with

$$\mathbf{h}_a = h_x \cos \omega t \hat{\mathbf{e}}_x + h_y \sin \omega t \hat{\mathbf{e}}_y + h_{DC} \hat{\mathbf{e}}_z. \quad (2.71)$$

As we saw in the last section, the time dependence of the applied field makes the system non-autonomous, however the time dependence can be removed by switching to a rotating reference frame if the field is circularly polarized.

Whenever the hypotheses of the previous section are not satisfied, time dependence is present also in the rotating reference frame. To see this let us substitute into the Gilbert equation magnetization and field in the rotating reference frame

$$\mathbf{m} = R(t)\mathbf{m}_{\text{rot}}, \quad \mathbf{h}_a = R(t)\mathbf{h}_{a,\text{rot}}, \quad (2.72)$$

where

$$R = \begin{bmatrix} \cos \omega t & -\sin \omega t & 0 \\ \sin \omega t & \cos \omega t & 0 \\ 0 & 0 & 1 \end{bmatrix}. \quad (2.73)$$

Since the vector product is invariant under rotations, i.e. $R(\mathbf{A} \times \mathbf{B}) = (R\mathbf{A}) \times (R\mathbf{B})$, Gilbert equation becomes

$$\begin{aligned} R(t) \frac{d\mathbf{m}_{\text{rot}}}{dt} + \frac{dR}{dt} \mathbf{m}_{\text{rot}} = & -R(t) [\mathbf{m}_{\text{rot}} \times (-R^{-1}(t)DR(t)\mathbf{m}_{\text{rot}} + \mathbf{h}_{a,\text{rot}})] + \\ & + \alpha R(t) \left(\mathbf{m}_{\text{rot}} \times \frac{d\mathbf{m}_{\text{rot}}}{dt} \right) + \alpha R(t) \mathbf{m}_{\text{rot}} \times \frac{dR}{dt} \mathbf{m}_{\text{rot}}, \end{aligned} \quad (2.74)$$

with

$$\mathbf{h}_{a,\text{rot}} = (h_x \cos^2 \omega t + h_y \sin^2 \omega t) \hat{\mathbf{e}}_{x'} + (h_y - h_x) \sin \omega t \cos \omega t \hat{\mathbf{e}}_{y'} + h_{DC} \hat{\mathbf{e}}_z. \quad (2.75)$$

To simplify notation we drop the subscript “rot” and we recall that $R^{-1} = R^\dagger$, where \dagger indicates the hermitian transpose and

$$\frac{dR}{dt} \mathbf{m} = R(t) (\omega \hat{\mathbf{e}}_z \times \mathbf{m}).$$

By multiplying (2.74) by R^\dagger , after some algebra, we obtain

$$\begin{aligned} \frac{d\mathbf{m}}{dt} - \alpha \left(\mathbf{m} \times \frac{d\mathbf{m}}{dt} \right) = \\ - [\mathbf{m} \times (-R^\dagger(t)DR(t)\mathbf{m} + \mathbf{h}_a)] + \omega\mathbf{m} \times \hat{\mathbf{e}}_z - \alpha\omega\mathbf{m} \times (\mathbf{m} \times \hat{\mathbf{e}}_z), \end{aligned} \quad (2.76)$$

where

$$\begin{aligned} R^\dagger DR = & \begin{bmatrix} \frac{D_x + D_y}{2} & 0 & 0 \\ 0 & \frac{D_x + D_y}{2} & 0 \\ 0 & 0 & D_z \end{bmatrix} + \\ & \begin{bmatrix} \frac{D_x - D_y}{2} \cos(2\omega t) & \frac{D_y - D_x}{2} \sin(2\omega t) & 0 \\ \frac{D_y - D_x}{2} \sin(2\omega t) & \frac{D_x - D_y}{2} \cos(2\omega t) & 0 \\ 0 & 0 & 0 \end{bmatrix}. \end{aligned} \quad (2.77)$$

Time depending terms in equation (2.75) and (2.77) have frequency ω or 2ω . On the other hand, if α is small enough and $h_{DC} \approx D_z - \frac{D_x + D_y}{2}$, the dynamic of (2.76) is slow compared to these fluctuating terms. This observation suggests the existence of two different time scales in the magnetization dynamic: a slow dynamic and a fast small ripple due to the fluctuating terms. This idea can be implemented mathematically using the Krylov-Boguliobov method [40]. We integrate (2.76) with respect to time for one period of external excitation $T = \frac{2\pi}{\omega}$. Since we suppose that magnetization does not have appreciable variations in one period, the following approximation can be applied

$$\int_{t-T}^t \mathbf{m}(\tau) v(\tau) d\tau \approx \mathbf{m}(t) \int_{t-T}^t v(\tau) d\tau. \quad (2.78)$$

By using (2.78), all the periodic terms in (2.76) disappear and the equation becomes

$$\frac{d\mathbf{m}}{dt} - \alpha \left(\mathbf{m} \times \frac{d\mathbf{m}}{dt} \right) = -[\mathbf{m} \times (-\bar{D}\mathbf{m} + \bar{\mathbf{h}}_a)] + \omega\mathbf{m} \times \hat{\mathbf{e}}_z - \alpha\omega\mathbf{m} \times (\mathbf{m} \times \hat{\mathbf{e}}_z), \quad (2.79)$$

where

$$\bar{D} = \begin{bmatrix} \frac{D_x + D_y}{2} & 0 & 0 \\ 0 & \frac{D_x + D_y}{2} & 0 \\ 0 & 0 & D_z \end{bmatrix} \quad (2.80)$$

and

$$\bar{\mathbf{h}}_a = \frac{h_x + h_y}{2} \hat{\mathbf{e}}_x + h_{DC} \hat{\mathbf{e}}_z \quad (2.81)$$

The equation represents an autonomous dynamic system, hence the methods of nonlinear dynamics (used in the previous section) can now be applied.

2.6 Hysteresis in ferromagnetic resonance

An evident effect of the bifurcations on the dynamics is hysteresis. A necessary condition for having hysteresis is the existence of more than one equilibrium point. Whenever the equilibrium is destroyed the system state changes abruptly. Even if the previous equilibrium is restored the system does not go back until the new one becomes unstable.

In this section numerical simulations are executed in order to show the effect of a bifurcation and to check the approximation introduced by Krylov-Boguliobov method in systems with small asymmetries. Let us consider a nanomagnet with $\kappa_{\text{eff}} = 0.5$, $\alpha = 0.05$, $h_{DC} = 0.3$ and $h_{AC} = 0.03$, the bifurcation map is shown in figure 2.12.

Starting from $\omega = 0.55$, the frequency is increased up to $\omega = 0.75$ and then decreased back to $\omega = 0.55$ as highlighted in the figure. The amplitude $m_{\perp} = \sqrt{1 - m_z^2}$ is shown in figure 2.13: the analytical fold over the curve is represented in blue, the interval in which m_{\perp} oscillates is represented in red. Starting from the lower curve, when the saddle-node bifurcation line is crossed the m_{\perp} jumps to a new equilibrium for $\omega \approx 0.69$ and stays on the higher curve. When the frequency is decreased m_{\perp} remains on the higher curve until the hopf bifurcation occurs at $\omega \approx 0.66$. Since the system is now in a stable limit cycle m_{\perp} oscillates and the cycle grows in amplitude until it collides with a saddle and gets destroyed by the homoclinic bifurcation at $\omega \approx 0.63$.

A similar simulation is executed for a slightly asymmetric system. Let us consider a nanomagnet with $D_x = -0.05$, $D_y = 0.05$ and $D_z = -0.5$, while all the remaining parameters are the same used for the previous simulation, so

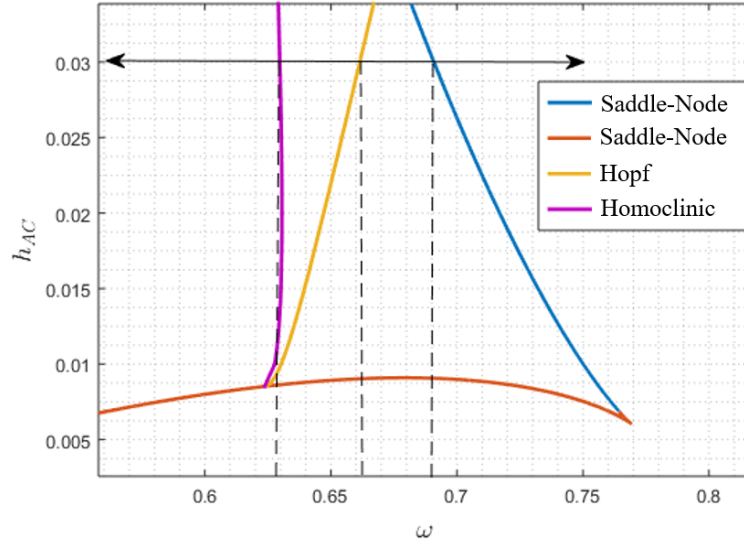


Figure 2.12: Bifurcation map of the system considered in section 2.6 obtained via numerical simulation. In the region indicated by the black double arrow, three bifurcation curves are crossed.

that the symmetrized model obtained with Krylov-Boguliobov method is unchanged.

Results of the simulation are in figure 2.14. As expected the asymmetry causes a ripple around the equilibrium state, nonetheless the averaged system still gives a good approximation of m_{\perp} as long as the asymmetry is small.

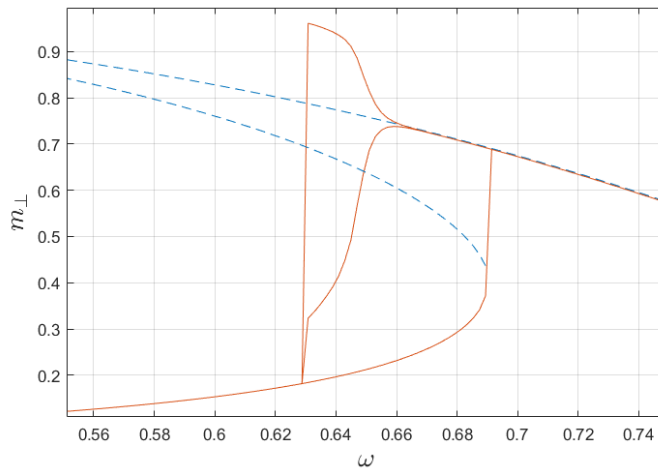


Figure 2.13: Simulation proposed in section 2.6 for a symmetrical system. Hysteresis are observed in the region between the homoclinic bifurcation curve and the saddle node bifurcation curve. The values of the equilibria - analytically obtained - are illustrated in blue

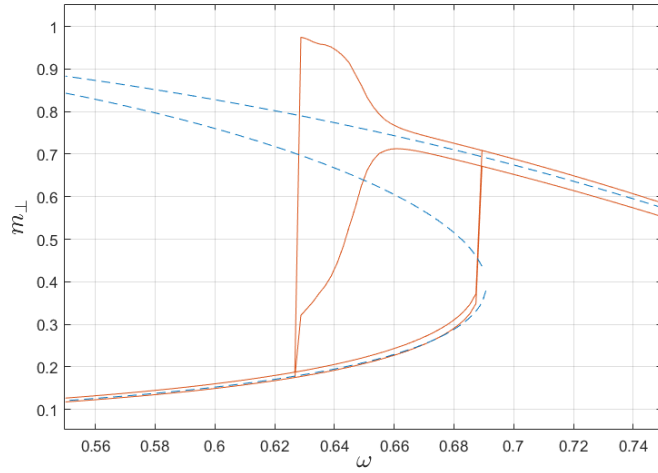


Figure 2.14: Simulation proposed in section 2.6 for a asymmetrical system. The equilibrium for the equivalent symmetrized system - obtained with the Krylov Boguliobov method - are illustrated in blue. Since the asymmetry is small, the magnetization amplitude m_{\perp} is similar to the one of the symmetric system except for a ripple.

Chapter 3

Noise in Nanosystems

In small systems the thermal fluctuations randomly influence the magnetization. Thermal fluctuations may allow the system to pass through an high energy barrier after a long enough time as depicted in the figure 3.1.

An example of the probability density function evolution is shown in figure 3.2. Starting from a potential well, the distribution quickly changes in the well. After a longer time the probability starts to grow in the other well and the equilibrium is reached.

The dimensions of magnetized devices used in magnetic storage technologies and spintronics are usually rather small and thermal effects must be included in the analysis.

These effects are usually studied by introducing an appropriate stochastic term in the Landau Lifshitz Gilbert (LLG) equation (1.82). The stochastic term usually added has the form of a random magnetic torque $\mathbf{m} \times \nu \mathbf{h}_N(t)$, where $\mathbf{h}_N(t)$ is a vector whose components are independent gaussian white noise processes, and ν is a parameter which measures the intensity of thermal perturbations

$$\frac{\partial \mathbf{m}}{\partial t} = -\mathbf{m} \times (\mathbf{h}_{\text{eff}} + \nu \mathbf{h}_N) - \alpha \mathbf{m} \times [\mathbf{m} \times (\mathbf{h}_{\text{eff}} + \nu \mathbf{h}_N)] . \quad (3.1)$$

The assumption that the thermal noise is gaussian is usually motivated by the central limit theorem: the random fluctuations are the result of a very large number of statistically independent random events, hence the sum of their effects tends to have a gaussian distribution. Moreover the choice of the gaussian distribution leads to results which are consistent with statistical mechanics.

On the other hand, the assumption that the noise has negligible correlation time reflects the hypothesis that the random perturbations are expected to have

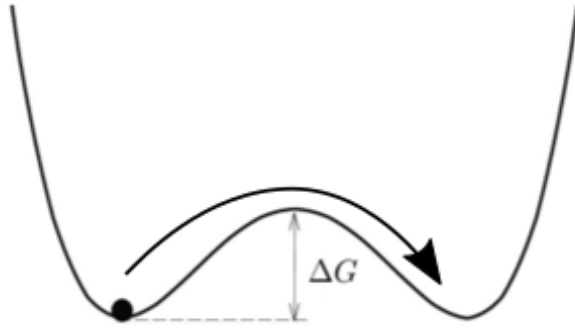


Figure 3.1: Qualitative representation a small bistable systems affected by thermal fluctuations

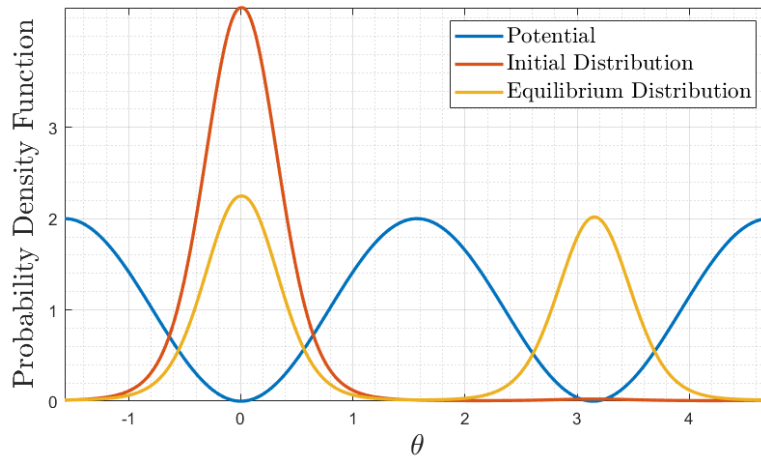


Figure 3.2: Evolution of the probability density function in a periodic potential. After a long enough time, the probability of finding the system state in potential well is the same regardless of the initial probability density function.

a correlation time much shorter than any time constant of magnetization dynamics.

Since equation (3.1) is stochastic, an analysis of the magnetization dynamics requires a large number of realizations of the process in order to have reliable statistics. Alternatively the time evolution of the probability density function of the magnetization could be directly determined. These two approaches are those conceptually proposed by Langevin in 1908 [51] and by Einstein in 1905 [50] respectively.

The study of the probability density function is generally preferable when the noise is rather big compared to the drift. The equation governing the probability density function evolution is called Fokker-Planck equation

$$\frac{\partial w}{\partial t} = -\nabla_{\Sigma} \cdot \left[(\mathbf{m} \times \nabla_{\Sigma} g - \alpha \nabla_{\Sigma} g) w - \frac{\nu^2}{2} \nabla_{\Sigma} w \right], \quad (3.2)$$

where w is the probability density function defined on the unit sphere, g is the Gibbs-Landau free energy and “ ∇_{Σ} ” and “ $\nabla_{\Sigma} \cdot$ ” are respectively the gradient and the divergence on the surface of the unit sphere.

In the following we consider the influence of the thermal fluctuations in two different scenarios: the switching times statistical distribution for magnetic memories [49] and the persistence of data in a magnetic grain.

3.1 Probability density function at equilibrium

In the second chapter we analyzed the equilibrium of a uniformly magnetized body. When there is noise the system can not have static equilibrium anymore since \mathbf{h}_N makes the system non-autonomous and non-periodic. The magnetization is expected to move, but at the same time it is expected to spend longer time in the regions with low free energy.

Let us consider the Fokker-Planck equation (3.2), at the equilibrium the probability density function must satisfy

$$\nabla_{\Sigma} \cdot \left[(-\mathbf{m} \times \nabla_{\Sigma} g + \alpha \nabla_{\Sigma} g) w + \frac{\nu^2}{2} \nabla_{\Sigma} w \right] = 0. \quad (3.3)$$

In order to solve (3.3) we impose that the term in square bracket is null, this procedure is also called detailed balance [43]. The solution can be found by applying separation of variables if we assume that the probability distribution depends only on the free energy, i.e.

$$w = w(g). \quad (3.4)$$

This assumption implies that the precessional term gives no contribution. Indeed we have

$$\nabla_{\Sigma} \cdot [(\mathbf{m} \times \nabla_{\Sigma} g) w] = \nabla_{\Sigma} \cdot (\mathbf{m} \times \nabla_{\Sigma} g) w + (\mathbf{m} \times \nabla_{\Sigma} g) \cdot \nabla_{\Sigma} w = 0. \quad (3.5)$$

The first term on the right hand side of (3.5) is zero because flows of Hamiltonian systems are divergenceless and the second term is null because $\nabla_{\Sigma} g$ and $\nabla_{\Sigma} w$ are parallel according to (3.4). Eventually we get

$$w = \frac{1}{Z} \exp \left(-\frac{2\alpha}{\nu^2} g \right), \quad (3.6)$$

where Z is a renormalization constant needed to ensure that the total probability is unitary. This result is also expected by statistical mechanics, in fact Boltzmann distribution reads

$$w = \frac{1}{Z} \exp \left(-\frac{\mu_0 M_S^2 V}{k_B T} g \right). \quad (3.7)$$

This last relation allows to find the value of ν , which is

$$\frac{\nu^2}{2\alpha} = \frac{k_B T}{\mu_0 M_S^2 V} \implies \nu = \sqrt{\frac{2\alpha k_B T}{\mu_0 M_S^2 V}}. \quad (3.8)$$

This relation is often referred to as the fluctuation-dissipation relation.

3.2 Data persistence in magnetic memories

Let us consider an axial symmetric particle with free energy given by

$$g = -\frac{1}{2} \kappa_{\text{eff}} m_z^2. \quad (3.9)$$

This situation appropriately models the state of a magnetic memory cell at rest. By equation (3.6) at thermal equilibrium the magnetization has an equal chance to be closer to the minimum $m_z = 1$ or to the minimum $m_z = -1$. In terms of data this means that we have an equal chance to read “0” or “1” regardless of what we wrote previously in the cell.

This worrying feature is actually present in every type of memory, nonetheless digital memories work properly because the time required to reach the equilibrium is long enough to retain the data for the entire lifetime of the product.

In magnetic memories this stability is achieved by increasing saturation, magnetization and anisotropy of the chosen material.

Let us consider Fokker-Planck equation for axialsymmetric particles

$$\frac{\partial w}{\partial t} = \frac{1}{\sin \theta} \frac{\partial}{\partial \theta} \left[\sin \theta \left(\alpha \frac{\partial g}{\partial \theta} w + \frac{\nu^2}{2} \frac{\partial w}{\partial \theta} \right) \right], \quad (3.10)$$

where the terms in round bracket correspond to the surface current density of the pdf.

If the energy barrier between the equilibria is high enough, we expect the probability density function to be approximated by

$$w(\theta) = \begin{cases} w(0) \exp \left(-\frac{G(\theta) - G(0)}{k_B T} \right) & \theta < \pi/2 \\ w(\pi) \exp \left(-\frac{G(\theta) - G(\pi)}{k_B T} \right) & \theta > \pi/2 \end{cases} \quad (3.11)$$

with $G = \mu_0 M_S^2 V g$. The idea behind this assumption is that the modes that redistribute the particles inside a potential well are much faster than the modes that bring the particles through the barrier.

We now define

$$n_1 = 2\pi w(0) \exp \left(\frac{G(0)}{k_B T} \right) I_1, \quad n_2 = 2\pi w(\pi) \exp \left(\frac{G(\pi)}{k_B T} \right) I_2, \quad (3.12)$$

with

$$I_1 = \int_0^{\theta_1} \exp \left(-\frac{G(\theta)}{k_B T} \right) \sin \theta \, d\theta, \quad I_2 = \int_{\theta_2}^{\pi} \exp \left(-\frac{G(\theta)}{k_B T} \right) \sin \theta \, d\theta. \quad (3.13)$$

The quantity n_1 and n_2 express the probability to find the magnetization in the upper or in the lower potential well respectively, while θ_1 and θ_2 delimit the region which is considered the center of the well. In fact, the exact values of θ_1 and θ_2 do not matter since the integrand term quickly vanishes if the energy barrier is high enough.

The integrals in equation (3.13) can be approximated by substituting $g(\theta)$ with its Taylor expansion up to the second order in $\theta = 0$ and $\theta = \pi$ respectively, using $\theta_1 = \infty$, $\theta_2 = -\infty$ and by replacing $\sin \theta$ by θ ; it yields

$$I_1 \approx \frac{k_B T}{G''(0)} \exp \left(-\frac{G(0)}{k_B T} \right), \quad I_2 \approx \frac{k_B T}{G''(\pi)} \exp \left(-\frac{G(\pi)}{k_B T} \right) \quad (3.14)$$

where $G''(\theta)$ is the second derivative of $G(\theta)$.

The flow of the probability density function is given by the Fokker Planck equation

$$I = -2\pi \sin \theta \left(\alpha \frac{\partial g}{\partial \theta} w + \frac{\nu^2}{2} \frac{\partial w}{\partial \theta} \right) \Rightarrow \frac{I}{2\pi \sin \theta} \frac{2}{\nu^2} = - \left(\frac{1}{k_B T} \frac{\partial G}{\partial \theta} w + \frac{\partial w}{\partial \theta} \right) \quad (3.15)$$

where we used equation (3.8). By multiplying (3.15) by $\exp(G/k_B T)$ and integrating with respect to θ we obtain

$$\frac{I}{\pi \nu^2} \int_{\theta_1}^{\theta_2} \frac{e^{G(\theta)/k_B T}}{\sin \theta} d\theta = w(\theta_1) \exp \left(\frac{G(\theta_1)}{k_B T} \right) - w(\theta_2) \exp \left(\frac{G(\theta_2)}{k_B T} \right). \quad (3.16)$$

By using equation (3.11) the right hand side of equation (3.16) is restated as

$$\begin{aligned} w(\theta_1) \exp \left(\frac{G(\theta_1)}{k_B T} \right) - w(\theta_2) \exp \left(\frac{G(\theta_2)}{k_B T} \right) = \\ w(0) \exp \left(\frac{G(0)}{k_B T} \right) - w(\pi) \exp \left(\frac{G(\pi)}{k_B T} \right). \end{aligned} \quad (3.17)$$

According to (3.12) we obtain

$$\frac{I}{\pi \nu^2} \int_{\theta_1}^{\theta_2} \frac{e^{G(\theta)/k_B T}}{2\pi \sin \theta} d\theta = \frac{1}{2\pi} \left(\frac{n_1}{I_1} - \frac{n_2}{I_2} \right). \quad (3.18)$$

Because of the high energy barrier we can assume that the probability density function is negligible in the area between θ_1 and θ_2 , hence

$$I = -\frac{dn_1}{dt} = \frac{dn_2}{dt}. \quad (3.19)$$

Eventually we have

$$\frac{dn_1}{dt} = -\frac{dn_2}{dt} = \frac{\nu^2}{2I_m} \left(\frac{n_2}{I_2} - \frac{n_1}{I_1} \right), \quad (3.20)$$

where

$$I_m = \int_{\theta_1}^{\theta_2} \frac{e^{G(\theta)/k_B T}}{2\pi \sin \theta} d\theta. \quad (3.21)$$

In matrix form equation (3.20) reads

$$\frac{d}{dt} \begin{bmatrix} n_1 \\ n_2 \end{bmatrix} = \begin{bmatrix} -\frac{\nu^2}{2I_m I_1} & \frac{\nu^2}{2I_m I_2} \\ \frac{\nu^2}{2I_m I_1} & -\frac{\nu^2}{2I_m I_2} \end{bmatrix} \begin{bmatrix} n_1 \\ n_2 \end{bmatrix}. \quad (3.22)$$

The secular equation is

$$\left(\frac{\nu^2}{2I_m I_1} + \lambda\right) \left(\frac{\nu^2}{2I_m I_2} + \lambda\right) - \frac{\nu^4}{4I_m^2 I_1 I_2} = \lambda^2 + \frac{\nu^2}{2I_m} \left(\frac{1}{I_1} + \frac{1}{I_2}\right) \lambda = 0 \quad (3.23)$$

and the eigenvalues are

$$\lambda_1 = 0, \quad \lambda_2 = -\frac{\nu^2}{2I_m} \left(\frac{1}{I_1} + \frac{1}{I_2}\right). \quad (3.24)$$

In particular λ_2 provides an estimate of the lowest non-zero eigenvalue of the Fokker Planck equation, its reciprocal is then the time constant for the thermal activation of the magnetic memory.

3.3 Pseudospectral methods

Let us consider again the Fokker Planck equation. If there is no drift, the equation becomes a diffusion equation on the unit sphere's surface. In such a case we have

$$\frac{\partial w}{\partial t} = \Delta_\Sigma w \quad (3.25)$$

where Δ_Σ is Laplace-Beltrami operator and its eigenmodes are the spherical harmonics.

When instead there is a drift term, no general analytic solution is available and numerical methods must be implemented.

For the analysis of these cases we consider the Pseudospectral method [52, 53]. This method has an excellent performance on equation (3.25) and the eigenvalues of the Laplace-Beltrami can be computed with machine precision as illustrated in figure 3.3.

Let us consider a set of functions $\varphi_i, i = 1, \dots, N$, to be used in the approximation of the real solution of Fokker Planck equation, we define our approximated solution as

$$w(\mathbf{m}, t) = \sum_{i=1}^N c_i(t) \varphi_i(\mathbf{m}). \quad (3.26)$$

If the exact w is a linear combination of the φ_i 's Fokker Planck equation can be solved everywhere with machine precision. Otherwise we can choose at most N cases where the equation is solved exactly and find the unknown coefficients consequently.

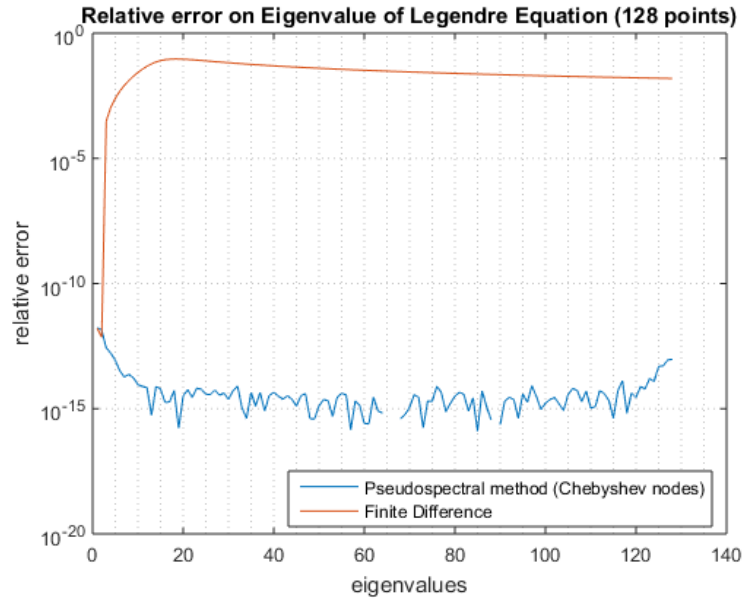


Figure 3.3: Comparison of the numerical errors in the computation of Laplace-Beltrami operator eigenvalues between finite differences and the pseudospectral method. The missing points in the blue curve correspond to null errors (or errors smaller than the machine precision).

To this purpose, we select a grid of points on the surface of the unit sphere $\mathbf{m}_i = (\theta_i, \phi_i)$, where we impose

$$\left. \frac{\partial w}{\partial t} \right|_{\mathbf{m}=\mathbf{m}_i} = -\nabla_{\Sigma} \cdot \left[(\mathbf{m} \times \nabla_{\Sigma} g - \alpha \nabla_{\Sigma} g) w - \frac{\nu^2}{2} \nabla_{\Sigma} w \right] \Big|_{\mathbf{m}=\mathbf{m}_i}. \quad (3.27)$$

This method is also called collocation method.

Then it is necessary to identify the basis function φ_i we want to use. According to the properties of these functions the numerical method has a different name. The simplest choice consists in piecewise linear functions which are zero in all the grid points but one; this choice classifies the method as the finite element method (FEM).

In some cases smooth functions are preferable. Smooth functions, with the whole domain as support, classify the method as the spectral method.

The pseudospectral method is somehow intermediate between the finite element method and the spectral method. We choose functions φ_i which are defined in the whole domain though they have the collocation property

$$\varphi_j(\mathbf{m}_i) = \delta_{ij}. \quad (3.28)$$

Let us use $z = \cos \theta$ as variable instead of θ . By using the Leibnitz formula for the derivatives we reformulate the Fokker Planck equation as follows

$$\frac{\partial w}{\partial t} = (\mathcal{L}_{\gamma} + \mathcal{L}_{\alpha} + \mathcal{L}_{\nu})w \quad (3.29)$$

with

$$\begin{aligned} \mathcal{L}_{\gamma} &= \frac{\partial g}{\partial \phi} \frac{\partial}{\partial z} - \frac{\partial g}{\partial z} \frac{\partial}{\partial \phi}, \\ \mathcal{L}_{\nu} &= \frac{\nu^2}{2} \left(-2z \frac{\partial}{\partial z} + (1 - z^2) \frac{\partial^2}{\partial z^2} + \frac{1}{1 - z^2} \frac{\partial^2}{\partial \phi^2} \right), \\ \mathcal{L}_{\alpha} &= \alpha \left(-2z \frac{\partial g}{\partial z} + (1 - z^2) \frac{\partial^2 g}{\partial z^2} + (1 - z^2) \frac{\partial g}{\partial z} \frac{\partial}{\partial \phi} \right. \\ &\quad \left. + \frac{1}{1 - z^2} \frac{\partial^2 g}{\partial \phi^2} + \frac{1}{1 - z^2} \frac{\partial g}{\partial \phi} \frac{\partial}{\partial \phi} \right). \end{aligned} \quad (3.30)$$

We choose a grid of points equispaced in θ and ϕ so that they are distributed as Chebyshev nodes in z . We have

$$(z_i, \phi_j) \quad \text{with } z \in \{z_1, \dots, z_{N_z}\} \text{ and } \phi \in \{\phi_1, \dots, \phi_{N_{\phi}}\}, \quad (3.31)$$

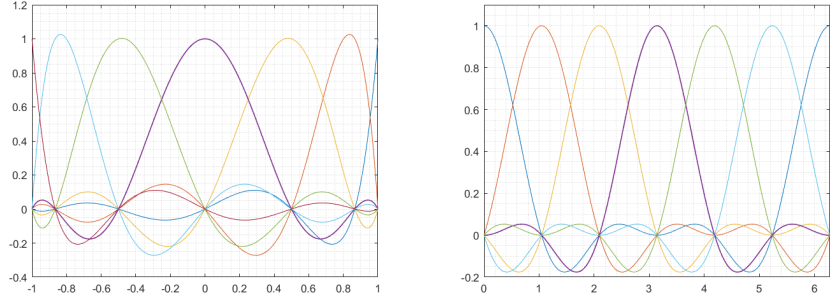


Figure 3.4: Plot of the basis functions defined in equation (3.33). On the left Lagrange polynomials with zeros distributed as Chebyshev nodes, on the right periodic sinc functions.

where N_z and N_ϕ are respectively the number of different values of z and ϕ used in the grid. Basis functions are given by

$$\varphi_{ij}(z, \phi) = Z_i(z)\Phi_j(\phi), \quad (3.32)$$

with

$$Z_i(z) = \prod_{m=1}^{N_z} \frac{z - z_m}{z_i - z_m}, \quad \Phi_j(\phi) = \frac{\sin(N_\phi(\phi - \phi_j)/2)}{N_\phi \tan((\phi - \phi_j)/2)}. \quad (3.33)$$

A representation of the functions Z and Φ is in figure 3.4. As benchmark for the pseudospectral method we consider the first non zero time constant obtained by the method of the previous section. The results are illustrated in the figure 3.5.

The pseudospectral method accurately reproduces the time constants for low to intermediate energy barriers. When the energy barrier increases the modes of the FokkerPlanck equation become very sharp in space and in order to accurately represent them an increasing number of basis functions is required, which inflates the computational costs.

Time constants for a wide interval of energy barriers are in figure 3.6. Industrial memories typically have $\Delta G/k_B T \approx 50$ which means $\tau \approx 10^{21} \text{ ns} \approx 30$ years.

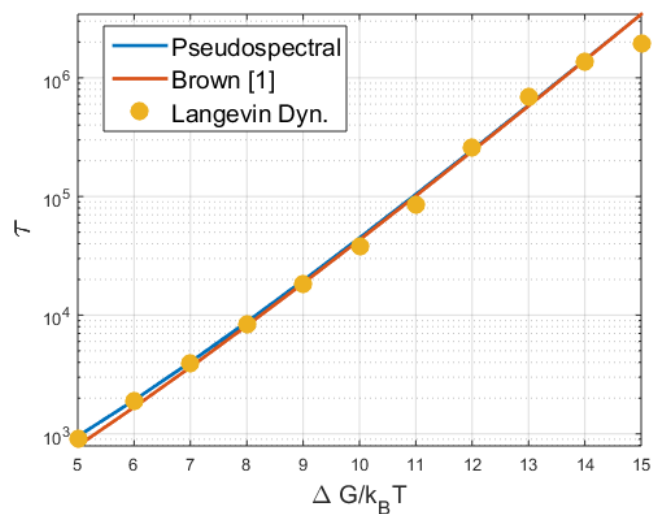


Figure 3.5: Comparison of the numerical solutions obtained with the pseudospectral method and Langevin dynamics and the analytical solution given by equation (3.24). The approximated analytical solution works well for high potential barriers, the numerical method instead works well for low or intermediate energy barrier. The analytical solution is used as benchmark.

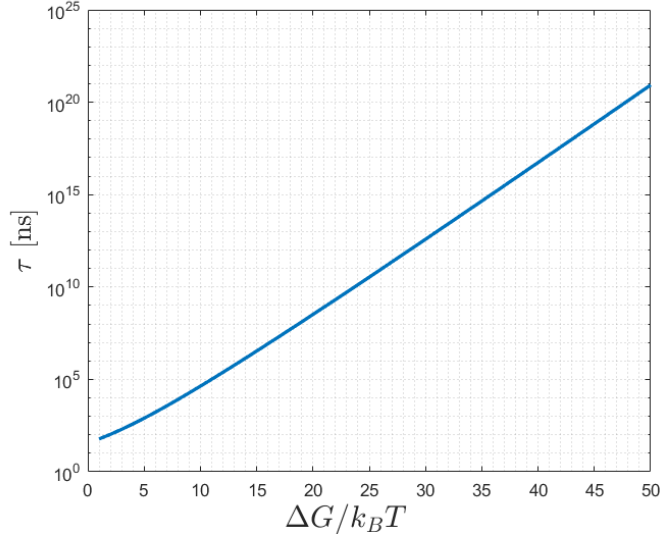


Figure 3.6: Extended plot of the analytical solution given in (3.24), energy barriers of $\Delta G \approx 50k_B T$ are used in recording devices.

3.4 Switching time distribution for a magnetic memory

In the previous sections we analyzed the magnetization dynamics when the memory cell is at rest. In particular we saw that no information can be stored permanently. Nonetheless if the time scales - we are interested in - are small compared with the time required to reach the equilibrium we can consider an initial distribution like (3.11).

We still have to consider how the thermal noise influences the writing process, which is our topic in the work [49].

Let us consider the Fokker Planck equation of a magnetic particle with uniaxial anisotropy along \hat{e}_z , applied magnetic field \mathbf{h}_a and with an injected current β polarized along the direction \mathbf{e}_p . We have

$$\frac{\partial w}{\partial t} = -\nabla_{\Sigma} \cdot \left[(\mathbf{m} \times \nabla_{\Sigma} g - \alpha \nabla_{\Sigma} \Phi) w - \frac{\nu^2}{2} \nabla_{\Sigma} w \right], \quad (3.34)$$

where

$$g = -\frac{1}{2} \kappa_{\text{eff}} m_z^2 - \mathbf{m} \cdot \mathbf{h}_a, \quad (3.35)$$

3.4. SWITCHING TIME DISTRIBUTION FOR A MAGNETIC MEMORY 81

$$\Phi = g + \frac{\beta \ln(1 + c_p \mathbf{m} \times \hat{\mathbf{e}}_p)}{c_p}, \quad (3.36)$$

and c_p controls the spin torque transfer.

Let us also assume axial symmetry, i.e. $\hat{\mathbf{e}}_z = \hat{\mathbf{e}}_p$ and $\hat{\mathbf{e}}_z$ parallel to \mathbf{h}_a , g and Φ are then restated as

$$g = -\frac{1}{2} \kappa_{\text{eff}} m_z^2 - h_a m_z \quad (3.37)$$

and

$$\Phi = g + \frac{\beta \ln(1 + c_p \mathbf{m} \times \hat{\mathbf{e}}_z)}{c_p}. \quad (3.38)$$

Before beginning the writing process, neither the applied field nor the current are present, hence the equilibrium probability density function is given by

$$w_{eq}(m_z) = \frac{1}{Z} \exp\left(\frac{\alpha}{\nu^2} \kappa_{\text{eff}} m_z^2\right), \quad (3.39)$$

with

$$Z = 2\pi \int_{-1}^1 \exp\left(\frac{\alpha}{\nu^2} \kappa_{\text{eff}} m_z^2\right) dm_z, \quad (3.40)$$

or in terms of the angle θ with the z axis

$$p_{eq}(\theta) = B \sin \theta \exp\left(\frac{\alpha}{\nu^2} \kappa_{\text{eff}} \sin^2 \theta\right), \quad (3.41)$$

where B is an appropriate normalization constant.

If the energy barrier is high enough, as in the case of magnetic memories, p_{eq} quickly goes to zero as θ grows, hence we can approximate $\sin \theta \approx \theta$ in the relevant neighborhood of $\theta = 0$ and obtain

$$\tilde{p}_{eq} = B\theta \exp\left(\frac{\alpha}{\nu^2} \kappa_{\text{eff}} \theta^2\right), \quad (3.42)$$

with the cumulative density function

$$F_{eq}(\theta) = 1 - \exp\left[-\mu \frac{\kappa_{\text{eff}}}{2} \theta^2\right]. \quad (3.43)$$

Closed form expressions can also be derived for the mean μ_θ and the variance σ_θ^2

$$\mu_\theta = \sqrt{\frac{4 - \pi}{2\mu\kappa_{\text{eff}}}}, \quad \sigma_\theta^2 = \frac{4 - \pi}{2\mu\kappa_{\text{eff}}}. \quad (3.44)$$

Let us now consider the switching process triggered by an applied field and a polarized current. Due to the small duration of the whole process we can ignore

the noise during the switch, although the noise affects the initial condition of the process which may modify the time required for the process.

The component m_z of the magnetization evolves according to

$$\frac{dm_z}{dt} = \alpha \left(\kappa_{\text{eff}} m_z + h_{az} - \frac{\beta}{\alpha} (1 + c_p m_z)^{-1} \right) (1 - m_z^2). \quad (3.45)$$

In order to switch the magnetization from \hat{e}_z to $-\hat{e}_z$, the current is required to be above a critical value β_{crit} given by

$$\beta > \beta_{\text{crit}} = \alpha(1 + c_p)(\kappa_{\text{eff}} + h_{az}), \quad (3.46)$$

whereas switching from $-\hat{e}_z$ to \hat{e}_z requires a current below the following critical value

$$\beta < \beta_{\text{crit}} = \alpha(1 - c_p)(-\kappa_{\text{eff}} + h_{az}). \quad (3.47)$$

The equation (3.45) can be integrated analytically by separation of variables. By setting the initial time $t = 0$ we have

$$\int_{m_{zi}}^{m_{zf}} \frac{dm_z}{[\kappa_{\text{eff}} + h_{az} - \beta/\alpha(1 + c_p m_z)^{-1}](1 - m_z^2)} = \alpha t. \quad (3.48)$$

We can hence define the switching time as the time required to reach an assigned value of magnetization, say $m_{zf} = -0.9$ starting from the initial condition m_{zi} .

In the case of a symmetric spin torque, namely $c_p = 0$, it is possible to analytically integrate (3.48). In this case the equation becomes

$$\int_{m_{zi}}^{m_{zf}} \frac{dm_z}{(\kappa_{\text{eff}} + \tilde{h})(1 - m_z^2)} = \alpha t. \quad (3.49)$$

with $\tilde{h} = h_{az} - \beta/\alpha$ and the solution is given by

$$t_s = \frac{1}{\alpha} \left[\frac{1}{2(\tilde{h} - \kappa_{\text{eff}})} \ln \left(\frac{1 + m_{zf}}{1 + m_{zi}} \right) - \frac{1}{2(\tilde{h} + \kappa_{\text{eff}})} \ln \left(\frac{1 - m_{zf}}{1 - m_{zi}} \right) - \frac{\kappa_{\text{eff}}}{\tilde{h}^2 - \kappa_{\text{eff}}^2} \ln \left(\frac{\tilde{h} + \kappa_{\text{eff}} m_{zf}}{\tilde{h} + \kappa_{\text{eff}} m_{zi}} \right) \right] = g(m_{zi}). \quad (3.50)$$

By using the composition rule for probability distribution functions we obtain the statistical distribution for switching times

$$f(t_s) = \tilde{p}_{eq}(\arccos(g^{-1}(t_s))) \left| \frac{1}{\sqrt{1 - (g^{-1}(t_s))^2}} \right| \left| \frac{dg^{-1}(t_s)}{dt_s} \right| \quad (3.51)$$

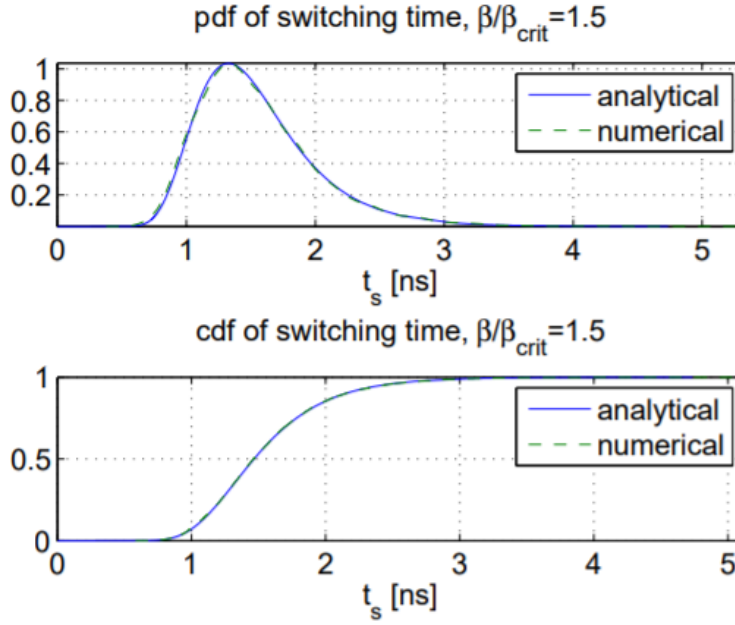


Figure 3.7: Comparison of the probability density function and cumulative density function obtained from the formulas (3.51) and (3.52) and the histograms generated by using (3.50).

and the cumulative distribution function

$$F(t_s) = \exp \left[-\frac{\alpha}{\nu^2} \kappa_{\text{eff}} \arccos^2(g^{-1}(t_s)) \right]. \quad (3.52)$$

The function $g^{-1}(t_s)$ cannot be easily expressed in closed form, but nevertheless it can be efficiently obtained by numerical inversion of the strictly monotone function $g(m_{zi})$ given by (3.50).

The probability and the cumulative distribution function are illustrated in figure 3.7 for the following material parameters $M_s = 106 \text{ A/m}$, $V = 7.07 \cdot 10^{-25} \text{ m}^3$, $T = 300 \text{ K}$, $D_x = D_y = 0.0464$, $D_z = -0.366$ resulting in $\kappa_{\text{eff}} = 0.412$ and $\mu \kappa_{\text{eff}} = 88.49$.

Finally, it is useful deriving simple analytical formulas for the mean and the variance of the switching time as function of the field and the current amplitudes. By using Taylor expansion of the function $g(m_{z0})$, it can be shown that

up to second order term the average is

$$E[T_s] = \frac{1}{\alpha\kappa_{\text{eff}}} \left[-\frac{1}{\tilde{h}^2 - 1} \log \left(\frac{\tilde{h} + m_{zf}}{\tilde{h} + \cos \mu_\theta} \right) - \frac{1}{2(\tilde{h} - 1)} \log \left(\frac{1 + m_{zf}}{1 + \cos \mu_\theta} \right) - \frac{1}{2(\tilde{h} + 1)} \log \left(\frac{1 - m_{zf}}{1 - \cos \mu_\theta} \right) \right], \quad (3.53)$$

while at first order the variance can be expressed as

$$\sigma_T^2 = \frac{4 - \pi}{2\mu\kappa_{\text{eff}}} \left[\frac{1}{\alpha\kappa_{\text{eff}} \cos^3 \mu_\theta + \tilde{h} \cos^2 \mu_\theta - \cos \mu_\theta - \tilde{h}} \right]^2. \quad (3.54)$$

In order to check the accuracy of the analytical prediction for the probability and the cumulative distribution function, we have performed numerical simulations of magnetization switching in the presence of noise, the material parameters are $M_s = 106 \text{ A/m}$, $V = 7.07 \cdot 10^{-25} \text{ m}^3$, $T = 300 \text{ K}$, $\kappa_{\text{eff}} = 0.412$. The switching time distributions for different values of the applied field are shown in figure 3.8. The figure shows also the distribution obtained from numerical simulations with macrospin model and micromagnetic simulations (1000 realizations).

Each realization of the stochastic dynamics has been performed starting from the initial condition $m_z = 1$ at $t = 0$ under zero external actions (field, current) and letting magnetization relax for a time interval of 2 ns, then a rectangular field pulse of amplitude $h_{az} < -\kappa_{\text{eff}}$ is applied and the time t_s for which $m_z = -0.9$ is determined. The distribution function is estimated from a collection of a large number of realizations.

The computed values of average and variance extracted from macrospin and micromagnetic simulation are shown in table 3.1. It can be seen that macrospin simulation exhibits a good agreement with the analytical formulas, especially for high field, when the drift term prevails on the noise. On the other hand micromagnetic simulation shows good agreement for intermediate fields, whereas high field can activate spatially inhomogeneous modes that increase the average swithing time with respect to the macrospin approximation.

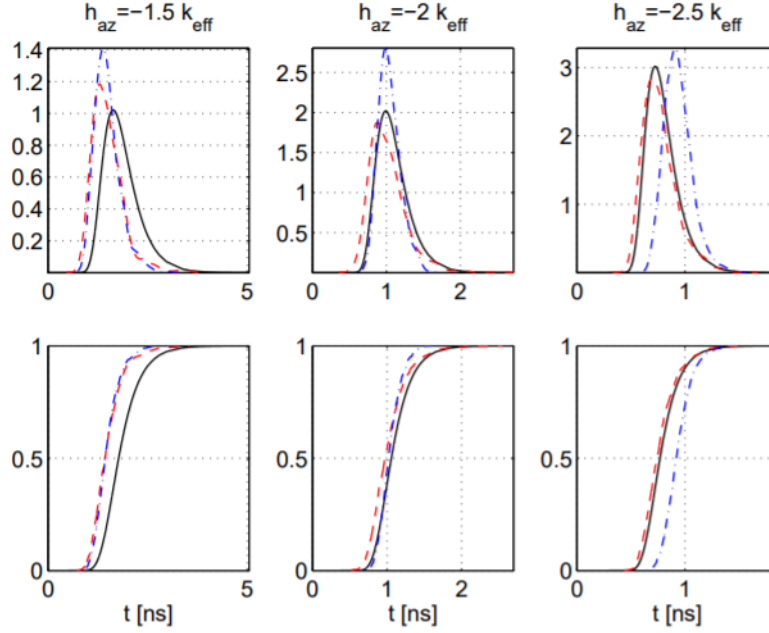


Figure 3.8: Probability density function (upper row) and cumulative probability function (lower row) of the switching time for different values of the applied field. Solid black lines refer to analytical formulas, dashed red lines refer to numerical results from macrospin simulation ($N = 1000$ realizations) and the blue dot-dashed line refer to numerical results from micromagnetic simulation ($N = 1000$ realizations)

— $h_{az}/\kappa_{\text{eff}}$	Analytical		Macrospin		Micromagnetic	
	$E[T_S]$	$\sigma_{T_S}^2$	$E[T_S]$	$\sigma_{T_S}^2$	$E[T_S]$	$\sigma_{T_S}^2$
-1.5	1.8294	0.1420	1.4927	0.1562	1.4866	0.1009
-2.0	1.0854	0.0361	1.0180	0.0631	1.0399	0.0219
-2.5	0.7874	0.0161	0.7674	0.0250	0.9360	0.0164

Table 3.1: Values of the mean and the variance obtained with (3.53) and (3.54), compared with the mean and the variance obtained from macrospin simulation and micromagnetic simulation for different values of the applied field (no spin polarized current).

Chapter 4

Ultrafast Magnetization Dynamics

Until 20 years ago, all of the relevant physics of magnetization dynamics were believed to be included in Landau-Lifshitz-Gilbert equation which was thought to be the only reference for the optimization of storage devices. However, the pioneering experiment of Bigot et al. in 1996 [54] revealed the occurrence of spin dynamics on the sub-picosecond scales that could not be described by the Landau-Lifshitz-Gilbert equation, giving birth to the field of ultrafast magnetism.

In 2004 Zhu et al. [59] showed that the dynamics of spins in a tunnelling barrier between two superconductors has an unusual behaviour in contrast to a simple spin precession and they named it 'Josephson nutation'. Kimel et al. [60] for the first time showed inertia-driven spin switching in antiferromagnetically ordered systems.

The concept of inertia in proper ferromagnetic systems appeared only in 2011 with the works of Ciornei et al. [55]. The Landau-Lifshitz-Gilbert equation was reformulated including a physically correct inertial response, which was surprisingly missing from the original formulation, and which predicts the appearance of spin nutations, similar to the ones of a spinning top, at a frequency much higher (in the terahertz range) than the spin precession described by the conventional Landau-Lifshitz-Gilbert equation, typically at gigahertz frequencies.

However, the lack of intense magnetic field sources at these high frequencies has hampered the experimental observation of such nutation dynamics.

This field is currently one of the most investigated and debated topic in con-

densed matter physics [63, 64, 65, 66, 67, 68, 69, 70, 71, 72, 73, 74, 75, 76], with implications for our fundamental understanding of magnetism as well as for possible applications for faster and more energy-efficient data manipulation.

4.1 Experimental techniques for ultrafast dynamics

Measuring magnetization in ultrafast phenomena is a complex challenge that requires appropriate method to be accomplished.

A physical effect widely used to measure magnetization is the Magneto Optic Kerr Effect (MOKE). It was noticed by Faraday in 1845 that light reflected by magnetized bodies manifests changes in the polarization depending on the magnetization of the body [61, 62]. This effect is due to a change in the electric permittivity. In particular it can be observed that electric susceptibility is represented by an antisymmetric matrix, i.e.

$$\underline{\underline{\varepsilon}} = \varepsilon \begin{bmatrix} 1 & 0 & 0 \\ 0 & 1 & 0 \\ 0 & 0 & 1 \end{bmatrix} + \varepsilon \begin{bmatrix} 0 & iQ_z & -iQ_y \\ -iQ_z & 0 & iQ_x \\ iQ_y & iQ_x & 0 \end{bmatrix}, \quad (4.1)$$

the electric induction vector will hence be given by

$$\mathbf{D} = \varepsilon \mathbf{E} + i\varepsilon \mathbf{E} \times \mathbf{Q}, \quad (4.2)$$

where we introduced the vector $\mathbf{Q} = [Q_x, Q_y, Q_z]$.

Phenomenologically, this can be answered by a simple argument based on time reversal symmetry. Under the time reversal operation, the electric displacement field \mathbf{D} and the electric field \mathbf{E} remain unchanged, but the magnetic field \mathbf{H} changes its sign. Thus, Onsager's relation gives $\varepsilon_{ij}(\mathbf{E}, \mathbf{H}) = \varepsilon_{ji}(\mathbf{E}, -\mathbf{H})$ [61, 26]. By expanding ε_{ij} up to terms linear in \mathbf{E} and \mathbf{H} it becomes obvious that the antisymmetric part of ε_{ij} is generated by the magnetic field. In general, any quantity that breaks time reversal symmetry could, in principle, generate antisymmetric elements of the permittivity matrix.

Maxwell's equations for plane waves become (assuming for simplicity $\mathbf{H} = \mathbf{B}$)

$$\begin{cases} \mathbf{k} \cdot \mathbf{E} + i\mathbf{k} \cdot (\mathbf{E} \times \mathbf{Q}) = 0 \\ \mathbf{k} \times \mathbf{E} = \frac{\omega}{c} \mathbf{H} \\ \mathbf{k} \cdot \mathbf{H} = 0 \\ \mathbf{k} \times \mathbf{H} = -\frac{\omega\varepsilon}{c} (\mathbf{E} + i\mathbf{E} \times \mathbf{Q}) \end{cases}. \quad (4.3)$$

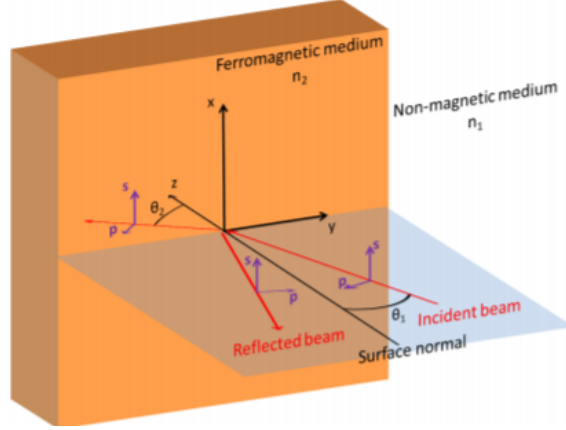


Figure 4.1: Reference frame for section 4.1

Let us consider the reference frame in figure 4.1 where a wave that propagates along the direction $\hat{\mathbf{k}}$ hits a ferromagnetic medium. The unit vector normal to the surface of the medium is called $\hat{\mathbf{e}}_z$. Let us choose $\hat{\mathbf{e}}_s$ to be perpendicular to $\hat{\mathbf{k}}$ and $\hat{\mathbf{e}}_z$ and $\hat{\mathbf{e}}_p$ perpendicular to $\hat{\mathbf{e}}_s$ and $\hat{\mathbf{k}}$, from Maxwell's equations we obtain the following wave equations

$$\begin{cases} \left(\frac{\omega^2 \varepsilon}{c^2} - k^2 \right) E_s + \frac{i\omega^2 \varepsilon \mathbf{Q} \cdot \hat{\mathbf{e}}_k}{c^2} E_p = 0, \\ \left(\frac{\omega^2 \varepsilon}{c^2} - k^2 \right) E_p - \frac{i\omega^2 \varepsilon \mathbf{Q} \cdot \hat{\mathbf{e}}_k}{c^2} E_s = 0. \end{cases} \quad (4.4)$$

If we consider a circularly polarized wave we have $E_s = \pm i E_p$ depending on whether the wave is right polarized or left polarized. From equation (4.4), by keeping only the first order term in \mathbf{Q} , we obtain as refractive index for circularly polarized waves

$$n_{R,L} = n \left(1 \pm \frac{1}{2} \mathbf{Q} \cdot \hat{\mathbf{e}}_k \right). \quad (4.5)$$

This means that left polarized waves or right polarized waves travel at a different speed producing a change of polarization of the transmitted waves, this is known as Faraday effect.

Consequently also the reflected waves have a different polarization depending

on the vector \mathbf{Q} , and hence on the magnetization \mathbf{M} . The reflected waves can be calculated using a matrix formalism

$$\begin{bmatrix} E_{rs} \\ E_{rp} \end{bmatrix} = \begin{bmatrix} r_{ss} & r_{sp} \\ r_{ps} & r_{pp} \end{bmatrix} \begin{bmatrix} E_{is} \\ E_{ip} \end{bmatrix} \quad (4.6)$$

where the first subscript of E denotes the reflected or the incident wave and the second subscript of E denotes the component along \hat{e}_s or along \hat{e}_p .

The reflectivity coefficients are given by

$$r_{pp} = \frac{n_2 \cos \theta_1 - n_1 \cos \theta_2}{n_2 \cos \theta_1 + n_1 \cos \theta_2} - \frac{2in_1n_2 \cos \theta_1 \sin \theta_2 Q_x}{(n_2 \cos \theta_1 + n_1 \cos \theta_2)^2} \quad (4.7)$$

$$r_{ps} = \frac{in_1n_2 \cos \theta_1 (Q_y \sin \theta_2 - Q_z \cos \theta_2)}{(n_2 \cos \theta_1 + n_1 \cos \theta_2)(n_1 \cos \theta_1 + n_2 \cos \theta_2) \cos \theta_2} \quad (4.8)$$

$$r_{sp} = \frac{in_1n_2 \cos \theta_1 (Q_y \sin \theta_2 + Q_z \cos \theta_2)}{(n_2 \cos \theta_1 + n_1 \cos \theta_2)(n_1 \cos \theta_1 + n_2 \cos \theta_2) \cos \theta_2} \quad (4.9)$$

$$r_{pp} = \frac{n_1 \cos \theta_1 - n_2 \cos \theta_2}{n_1 \cos \theta_1 + n_2 \cos \theta_2} \quad (4.10)$$

where n_1 and n_2 are the refractive indexes of the two media in absence of contribution from magnetization, and θ_1 and θ_2 are the angles of the incident and transmitted waves with the normal to the interface between the two media. In the experiments the rotation ϕ' and the ellipticity ϕ'' of the reflected wave are measured. In the case of incident electric field aligned with \hat{e}_s , these are given by

$$\phi' = \text{Re} \left[\frac{E_{rs}}{E_{rp}} \right] = \text{Re} \left[\frac{r_{ps}}{r_{ss}} \right], \quad \phi'' = \text{Im} \left[\frac{E_{rs}}{E_{rp}} \right] = \text{Im} \left[\frac{r_{ps}}{r_{ss}} \right], \quad (4.11)$$

while in case of incident electric field linearly polarized along \hat{e}_p they are given by

$$\phi' = \text{Re} \left[\frac{E_{rp}}{E_{rs}} \right] = \text{Re} \left[\frac{r_{sp}}{r_{pp}} \right], \quad \phi'' = \text{Im} \left[\frac{E_{rp}}{E_{rs}} \right] = \text{Im} \left[\frac{r_{sp}}{r_{pp}} \right]. \quad (4.12)$$

In order to measure dynamics that evolves in few picosecond, or even in few femtoseconds, it is useful the pump probe method. Assuming that it is possible to repeat the same experiment, the pump probe technique consists in sending the pump signal and the probe signal with a different delay in every replication of the experiment.

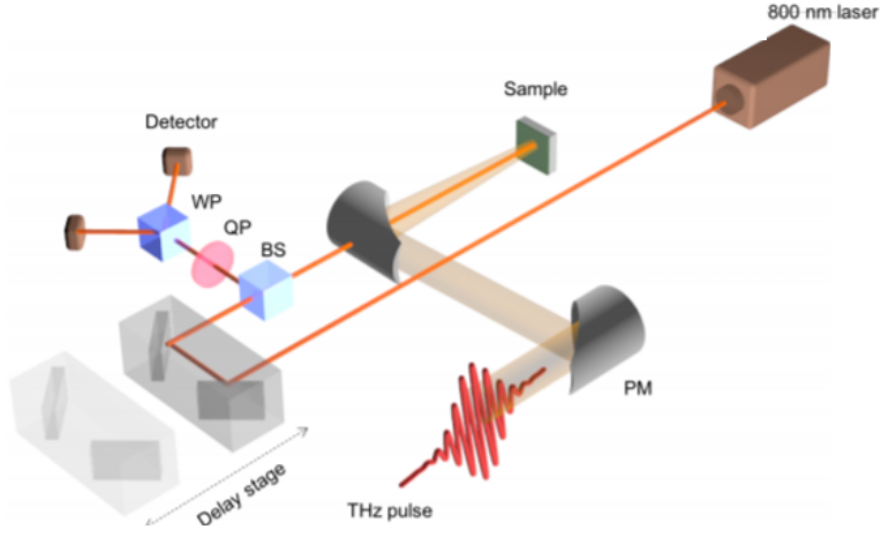


Figure 4.2: Setup of an experiment with pump probe measurement.

The pump signal is the one with high energy that triggers the phenomena of interest, while the probe signal is the one sent to the detector for the measurement. The signal is then reconstructed by using as elapsed time the delay between pump and probe instead of the actual time when the measure is obtained. An example of setup for the pump probe measurement is in figure 4.2.

4.2 Inertial magnetization dynamics

According to the Landau-Lifshitz-Gilbert equation, the dynamics of the magnetization \mathbf{M} in a ferromagnetic sample is described by the equation (1.82) here reported

$$\frac{d\mathbf{M}}{dt} = -\gamma_G \mathbf{M} \times \left(\mathbf{H}_{\text{eff}} - \frac{\alpha_G}{M_S} \frac{d\mathbf{M}}{dt} \right).$$

In the derivation of this equation, Gilbert introduced a Lagrangian for the ferromagnetic systems with an ad hoc inertia tensor. In this mechanical approach for describing the motion of spins the two principal moments of inertia are set to zero so that the inertial terms disappear from the dynamic equation. An inertial tensor of such kind is not physically correct as the same Gilbert noticed.

Despite its crudeness, this approximation turned out to be good enough to describe the dynamics of magnetization on time scales of 0.1 nanoseconds or longer, and the general validity of the equation at faster time scales was not questioned.

A full derivation of the inertial LLG equation was given later by Wegrowe et al. [56], and the three principal momenta of inertia were realistically set to non-zero values, which led to the so-called inertial LLG equation

$$\frac{d\mathbf{M}}{dt} = -\gamma_G \mathbf{M} \times \left[\mathbf{H}_{\text{eff}} - \frac{\alpha_G}{M_S} \left(\frac{d\mathbf{M}}{dt} + \tau \frac{d^2\mathbf{M}}{dt^2} \right) \right]. \quad (4.13)$$

The last term of equation (4.13) has a second derivative term due to angular momentum relaxation, in addition to the spin precession and the damping. It is noticed from simulations that, on time scales shorter than τ , nutation oscillations are observed on top of the precession motion, identifying a novel ‘nutation regime’ driven by the inertia that had never been experimentally observed before. On time scales longer than τ the usual Landau-Lifshitz-Gilbert equation is recovered. The possible large separation between the time scales of the two regimes would then explain the success of the standard Landau-Lifshitz-Gilbert equation in correctly describing magnetization dynamics for times larger than τ . The determination of the value of τ is however an open problem which needs to be addressed experimentally, as different theoretical works indicate values ranging from a few femtoseconds to hundreds of picoseconds. The qualitative difference of magnetization dynamics of (1.82) and (4.13) is shown in figure 4.3. In the following of the chapter the subscript G of α_G and γ_G are dropped to keep the notation simple.

4.3 Derivation of the inertial LLG equation

The derivation of the inertial Landau-Lifshitz-Gilbert equation (4.13) is based on the Lagrangian mechanic approach similar to the one developed in section 1.5.3. As a starting point we consider the equation of a rotating rigid body, in a body-fixed reference frame. The angular velocity vector reads

$$\begin{aligned} \Omega_1 &= \dot{\varphi} \sin \theta \sin \psi + \dot{\theta} \cos \psi, \\ \Omega_2 &= \dot{\varphi} \sin \theta \cos \psi - \dot{\theta} \sin \psi, \\ \Omega_3 &= \dot{\varphi} \cos \theta + \dot{\psi}. \end{aligned} \quad (4.14)$$

An illustration of the reference is shown in figure 4.4. For any vector \mathbf{M} of

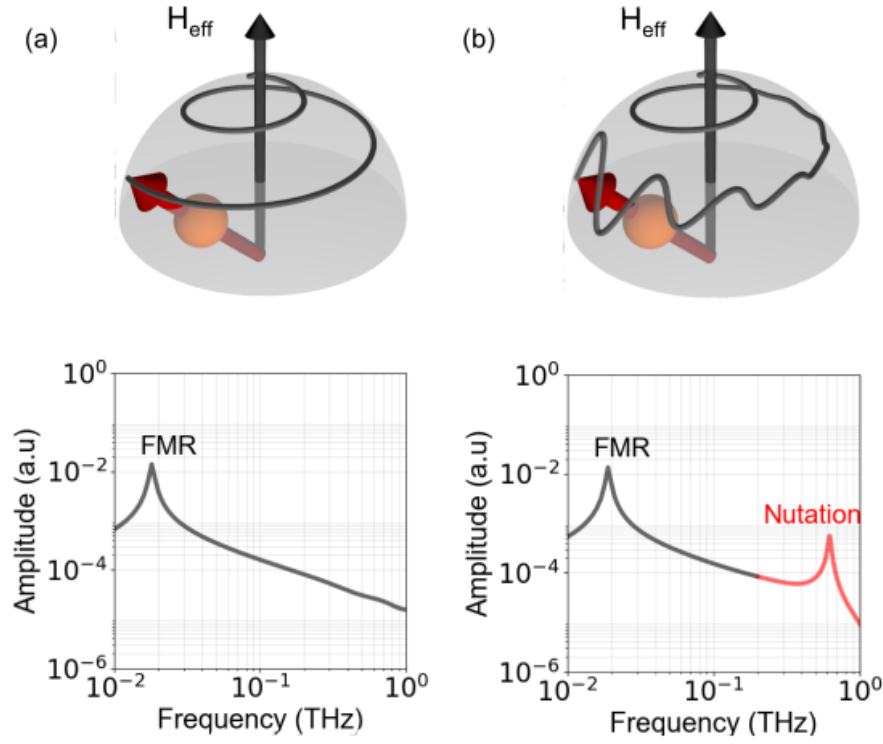


Figure 4.3: Magnetization dynamics without inertia (on the left) and with inertia (on the right). The inertial term causes the appearance of an oscillation around the usual precessional motion at high frequency. This oscillation is called nutation. The frequency response of the system has a second small resonance peak at higher frequencies.

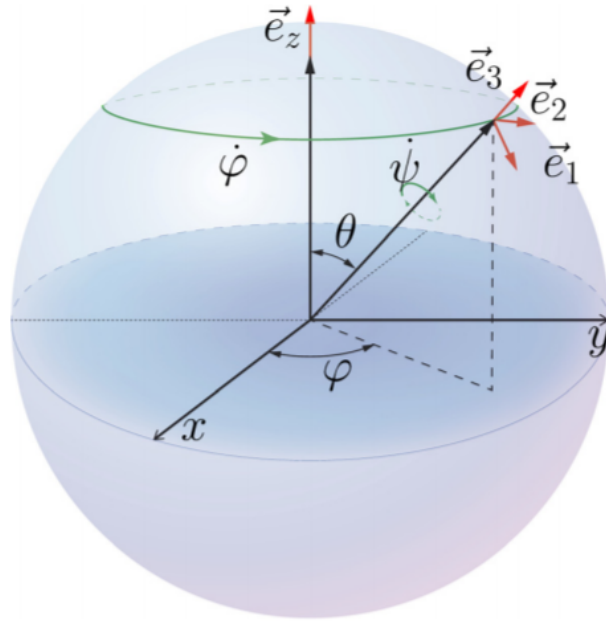


Figure 4.4: . Illustration of the coordinates system of the body fixed reference frame.

constant magnitude carried with the rotating body we have

$$\frac{d\mathbf{M}}{dt} = \boldsymbol{\Omega} \times \mathbf{M} . \quad (4.15)$$

This relation can be inverted by cross product multiplication of (4.15) by \mathbf{M} . By using $\mathbf{M} = M_S \hat{\mathbf{e}}_3$ we have

$$\boldsymbol{\Omega} = \frac{1}{M_S^2} \mathbf{M} \times \frac{d\mathbf{M}}{dt} + \Omega_3 \hat{\mathbf{e}}_3 . \quad (4.16)$$

Let us define the Lagrangian of the system as

$$\mathcal{L} = \frac{1}{2} I_1 (\Omega_1^2 + \Omega_2^2) + \frac{1}{2} I_3 \Omega_3^2 - G(\theta, \varphi) , \quad (4.17)$$

where G is the Gibbs-Landau free energy and we assume that two of the three principal momenta of inertia are equal.

The Euler-Lagrange equation, including the Rayleigh dissipation term, reads as in equation (1.80)

$$\frac{d}{dt} \frac{\partial \mathcal{L}(\mathbf{M}, \dot{\mathbf{M}})}{\partial \dot{\mathbf{M}}} - \frac{\partial \mathcal{L}(\mathbf{M}, \dot{\mathbf{M}})}{\partial \mathbf{M}} + \frac{\partial \mathcal{R}(\dot{\mathbf{M}})}{\partial \dot{\mathbf{M}}} = 0 ,$$

with $\mathcal{R} = \frac{\eta}{2} \dot{\mathbf{M}}^2 = \frac{1}{2} \eta M_S (\Omega_1^2 + \Omega_2^2)$.

By inserting (4.17) into it and using the expression of $\boldsymbol{\Omega}$ given in (4.14) we obtain

$$\begin{aligned} \frac{d}{dt} (I_1 \dot{\theta}) - I_1 \dot{\varphi}^2 \sin \theta \cos \theta + I_3 \dot{\varphi} \sin \theta (\dot{\varphi} \cos \theta + \dot{\psi}) &= \frac{\partial \mathcal{R}}{\partial \dot{\theta}} - \frac{\partial G}{\partial \theta} , \\ \frac{d}{dt} [I_1 \dot{\varphi} \sin^2 \theta + I_3 (\dot{\varphi} \cos \theta + \dot{\psi}) \cos \theta] &= \frac{\partial \mathcal{R}}{\partial \dot{\varphi}} - \frac{\partial G}{\partial \varphi} , \\ \frac{d}{dt} [I_3 (\dot{\varphi} \cos \theta + \dot{\psi})] &= \frac{d}{dt} (I_3 \Omega_3) = - \frac{\partial \mathcal{R}}{\partial \dot{\psi}} = 0 . \end{aligned} \quad (4.18)$$

The angular momentum is given by

$$\begin{bmatrix} L_1 \\ L_2 \\ L_3 \end{bmatrix} = \begin{bmatrix} I_1 & 0 & 0 \\ 0 & I_1 & 0 \\ 0 & 0 & I_3 \end{bmatrix} \begin{bmatrix} \Omega_1 \\ \Omega_2 \\ \Omega_3 \end{bmatrix} , \quad (4.19)$$

and the magnetization is proportional to the the angular momentum

$$\mathbf{M} = -\gamma L_3 \hat{\mathbf{e}}_3 = -\gamma I_3 \Omega_3 \hat{\mathbf{e}}_3 , \quad (4.20)$$

where γ is the gyromagnetic ratio already defined in section 1.5.1. The third equation of (4.18) simply states the conservation of the magnetization module, already stated in (4.15). After some calculations the first two equations of (4.18) yield

$$\begin{aligned}\dot{\Omega}_1 &= -\frac{\eta M_S^2}{I_1} \Omega_1 + \left(1 + \frac{I_3}{I_1}\right) \Omega_2 \Omega_3 - \frac{1}{I_1} \frac{\partial G}{\partial \theta}, \\ \dot{\Omega}_2 &= \frac{\eta M_S^2}{I_1} \Omega_2 - \left(1 + \frac{I_3}{I_1}\right) \Omega_1 \Omega_3 - \frac{1}{I_1 \sin \theta} \frac{\partial G}{\partial \varphi}.\end{aligned}\quad (4.21)$$

The two terms containing the derivative of the free energy are the components of the effective field perpendicular to \hat{e}_3 , namely

$$\mathbf{H}_{\text{eff}} \cdot \hat{e}_2 = \frac{1}{M_S} \frac{\partial G}{\partial \theta}, \quad \mathbf{H}_{\text{eff}} \cdot \hat{e}_1 = -\frac{1}{M_S \sin \theta} \frac{\partial G}{\partial \varphi}. \quad (4.22)$$

Since $\dot{\Omega}_3 = 0$, the equation (4.21) can be reformulated as

$$\dot{\boldsymbol{\Omega}} = -\frac{\eta M_S^2}{I_1} (\boldsymbol{\Omega} - \Omega_3 \hat{e}_3) + \frac{M_S}{\gamma} \left(\frac{1}{I_3} - \frac{1}{I_1} \right) (\boldsymbol{\Omega} \times \hat{e}_3) + \frac{M_S}{I_1} (\hat{e}_3 \times \mathbf{H}_{\text{eff}}). \quad (4.23)$$

Finally, replacing (4.16) and (4.20) into the last equation yields

$$\frac{d\mathbf{M}}{dt} = -\gamma \mathbf{M} \times \mathbf{H}_{\text{eff}} - \gamma \eta \mathbf{M} \times \frac{d\mathbf{M}}{dt} - \gamma \eta \tau \mathbf{M} \times \frac{d^2 \mathbf{M}}{dt^2}, \quad (4.24)$$

where we set $\tau = \frac{I_1}{\eta M_S}$.

It is worthy to notice that the standard Gilbert equation is obtained if $I_1 = 0$, and the proportionality between the angular momentum \mathbf{L} and the magnetization \mathbf{M} is also restored.

4.4 Analysis of the iLLG equation

In order to clearly understand the experimental data, some analytics on the LLG equation with inertia must be introduced. Let us consider a ferromagnetic thin film, and denote \hat{e}_z the unit vector perpendicular to the film. An external magnetic field is applied and no material anisotropy is present. Moreover we assume the magnetization to be uniform over space. The applied field is given

by the sum of a constant field perpendicular to \hat{e}_x and a time varying magnetic field H_{THz} parallel to \hat{e}_x

$$\mathbf{H}_a = H_{\text{THz}}(t)\hat{e}_x + H_{\parallel}\hat{e}_y + H_{\perp}\hat{e}_z . \quad (4.25)$$

We also define a spherical coordinates system, the semiaxis $\theta = 0$ is the positive part of the z axis, while the semiaxis $\varphi = 0$ is represented by the positive part of the x axis. In this case the transformation from cartesian to polar coordinates is given by

$$\begin{aligned} H_r &= H_x \cos \varphi \sin \theta + H_y \sin \varphi \sin \theta + H_z \cos \theta , \\ H_{\theta} &= H_x \cos \varphi \cos \theta + H_y \sin \varphi \cos \theta - H_z \sin \theta , \\ H_{\varphi} &= -H_x \sin \varphi + H_y \cos \varphi . \end{aligned} \quad (4.26)$$

The LLG equation can hence be written in spherical coordinates as

$$\alpha\tau\ddot{\theta} = \alpha\tau\dot{\varphi}^2 \sin \theta \cos \theta + \gamma H_{\text{eff}\theta} - \alpha\dot{\theta} - \dot{\varphi} \sin \theta , \quad (4.27)$$

$$\alpha\tau \sin \theta \ddot{\varphi} = -2\alpha\tau\dot{\theta}\dot{\varphi} \cos \theta + \gamma H_{\text{eff}\varphi} - \alpha\dot{\varphi} \sin \theta + \dot{\theta} . \quad (4.28)$$

From these equations the equilibrium $\{\theta_0, \varphi_0\}$ can be immediately found by setting all the derivatives equal to zero. These are of course also the equilibrium points of the standard Landau-Lifshitz-Gilbert equation

$$\begin{aligned} H_{\text{eff}\varphi} &= H_y \cos \varphi_0 = 0 \implies \varphi_0 = \pm \frac{\pi}{2} , \\ H_{\text{eff}\theta} &= \pm H_{\parallel} \cos \theta_0 - H_z \sin \theta_0 + \frac{1}{2}DM_s \sin 2\theta_0 = 0 . \end{aligned} \quad (4.29)$$

Linearization of the Gilbert equation with inertia

For the linearization of the iLLG equation (4.13) it is convenient to define an appropriate cartesian reference frame depending on the equilibrium point. Let $\{\theta_0, \pi/2\}$ be the angular coordinates of the equilibrium point. The cartesian reference frame is defined by three axis $\{\hat{e}_r, \hat{e}_{\theta}, \hat{e}_{\varphi}\}$, where \hat{e}_r is parallel to the magnetization at equilibrium, and \hat{e}_{φ} and \hat{e}_{θ} point in the direction of increasing φ and θ respectively

$$\begin{aligned} \hat{e}_r &= \sin \theta_0 \hat{e}_y + \cos \theta_0 \hat{e}_z & \hat{e}_{\varphi} &= -\hat{e}_x \\ \hat{e}_{\theta} &= \sin \theta_0 \hat{e}_y - \cos \theta_0 \hat{e}_z \end{aligned} \quad (4.30)$$

The reference frame is shown in figure 4.5.

The projections of equations (4.27) and (4.28) on \hat{e}_φ and \hat{e}_θ , approximated to the first order in δM_φ and δM_θ , and their derivatives give

$$\begin{aligned}\alpha\tau\delta\ddot{M}_\varphi &= \gamma M_s H_\varphi - \gamma H_r \delta M_\varphi - \alpha\delta\dot{M}_\varphi + \delta\dot{M}_\theta, \\ \alpha\tau\delta\ddot{M}_\theta &= \gamma M_s H_\theta - \gamma H_r \delta M_\theta - \alpha\delta\dot{M}_\theta - \delta\dot{M}_\varphi,\end{aligned}\quad (4.31)$$

where the magnetic fields H_φ , H_θ and H_r are given by

$$\begin{aligned}H_\varphi &= -H_{\text{THz}} & H_\theta &= D\delta M_\theta \sin^2 \theta_0 & \text{to order one} \\ H_r &= H_\parallel \sin \theta_0 + H_\perp \cos \theta_0 - DM_s \cos^2 \theta_0 & & & \text{to order zero}\end{aligned}\quad (4.32)$$

Equations (4.31) then become

$$\begin{aligned}\alpha\tau\delta\ddot{M}_\varphi &= -\gamma(H_\parallel \sin \theta_0 + H_\perp \cos \theta_0 - DM_s \cos^2 \theta_0)\delta M_\varphi \\ &\quad - \alpha\delta\dot{M}_\varphi + \delta\dot{M}_\theta - \gamma M_s H_{\text{THz}}, \\ \alpha\tau\delta\ddot{M}_\theta &= -\gamma(H_\parallel \sin \theta_0 + H_\perp \cos \theta_0 - DM_s \cos^2 \theta_0)\delta M_\theta \\ &\quad - \alpha\delta\dot{M}_\theta - \delta\dot{M}_\varphi - \gamma DM_s \sin^2 \theta_0 \delta M_\theta.\end{aligned}\quad (4.33)$$

By using $h(H_\parallel, H_\perp, DM_s) = H_\parallel \sin \theta_0 + H_\perp \cos \theta_0 - DM_s \cos^2 \theta_0$, (4.31) can be expressed in its state-space form as

$$\begin{aligned}\alpha\tau \frac{d}{dt} \begin{bmatrix} \delta M_\varphi \\ \delta M_\theta \\ \delta\dot{M}_\varphi \\ \delta\dot{M}_\theta \end{bmatrix} &= \begin{bmatrix} 0 & 0 & \alpha\tau & 0 \\ 0 & 0 & 0 & \alpha\tau \\ -\gamma h & 0 & -\alpha & +1 \\ 0 & -\gamma(h + DM_s \sin^2 \theta_0) & -1 & -\alpha \end{bmatrix} \begin{bmatrix} \delta M_\varphi \\ \delta M_\theta \\ \delta\dot{M}_\varphi \\ \delta\dot{M}_\theta \end{bmatrix} - \gamma M_s \begin{bmatrix} 0 \\ 0 \\ H_{\text{THz}} \\ 0 \end{bmatrix}.\end{aligned}\quad (4.34)$$

Alternatively the transfer function representation can be used, by Fourier transforming equation (4.33). It yields

$$\begin{aligned}(\alpha\tau\omega^2 - i\alpha\omega - \gamma h)\delta\hat{M}_\varphi + i\omega\delta\hat{M}_\theta &= \gamma M_s \hat{H}_{\text{THz}} \\ -i\omega\delta\hat{M}_\varphi + (\alpha\tau\omega^2 - i\alpha\omega - \gamma(h + DM_s \sin^2 \theta_0))\delta\hat{M}_\theta &= 0\end{aligned}\quad (4.35)$$

where the hat “^” indicates the Fourier transform, in matrix form it reads

$$\begin{bmatrix} \delta \hat{M}_\varphi \\ \delta \hat{M}_\theta \end{bmatrix} = \begin{bmatrix} \alpha\tau\omega^2 - i\alpha\omega - \gamma h & i\omega \\ -i\omega & \alpha\tau\omega^2 - i\alpha\omega - \gamma(h + DM_s \sin^2 \theta_0) \end{bmatrix}^{-1} \begin{bmatrix} \gamma M_s \hat{H}_{\text{THz}} \\ 0 \end{bmatrix}. \quad (4.36)$$

The imaginary parts of the eigenvalues of the matrices in (4.34) give the frequencies of the ferromagnetic resonance and the nutation. In order to easily find these frequencies we neglect the imaginary part and look for the poles of the transfer function (4.36). The following equation in ω^2 is obtained

$$\alpha^2 \tau^2 \omega^4 - (2\gamma\alpha\tau h + \gamma\alpha\tau DM_s \sin^2 \theta_0 + 1)\omega^2 + \gamma^2 h(h + DM_s \sin^2 \theta_0) = 0. \quad (4.37)$$

Formula (4.37) contains as special case the Kittel frequency, seen in section 2.3. By choosing $\tau = 0$ equation (4.37) becomes

$$\omega = |\gamma| \sqrt{(H_\parallel \sin \theta_0 + H_\perp \cos \theta_0 - DM_s \cos^2 \theta_0)} \cdot \sqrt{(H_\parallel \sin \theta_0 + H_\perp \cos \theta_0 - DM_s (\cos^2 \theta_0 - \sin^2 \theta_0))}. \quad (4.38)$$

It can be particularized for $H_\parallel = 0$ or $H_\perp = 0$ and yields respectively

$$\omega_{k\perp} = |\gamma| \sqrt{(H_\perp - DM_s)^2} \quad \text{and} \quad \omega_{k\parallel} = |\gamma| \sqrt{H_\parallel (H_\parallel + DM_s)}$$

where the formula for $\omega_{k\perp}$ holds only for $H_\perp \geq DM_s$, otherwise no stable equilibrium is possible.

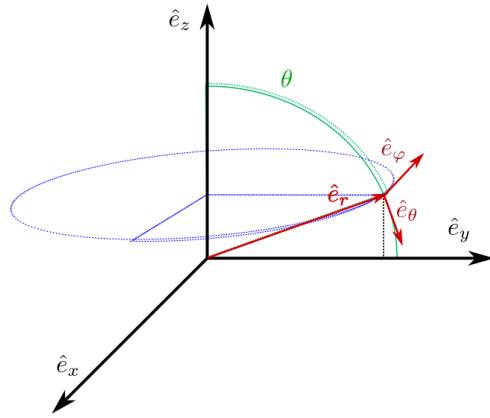


Figure 4.5: Reference frame used for the linearization in section 4.4

In Plane Applied Field

It is worthy giving particular attention to the case of an in-plane applied field, since it is used for the setup of the experiment of the next section. We have

$$H_{\perp} = 0 \implies \theta_0 = \pi/2 \implies h = H_{\parallel}.$$

In this specific condition (4.36) becomes

$$\begin{bmatrix} \delta \hat{M}_{\varphi} \\ \delta \hat{M}_{\theta} \end{bmatrix} = \begin{bmatrix} \alpha\tau\omega^2 - i\alpha\omega - \gamma H_{\parallel} & i\omega \\ -i\omega & \alpha\tau\omega^2 - i\alpha\omega - \gamma(H_{\parallel} + DM_s) \end{bmatrix}^{-1} \begin{bmatrix} \gamma M_s \hat{H}_{\text{THz}} \\ 0 \end{bmatrix}. \quad (4.39)$$

By computing the inverse matrix the expressions for $\delta \hat{M}_{\varphi}$ and $\delta \hat{M}_{\theta}$ are obtained

$$\delta M_{\theta} = - \frac{(\alpha\tau\omega^2 - i\alpha\omega - \gamma H_{\parallel} - \gamma DM_s) \gamma M_s \hat{H}_{\text{THz}}}{(\alpha\tau\omega^2 - \gamma H_{\parallel} - i\alpha\omega)(\alpha\tau\omega^2 - \gamma H_{\parallel} - \gamma DM_s - i\alpha\omega) - \omega^2}, \quad (4.40)$$

$$\delta M_{\varphi} = - \frac{i\omega \gamma M_s \hat{H}_{\text{THz}}}{(\alpha\tau\omega^2 - \gamma H_{\parallel} - i\alpha\omega)(\alpha\tau\omega^2 - \gamma H_{\parallel} - \gamma DM_s - i\alpha\omega) - \omega^2}. \quad (4.41)$$

If the imaginary part is neglected (which means neglecting the damping), the maximum of the response occurs at the zero of the denominator, i.e.

$$\alpha^2 \tau^2 \omega^4 - (\gamma \alpha \tau (2H_{\parallel} + M_s) + 1) \omega^2 + \gamma^2 H_{\parallel} (H_{\parallel} + M_s) = 0. \quad (4.42)$$

A further simplification arises if the ferromagnetic resonance frequency is much smaller than the nutation frequency

$$\omega \approx \sqrt{\frac{\gamma \alpha \tau (2H_{\parallel} + M_s) + 1}{\alpha^2 \tau^2}} \approx \frac{1}{\alpha \tau}. \quad (4.43)$$

The amplitude and the phase of (4.39) are reported (in logarithmic scale) in figure 4.6 for δM_{θ} and in figure 4.7 for δM_{φ} .

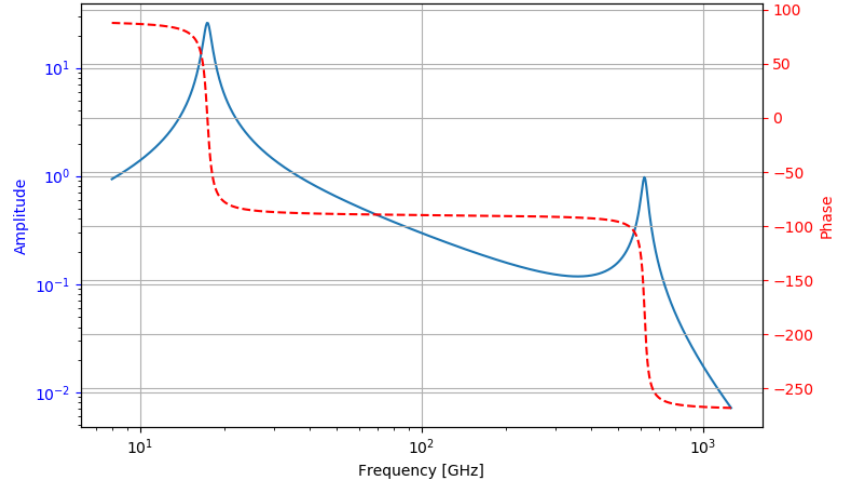


Figure 4.6: Amplitude and phase of the Transfer function (4.41) in logarithmic scale. The parameters are $\tau = 10.66$ ps, $\alpha = 0.025$ and $\mu_0 H_{\text{DC}} = 0.3$ T

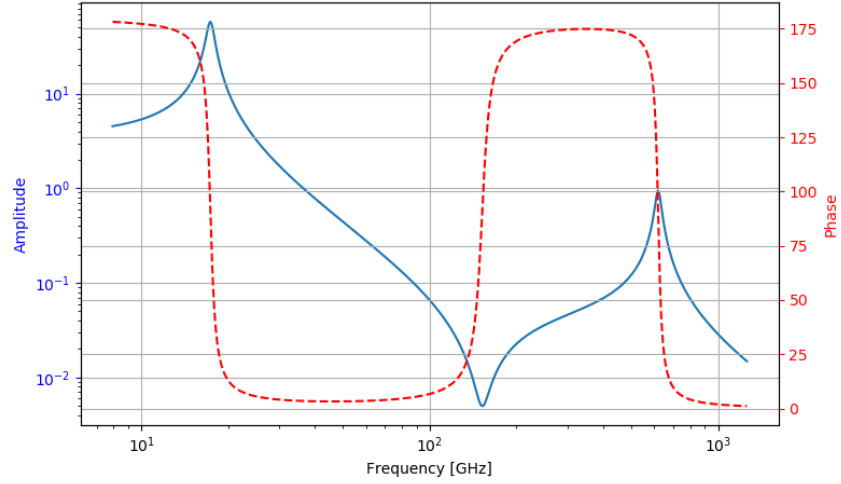


Figure 4.7: Amplitude and phase of the Transfer function (4.40) in logarithmic scale. The parameters are $\tau = 10.66$ ps, $\alpha = 0.025$ and $\mu_0 H_{\text{DC}} = 0.3$ T

4.5 Experimental evidence of inertial dynamics in a ferromagnet

In order to experimentally detect nutations, it is necessary to perform magnetic field spectroscopy in the terahertz range, a task which was technically unfeasible until very recently, when intense terahertz sources started becoming available.

Intense and tunable narrow-band terahertz magnetic fields can now be generated at superradiant electron sources such as the TELBE facility in Dresden, Germany [78], [79], where the experiments reported in [81] were executed.

In such experiments Neeraj et al [81] used intense narrow-band terahertz magnetic fields to detect inertial magnetization effects in ferromagnetic thin films. The basic idea is to perform a forced oscillator experiment as a function of the frequency of the terahertz magnetic field \mathbf{H}_{THz} , and detect amplitude and phase of the response with the femtosecond MOKE, in the attempt to observe the signature of a resonance.

Three different thin film samples were investigated, all with easy-plane magnetization: amorphous CoFeB grown on Si/SiO₂ substrate, and two epitaxial and polycrystalline permalloy grown on single crystal MgO (100) and (111) substrates respectively.

Figure 4.8 shows the amplitude of the femtosecond MOKE response of the three ferromagnetic thin film samples after excitation with narrowband terahertz pulses with a center frequency of 0.4, 0.6 and 0.8 THz.

In all cases, the observed response of the magnetization confirms the analogy with a forced oscillator, where the terahertz magnetic field acts as the driving periodic force.

The modulation of the amplitude of the response suggests already the presence of an underlying resonance at approximately 0.6 THz superimposed to the purely off-resonant forced response of lower amplitude. To further validate this point, Fig. 4.9 shows the relative phase shift between the integral of the driving force (reconstructed independently via experimental electrooptical sampling) and the experimental MOKE signal far away from the maximum response (0.4 THz) and at the maximum response (0.6 THz).

The data show that at 0.4 THz the magnetization precession is in phase with the driving field. This is also reproduced by simulations solving the inertial LLG equation (4.13) including the experimentally measured terahertz magnetic field as the driving force.

At 0.6 THz, on the other hand, magnetization precession and driving field are

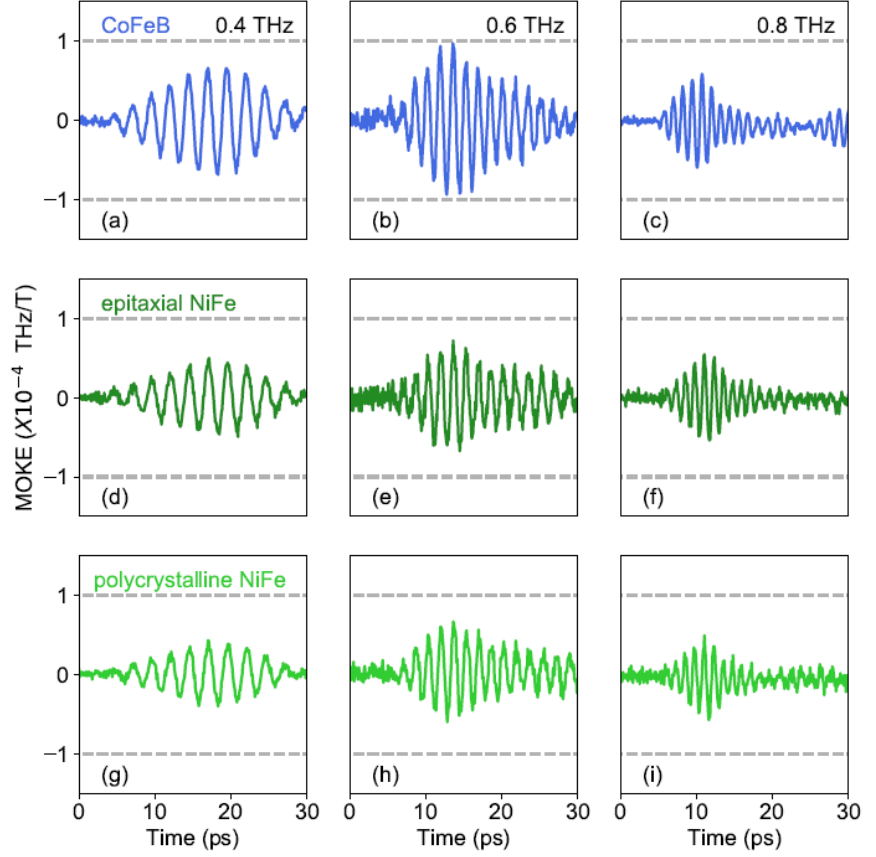


Figure 4.8: Time-resolved magneto-optical Kerr (MOKE) response of the magnetisation to narrowband terahertz fields centered around 0.4, 0.6 and 0.8 THz for (a)-(c) an amorphous CoFeB film on silicon, (d)-(f) an epitaxial $\text{Ni}_{81}\text{Fe}_{19}$ (permalloy) film grown on MgO (100) substrate and (g)-(i) of a polycrystalline $\text{Ni}_{81}\text{Fe}_{19}$ deposited on MgO (111) substrate [81].

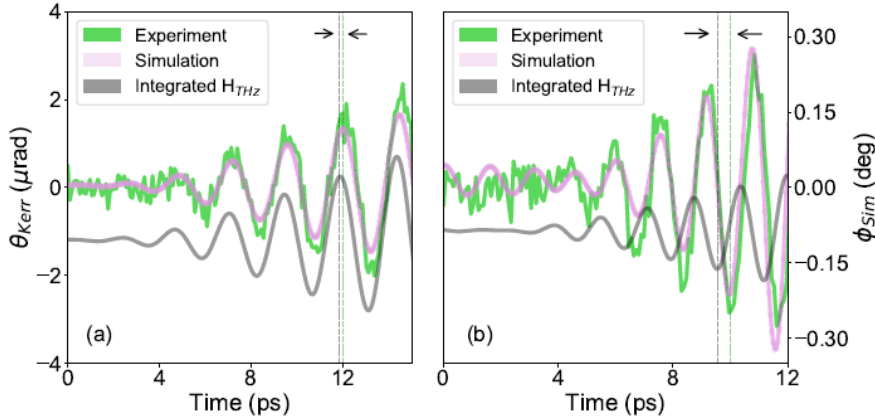


Figure 4.9: Comparison of the phase resolved response at (a) 0.4 THz and (b) 0.6 THz center frequency of the terahertz magnetic field pulse for the polycrystalline permalloy film. Green curves: experimentally measured magneto-optical Kerr rotations. Pink curves: simulated response using the inertial LLG equation (4.13) with $\tau = 11.3$ ps and using the experimentally measured \mathbf{H}_{THz} field amplitude. The right vertical axis is the simulated nutation angle. Grey curves: time integral of the experimental terahertz magnetic field \mathbf{H}_{THz} .

approximately 90 degrees out of phase, as reproduced also by the simulations. This evidence provides further support to the statement that an underlying resonance is present in the system, at a frequency two orders of magnitude higher than any known ferromagnetic resonance, and which is determined by one single parameter τ .

In order to estimate the value of τ from the experiments, figure 4.10 plots the amplitude of the measured response at six different frequencies. A fit with a Lorentzian curve was used to return the center frequency ω_n and the nutation frequency, which is

$$\omega_n \approx \frac{1}{\alpha\tau}. \quad (4.44)$$

Gilbert damping constant α was measured independently with ferromagnetic resonance spectroscopy in all three samples and the corresponding τ was extracted, with the results summarized in Table 4.1. The outcome of numerical calculations that solve the inertial LLG equation with these values of τ are shown in figure 4.10, and reproduce the main features of the experimental

data.

In conclusion, a narrowband terahertz magnetic fields is used to drive magne-

Sample	$\frac{\omega_n}{2\pi}$ (THz)	FWHM (THz)	α	τ (ps)
CoFeB	0.59 ± 0.13	0.52	0.0044	60.5 ± 13.3
epitaxial NiFe	0.62 ± 0.12	0.57	0.0058	44.0 ± 8.5
polycrystalline Nife	0.61 ± 0.12	0.58	0.0230	11.3 ± 2.2

Table 4.1: The center frequency $f_n = \omega_n/(2\pi)$ and the full-width half maximum (FWHM) are the parameters extracted from the Lorentzian fit of the experimental data plotted in figure 4.10 for all three samples. The Gilbert damping α was measured independently. The angular momentum relaxation time τ is calculated using the approximation of equation (4.44).

tization dynamics in thin ferromagnetic films, which is probed with the femtosecond magneto-optical Kerr effect. By analyzing both amplitude and phase of the response, a broad resonance at approximately 0.6 THz is detected, which is ascribed to the presence of a nutation spin resonance excited by the terahertz magnetic field. Experimental observations are in good agreement with numerical simulations performed with the inertial version of the LLG equation using the angular momentum relaxation time τ extracted from the experimental data. These results allow a better understanding of the fundamental mechanisms of ultrafast demagnetization and reversal, with interesting implications for the realization of faster and more efficient magnetic data storage.

4.6 Spin waves in thin films

A strong magnetic field is used in the experiment for the detection of nutations. The field can cause the generation of nonuniformities in the magnetization even when the field is uniform. For this reason an investigation on the entity of such nonuniformities is necessary to motivate the use of a macrospin model.

SpinWave Calculation

The system considered here and the reference frame are the same used in section 4.2, i.e. a thin film with normal unit vector \hat{e}_z , a constant applied field

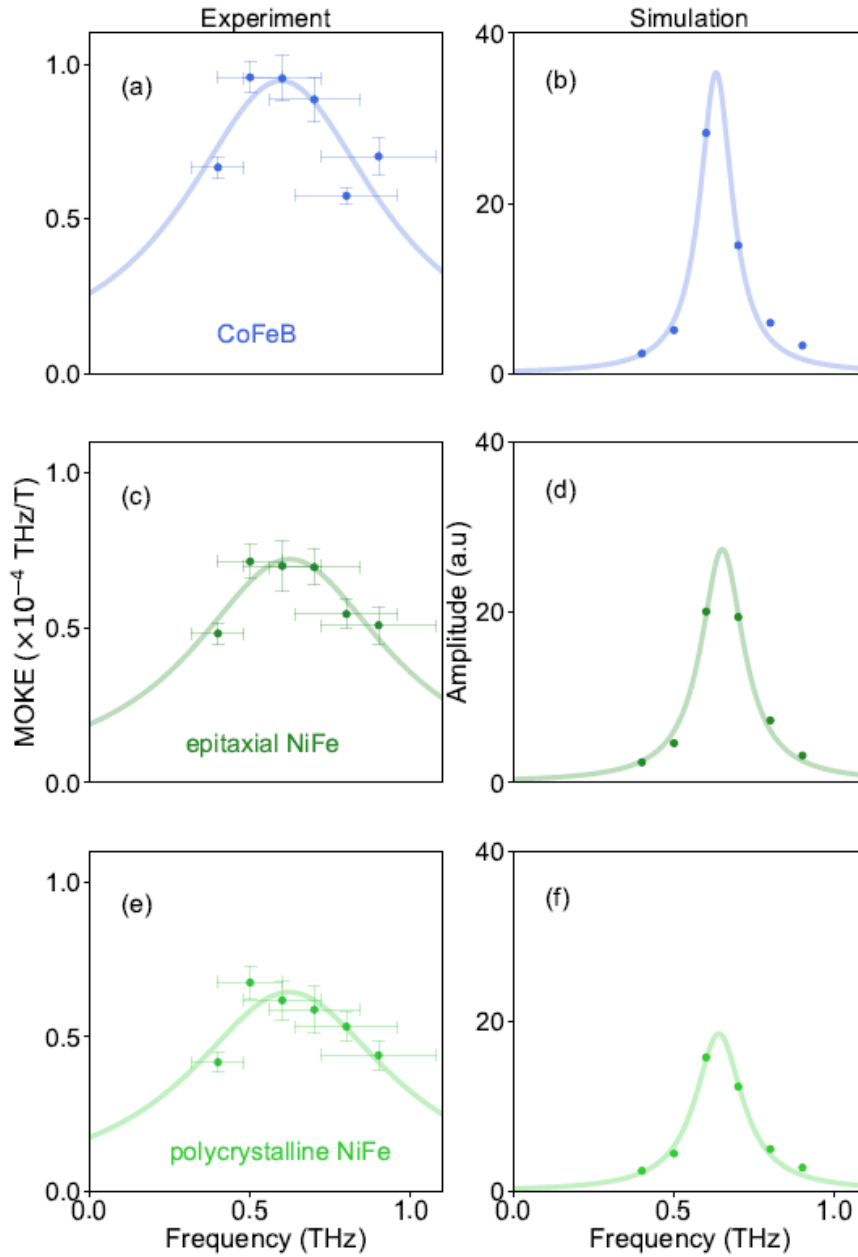


Figure 4.10: Symbols: (a), (c), (e) experimentally measured maximum MOKE amplitude normalized according to equation (3) for CoFeB, epitaxial NiFe and, respectively, polycrystalline NiFe; (b), (d), (f) calculated maximum magnetization response amplitude solving the inertial LLG equation. Solid lines: Lorentzian fit to the data points.

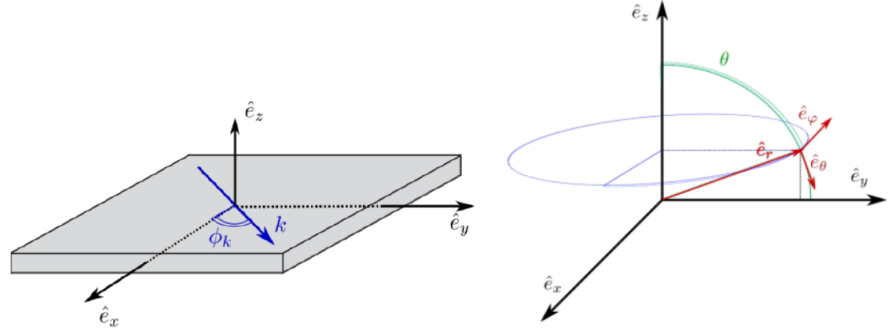


Figure 4.11: Reference frame for the calculations of section 4.6.

in the zy plane and a time dependent magnetic field in the x direction. The geometry is represented in figure (4.11).

We assume the magnetization to be a function of x and y only and the film to be large enough to neglect the effect of boundaries in the area of interest.

We expect the equilibrium magnetization to be homogeneous. The stable equilibrium can be represented in angular coordinates $\{\theta_0, \pi/2\}$ where θ_0 must satisfy $\mathbf{M} \cdot \mathbf{H}_a > 0$ and

$$H_{\parallel} \cos \theta_0 + H_{\perp} \sin \theta_0 - M_S \cos \theta_0 \sin \theta_0 = 0, \quad (4.45)$$

where H_{\parallel} and H_{\perp} are the components of \mathbf{H}_a along \hat{e}_y and \hat{e}_z respectively.

Let us consider a different cartesian reference frame for the linearization, as in section 4.2,

$$\hat{e}_r = \sin \theta_0 \hat{e}_y + \cos \theta_0 \hat{e}_z, \quad \hat{e}_{\varphi} = -\hat{e}_x, \quad \hat{e}_{\theta} = \cos \theta_0 \hat{e}_y - \sin \theta_0 \hat{e}_z. \quad (4.46)$$

The reference frame is shown in the right panel of figure 4.11.

At the equilibrium we have $M_{r0} = M_S$, $M_{\varphi 0} = 0$ and $M_{\theta 0} = 0$. Developing the Landau-Lifshitz-Gilbert equation with the perturbation method up to the first order in δM_{ϕ} and δM_{θ} yields

$$\begin{aligned} \delta \dot{M}_{\theta} - \alpha \delta \dot{M}_{\varphi} &= -M_S \gamma \delta H_{\text{eff}, \varphi} + \gamma H_{\text{eff}, r0} \delta M_{\varphi}, \\ \delta \dot{M}_{\varphi} + \alpha \delta \dot{M}_{\theta} &= +M_S \gamma \delta H_{\text{eff}, \theta} - \gamma H_{\text{eff}, r0} \delta M_{\theta}, \end{aligned} \quad (4.47)$$

where the equilibrium effective field is a known term

$$H_{\text{eff}, r0} = H_{\parallel} \sin \theta_0 + H_{\perp} \cos \theta_0 - M_S \cos^2 \theta_0. \quad (4.48)$$

Including the Teraheartz applied field as perturbation of the applied field, the first order perturbation of the effective field is given by

$$\begin{aligned}\delta H_{\text{eff},\varphi} &= -\delta H_x(\mathbf{r}, t) + \ell_{EX}^2 \nabla^2 \delta M_\varphi + \delta H_{M\varphi}[\delta \mathbf{M}] , \\ \delta H_{\text{eff},\theta} &= \ell_{EX}^2 \nabla^2 \delta M_\theta + \delta H_{M\theta}[\delta \mathbf{M}] ,\end{aligned}\quad (4.49)$$

where $\delta H_{M\theta}$ and $\delta H_{M\varphi}$ are the demagnetizing field generated along \hat{e}_θ and along \hat{e}_φ respectively, their expression are in appendix D.

Let us consider solutions of the type

$$\delta \mathbf{M} = \text{Re} \left[c_{\theta \mathbf{k}}(t) e^{j\mathbf{k}\cdot\mathbf{r}} \right] \hat{e}_\theta + \text{Re} \left[c_{\varphi \mathbf{k}}(t) e^{j\mathbf{k}\cdot\mathbf{r}} \right] \hat{e}_\varphi , \quad (4.50)$$

with \mathbf{k} lying in the xy plane and where the c 's are complex coefficients. Under this hypothesis the demagnetizing field can be calculated exactly. The detailed calculations are shown in the appendix D, eventually we have for the demagnetizing field

$$\delta \mathbf{H}_M = (1 - S_{\mathbf{k}})(\delta M_\varphi \cos \phi_k - \delta M_\theta \cos \theta_0 \sin \phi_k) \hat{e}_{\mathbf{k}} + S_{\mathbf{k}} \delta M_\theta \sin \theta_0 \hat{e}_z \quad (4.51)$$

where ϕ_k is the angle between \mathbf{k} and \hat{e}_x ,

$$S_{\mathbf{k}} = \frac{1 - \exp(-|\mathbf{k}|d)}{|\mathbf{k}|d} , \quad (4.52)$$

and d is the thickness of the thin film.

To keep notation simple we define

$$\begin{aligned}D_{\theta\theta} &= -((1 - S_{\mathbf{k}}) \cos^2 \theta_0 \sin^2 \phi_k + S_{\mathbf{k}} \sin^2 \theta_0) , \\ D_{\theta\varphi} &= \frac{1}{2}(1 - S_{\mathbf{k}}) \cos \theta_0 \sin(2\phi_k) = D_{\varphi\theta} , \\ D_{\varphi\varphi} &= -(1 - S_{\mathbf{k}}) \cos^2 \phi_k .\end{aligned}$$

The components of the effective field are given by

$$\begin{aligned}\delta H_{M\theta} &= D_{\theta\theta} \delta M_\theta + D_{\theta\varphi} \delta M_\varphi & \nabla^2 \delta M_\theta &= -k^2 \delta M_\theta \\ \delta H_{M\varphi} &= D_{\varphi\theta} \delta M_\theta + D_{\varphi\varphi} \delta M_\varphi & \nabla^2 \delta M_\varphi &= -k^2 \delta M_\varphi\end{aligned} , \quad (4.53)$$

where the coefficients D depend on \mathbf{k} although not explicitly shown in the notation.

By applying space Fourier transform to the LLG equation

$$\mathcal{F}_{\mathbf{x}}[\mathbf{M}](\mathbf{k}, t) = \int_{\mathbb{R}^3} \mathbf{M}(\mathbf{x}, t) e^{-i\mathbf{k}\cdot\mathbf{x}} dV , \quad (4.54)$$

the space dependence of the magnetization is removed. In matrix form it reads

$$\begin{bmatrix} 1 & -\alpha \\ +\alpha & 1 \end{bmatrix} \frac{d}{dt} \begin{bmatrix} c_{\theta\mathbf{k}} \\ c_{\varphi\mathbf{k}} \end{bmatrix} = \gamma M_S \begin{bmatrix} \mathcal{F}_{\mathbf{x}}[\delta H_x] \\ 0 \end{bmatrix} + \gamma \begin{bmatrix} -M_S D_{\varphi\theta} & M_S(\ell_{EX}^2 k^2 - D_{\varphi\varphi}) + H_{\text{eff},r0} \\ -M_S(\ell_{EX}^2 k^2 - D_{\theta\theta}) - H_{\text{eff},r0} & M_S D_{\theta\varphi} \end{bmatrix} \begin{bmatrix} c_{\theta\mathbf{k}} \\ c_{\varphi\mathbf{k}} \end{bmatrix} \quad (4.55)$$

The equation (4.55) can be used to compute the dispersion relation of the system. If we set $\alpha = 0$ the eigenvalues of the dynamic matrix of the system are pure imaginary. The secular equation gives

$$\lambda^2 = \gamma^2 M_S^2 \left[D_{\varphi\theta}^2 - \left(\ell_{EX}^2 k^2 - D_{\varphi\varphi} + \frac{H_{\text{eff},r0}}{M_S} \right) \left(\ell_{EX}^2 k^2 - D_{\theta\theta} + \frac{H_{\text{eff},r0}}{M_S} \right) \right] \quad (4.56)$$

This formula contains also the Kittel frequency (2.43) for the ferromagnetic resonance in the limit $k \rightarrow 0$ and the above equation becomes

$$\lambda^2 = -\gamma^2 [H_{\text{eff},r0} (H_{\text{eff},r0} + M_S \sin^2 \theta_0)] . \quad (4.57)$$

Notice that equation (4.57) also shows that when $k \rightarrow 0$ the dependence on ϕ disappears as expected.

Dispersion relation of forward and backward spin waves are contained in equation (4.56) as well. In particular if $H_{\perp} > M_S$ and, $H_{\parallel} = 0$ the equilibrium magnetization occurs out of plane and we have forward volume spin waves

$$\lambda^2 = -\gamma^2 (H_{\perp} - M_S) (H_{\perp} - M_S S_{\mathbf{k}}) . \quad (4.58)$$

If instead we have $H_{\perp} = 0$ the equilibrium magnetization is in plane and (4.56) becomes

$$\lambda^2 = -\gamma^2 (M_S(1 - S_{\mathbf{k}}) \cos^2 \phi_k + H_{\parallel}) (M_S S_{\mathbf{k}} + H_{\parallel}) . \quad (4.59)$$

In particular for $\phi_k = \pi/2$ the vector \mathbf{k} and the equilibrium magnetization are aligned and we have the formula of the backward volume spin waves

$$\lambda^2 = -\gamma^2 H_{\parallel} (H_{\parallel} + M_S S_{\mathbf{k}}) . \quad (4.60)$$

Demagnetization due to spin waves

In order to quantify the impact of nonuniformity in Teraheertz experiments we consider a different experimental case described in [82]. This experiment

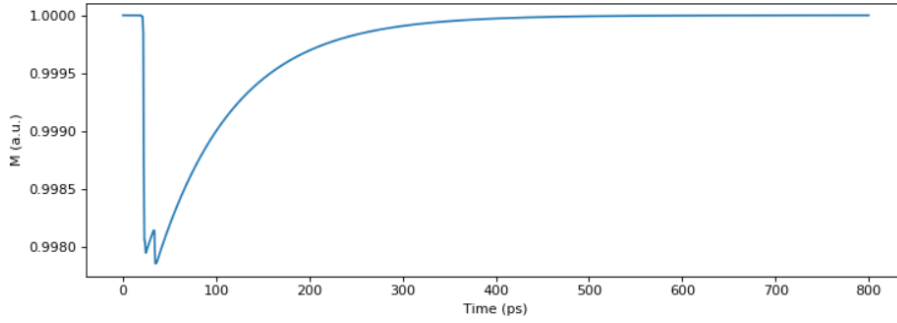


Figure 4.12: Relative reduction of magnetization module measured in the experiment [82].

is based on a similar experimental setup relying on the MOKE and the pump probe method.

It is noticed that an intense ultrafast magnetic pulse can cause a reduction of the magnetization module measured of 0.2%, as shown in figure 4.12.

Let us consider a thin film with $\alpha = 0.007$, $\ell_{EX} = 4.4$ nm and $M_S = 1.84$ T. A constant magnetic field of 0.448 T is applied along the out of plane direction and a weaker constant field of 0.056 T is applied in plane as pictured in the figure 4.13. A Teraheertz magnetic field is applied in plane. This field is perpendicular to the constant applied field. According to experimental measurements we assume

$$\mathbf{H}_{\text{THz}} = -0.06(\sigma_t^2 - t^2) \exp\left(\frac{1}{2} \frac{t^2}{\sigma_t^2}\right) \exp\left(\frac{x^2}{\sigma_x^2}\right) \hat{\mathbf{e}}_x, \quad (4.61)$$

with $\sigma_t = 0.5$ ps and $\sigma_x = 0.5$ mm. The field intensity as function of time is shown in figure 4.14 while the space distribution and its fourier transform are in figure 4.15.

Let us decompose the magnetization as follow

$$\mathbf{M} = M_S(\mathbf{m}_0 + \delta\mathbf{m}(\mathbf{x}, t)), \quad (4.62)$$

and expand the perturbative term into spin waves

$$\delta\mathbf{m} = \text{Re} \left[\sum_{\mathbf{k}} c_{\theta\mathbf{k}}(t) e^{i\mathbf{k}\cdot\mathbf{x}} \hat{\mathbf{e}}_{\theta} + \sum_{\mathbf{k}} c_{\varphi\mathbf{k}}(t) e^{i\mathbf{k}\cdot\mathbf{x}} \hat{\mathbf{e}}_{\varphi} \right], \quad (4.63)$$

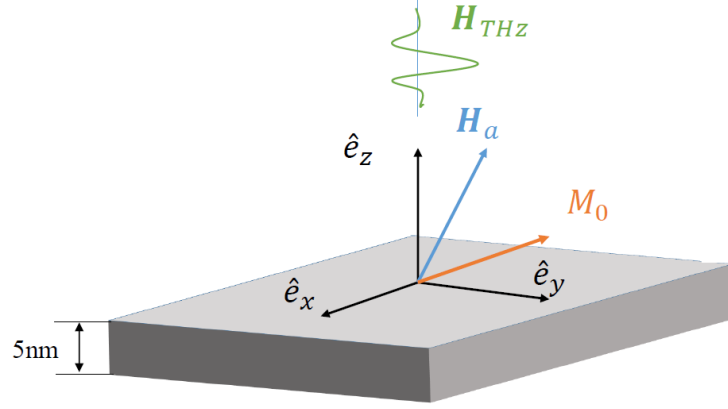


Figure 4.13: System of section 4.6, this is also the setup of the experiment described in [82].

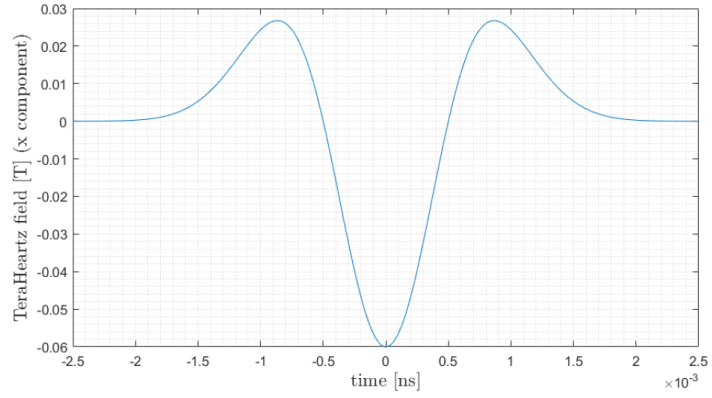


Figure 4.14: Time profile of the magnetic field considered in section 4.6, this is also the model of the field in the experiment reported in [82]

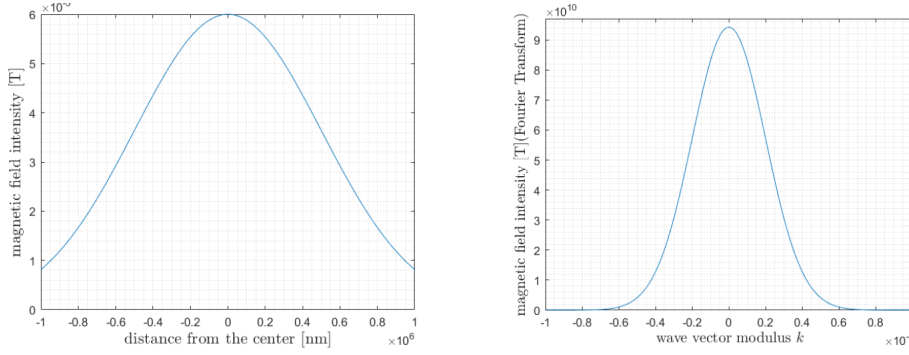


Figure 4.15: Space distribution (on the left) and its Fourier transform (on the right) of the magnetic field used for the simulation of section 4.6, this is also a realistic model for the experiment described in [82]

The time evolution of the $c_{\theta\mathbf{k}}$'s and the $c_{\varphi\mathbf{k}}$'s, for any value of \mathbf{k} , can be simulated using (4.55). In order to estimate the observed demagnetization we normalize the magnetization as

$$\mathbf{M} = M_S \frac{\mathbf{m}_0 + \delta\mathbf{m}(\mathbf{x}, t)}{\|\mathbf{m}_0 + \delta\mathbf{m}(\mathbf{x}, t)\|} \quad (4.64)$$

and we assume that the measured magnetization is given by an averaged value of the magnetization over the measuring area (circular spot with $250\mu\text{m}$ of diameter)

$$M_{\text{meas}} = \frac{1}{|\Omega_M|^2} \left\| \int \mathbf{M}(\mathbf{x}, t) dS \right\|^2. \quad (4.65)$$

Replacing (4.64) into the latter equation yields

$$M_{\text{meas}} = M_S \int \frac{\mathbf{m}_0}{\sqrt{\mathbf{m}_0^2 + \delta\mathbf{m}^2}} dS + M_S \int \frac{\delta\mathbf{m}}{\sqrt{\mathbf{m}_0^2 + \delta\mathbf{m}^2}} dS, \quad (4.66)$$

where we use $\mathbf{m}_0 \cdot \delta\mathbf{m} = 0$.

We expand in Taylor series the square root and neglect the terms of order greater than 2 in $\delta\mathbf{m}$. Hence we get the approximation

$$\int \mathbf{M}(\mathbf{x}, t) dS \approx M_S \mathbf{m}_0 \int \left(1 - \frac{1}{2} \|\delta\mathbf{m}\|^2 \right) dS + \int \delta\mathbf{m} dS. \quad (4.67)$$

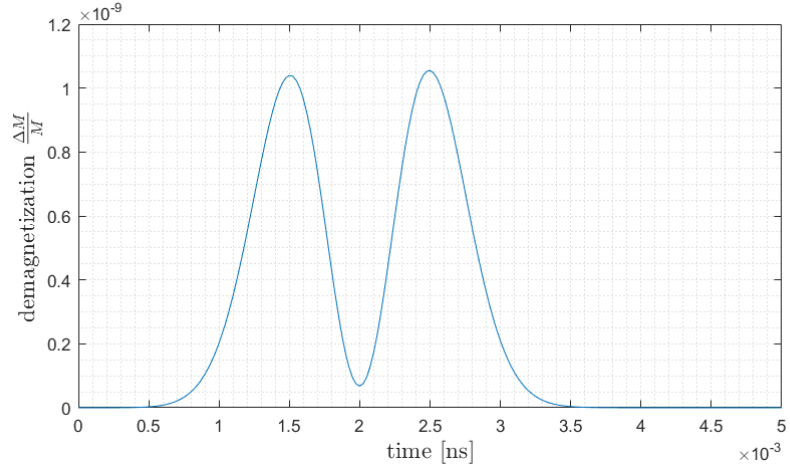


Figure 4.16: Magnetization module observed in the spin wave simulation described in section 4.6, demagnetization measured in [82] is orders of magnitude larger, hence it is not due to nonuniformity.

Finally we obtain the expression for the demagnetization

$$\Delta M = M_{\text{meas}} - M_S = \frac{M_S}{|\Omega_M|} \int \|\delta \mathbf{m}\| \, dS - \frac{M_S^2}{|\Omega_M|^2} \left\| \int \delta \mathbf{m} \, dS \right\|^2, \quad (4.68)$$

where we neglect the terms of order higher than 2 in $\delta \mathbf{m}$.

The resulting magnetization is reported in figure 4.16.

By the end, we can confirm that demagnetization observed in experiments (roughly 0.1% of total magnetization) is not due to nonuniformity in the magnetization. Indeed we can assert that non homogeneous modes barely appear and do not have any significant impact on the measurements. Consequently the macrospin model accurately describes the magnetization dynamics.

Conclusion

In the thesis the micromagnetic theory is used to analyze the physics of digital memories based on ferromagnetic materials. After introducing the fundamental theory, an analysis of uniformed magnetized bodies is proposed. This is a common feature of both hard disk memories and Magnetic Random Access Memories (MRAM), since the small size of the memory cell forces the magnetization to be uniform.

A particular attention is given to the nonlinear magnetic resonance, since it is of central importance in the implementation of Microwave Assisted Magnetic Switching, a technology which can significantly enhance the data capacity of magnetic storage devices. With this aim, the thesis develops analytical models and methods for the analysis of these systems.

The second and third chapters consider corrections of the LLG equation which allow its application to an extremely small length scale or an extremely fast time scale. These topics are of great interest since they are related to the increase of the capacity and the increase of the speed of memories, respectively.

When the memory cell size is small, effects of thermal fluctuations must be taken into account as they could reduce the data retention of the device and the reliability of the switching process. For this reason, materials with strong anisotropy and high saturation magnetization are required. On the other hand, these properties make harder and slower the writing process.

The thesis proposes analytical models for the analysis of the damped switching reliability and a numerical tool for the simulation of systems with low to intermediate drift term compared to the diffusive term.

The last chapter deals with the ultrafast dynamics in magnetic materials, where the term ultrafast denotes phenomena that occur in the time scale of picoseconds or even less. Because of experimental difficulties, ultrafast dynamics have been studied experimentally only recently, when appropriate instruments have become available.

In the ultrafast regime, there is a new relevant mode of the magnetization dynamics, this mode has been neglected for a long time because of the difficulties in exciting and measuring it. A direct experimental observation of the ultrafast mode was done for the first time by Neeraj et al [81]. On this occasion analytical models and numerical simulations were provided as theoretical support to the experimental work. Analysis of the ultrafast mode is not only an important result for the fundamental physics of magnetism, but it may also play a fundamental role in the development of future memories with high speed.

List of Publications

Journal Articles

D'Aquino M., Scalera V., Serpico C. (2019), "Analysis of switching times statistical distributions for perpendicular magnetic memories", *Journal of Magnetism and Magnetic Materials*, Vol. 475, pag. 652-661

Quercia A., Serpico C., D'Aquino M., Perna S., Scalera V., Mayergoyz I.D. (2018), "Normal form of nonlinear oscillator model relevant to spin-torque nano-oscillator theory", *Physica B: Condensed Matter*, Vol. 549, pag.: 87-90

D'Aquino M., Perna S., Quercia A., Scalera V., Serpico C. (2017), "Current-Driven Hysteretic Synchronization in Vortex Nanopillar Spin-Transfer Oscillators", *IEEE Magnetics Letters*, Vol. 8

D'Aquino M., Quercia A., Scalera V., Perna S., Bertotti G., Mayergoyz I.D., Serpico C. (2017), "Analytical Treatment of Nonlinear Ferromagnetic Resonance in Nanomagnets", *IEEE Transactions on Magnetics*, Vol. 53, N. 11,

D'Aquino M., Perna S., Quercia A., Scalera V., Serpico C. (2017), "Effect of Temperature in Hysteretic Synchronization of Magnetic Vortex Spin-Torque Nano-Oscillators", *IEEE Transactions on Magnetics*, Vol. 53, N. 11

Proceedings

Isernia N., Scalera V., Serpico C., Villone F., (2019) “Energy Balance During Disruptions” Proceedings of the 46th EPS Conference on Plasma Physics, P4.1053

Preprint

Neeraj K., Awari N., Kovalev S., Polley D., Hagstrom N.Z., Arekapudi S., Semisalova A., Lenz K., Green B., Deinert J.C., Ilyakov I., Chen M., Bawatna M., Scalera V., d’Aquino M., Serpico C., Hellwig O., Wegrowe J.E., Gensch M., Bonetti S. (2019), ”Experimental evidence of inertial dynamics in ferromagnets“, <https://arxiv.org/pdf/1910.11284.pdf>
(under revision for Nature Physics)

Appendix A

Helmholtz and Tellegen Theorems

In this appendix some theorems of mathematical analysis useful in electrodynamics are recalled.

Before listing the theorems, we quickly summarize the fundamental definitions used for vector fields.

By definition a vector field $\mathbf{V} : \Omega \rightarrow \mathbb{R}^3$ is conservative if every line integral over a closed line is zero, i.e.

$$\mathbf{V} \text{ is conservative} \iff \int_{\gamma} \mathbf{V} \cdot \hat{\mathbf{t}} d\ell = 0 \quad \forall \gamma, \quad (\text{A.1})$$

where γ are curves contained in Ω and $\hat{\mathbf{t}}$ is the unit vector tangent to the curve. An equivalent definition states that every line integral depends only on the initial and final point and not on the path. Moreover conservative fields are irrotational, i.e.

$$\mathbf{V} \text{ is conservative} \implies \nabla \times \mathbf{V} = 0. \quad (\text{A.2})$$

The converse is true if Ω is simply connected.

A conservative field can be written as the gradient of a scalar field

$$\mathbf{V} \text{ is conservative} \iff \exists \varphi : \mathbf{V} = \nabla \varphi. \quad (\text{A.3})$$

Another class of important fields are the solenoidal fields. By definition a field \mathbf{V} is solenoidal if its flux through any surface is zero, i.e.

$$\mathbf{V} \text{ is solenoidal} \iff \int_{\Sigma} \mathbf{V} \cdot \hat{\mathbf{n}} dS = 0 \quad \forall \Sigma, \quad (\text{A.4})$$

where Σ is a surface contained in Ω and $\hat{\mathbf{n}}$ is the unit vector pointing outside the surface.

Solenoidal fields are also divergenceless, which means

$$\mathbf{V} \text{ is solenoidal} \implies \nabla \cdot \mathbf{V} = 0, \quad (\text{A.5})$$

while the converse is true if the domain is simply connected.

An equivalent condition for fields to be solenoidal is to be equal to the curl of a field

$$\mathbf{V} \text{ is solenoidal} \iff \exists \mathbf{A} : \mathbf{V} = \nabla \times \mathbf{A}. \quad (\text{A.6})$$

A.1 Helmholtz Theorem

Let $\mathbf{V} : \mathbb{R}^3 \rightarrow \mathbb{R}^3$ be a vector field defined in the whole euclidean space and regular at infinity, i.e.

$$\lim_{\mathbf{x} \rightarrow \infty} |\mathbf{x}|^2 |\mathbf{V}| < \infty. \quad (\text{A.7})$$

Helmholtz decomposition theorem states that \mathbf{V} can be written as the sum of a conservative field and a solenoidal field, i.e.

$$\mathbf{V} = \nabla \phi + \nabla \times \mathbf{A}. \quad (\text{A.8})$$

In order to prove (A.8) we apply the sampling property of Dirac's delta

$$\mathbf{V}(\mathbf{x}) = \int_{\mathbb{R}^3} \mathbf{V}(\mathbf{y}) \delta(\mathbf{x} - \mathbf{y}) dV_{\mathbf{y}}, \quad (\text{A.9})$$

and we substitute the following expression

$$\delta(\mathbf{x} - \mathbf{y}) = -\frac{1}{4\pi} \nabla_{\mathbf{x}}^2 \frac{1}{|\mathbf{x} - \mathbf{y}|}, \quad (\text{A.10})$$

into (A.9). It yields

$$\mathbf{V}(\mathbf{x}) = -\frac{1}{4\pi} \nabla^2 \int_{\mathbb{R}^3} \frac{\mathbf{V}(\mathbf{y})}{|\mathbf{x} - \mathbf{y}|} dV_{\mathbf{y}}. \quad (\text{A.11})$$

By applying the vector identity $\nabla^2 \mathbf{V} = \nabla \nabla \cdot \mathbf{V} - \nabla \times \nabla \times \mathbf{V}$ we finally obtain

$$\mathbf{V}(\mathbf{x}) = \nabla \left(\frac{1}{4\pi} \nabla \cdot \int_{\mathbb{R}^3} \frac{\mathbf{V}(\mathbf{y})}{|\mathbf{x} - \mathbf{y}|} dV_{\mathbf{y}} \right) - \nabla \times \left(\frac{1}{4\pi} \nabla \times \int_{\mathbb{R}^3} \frac{\mathbf{V}(\mathbf{y})}{|\mathbf{x} - \mathbf{y}|} dV_{\mathbf{y}} \right), \quad (\text{A.12})$$

and equation (A.12) proves the theorem. Indeed we have

$$\phi = \frac{1}{4\pi} \nabla \cdot \int_{\mathbb{R}^3} \frac{\mathbf{V}(\mathbf{y})}{|\mathbf{x} - \mathbf{y}|} dV_{\mathbf{y}}, \quad \mathbf{A} = \frac{1}{4\pi} \nabla \times \int_{\mathbb{R}^3} \frac{\mathbf{V}(\mathbf{y})}{|\mathbf{x} - \mathbf{y}|} dV_{\mathbf{y}}. \quad (\text{A.13})$$

A.2 Tellegen theorem

Let $\mathbf{V} : \mathbb{R}^3 \rightarrow \mathbb{R}^3$ be a conservative field defined on the whole space and let $\mathbf{W} : \mathbb{R}^3 \rightarrow \mathbb{R}^3$ be a solenoidal field also defined on the whole space.

Furthermore let both fields be regular at infinity. The Tellegen theorem states that

$$\int_{\mathbb{R}^3} \mathbf{V} \cdot \mathbf{W} \, dV_{\mathbf{x}} = 0 . \quad (\text{A.14})$$

To prove the theorem, let us write the conservative field as $\mathbf{V} = \nabla\varphi$. The integral in equation (A.14), after integrating by parts and applying the divergence theorem, becomes

$$\int_{\mathbb{R}^3} \nabla\varphi \cdot \mathbf{W} \, dV_{\mathbf{x}} = \int_{\partial\mathbb{R}^3} \nabla(\varphi \cdot \mathbf{W}) \, dS_{\mathbf{x}} - \int_{\mathbb{R}^3} \varphi(\nabla \cdot \mathbf{W}) \, dV_{\mathbf{x}} . \quad (\text{A.15})$$

The proof is complete since the surface integral is null thanks to the regularity conditions at infinity and the volume integral contains the divergence of a solenoidal field which is zero.

Appendix B

Poynting Theorem

Poynting theorem is a vector identity coming from Maxwell's equations and it is also an energy balance involving the electromagnetic field.

Let us calculate

$$\nabla \cdot (\mathbf{E} \times \mathbf{H}) = \mathbf{H} \cdot (\nabla \times \mathbf{E}) - \mathbf{E} \cdot (\nabla \times \mathbf{H}) . \quad (\text{B.1})$$

By substituting the curl of the electric and magnetic field from the Maxwell's equations we obtain

$$\nabla \cdot (\mathbf{E} \times \mathbf{H}) = -\mathbf{H} \cdot \frac{\partial \mathbf{B}}{\partial t} - \mathbf{E} \cdot \mathbf{J} - \mathbf{E} \times \frac{\partial \mathbf{D}}{\partial t} . \quad (\text{B.2})$$

Dimensionally the terms in the equation (B.2) are powers. Moreover it contains $\mathbf{E} \cdot \mathbf{J}$ which is known to be the power dissipated by joule effect. This suggests that the equation can be interpreted as a power balance of energy involved in electromagnetic phenomena.

If no medium is present we can use the constitutive relation of the void and get

$$\frac{\partial}{\partial t} \left(\frac{\mathbf{E}^2 \varepsilon_0}{2} + \frac{\mathbf{B}^2}{2\mu_0} \right) = -\nabla \cdot \mathbf{S} - \mathbf{E} \cdot \mathbf{J} \quad (\text{B.3})$$

where $\mathbf{S} = \mathbf{E} \times \mathbf{H}$ is called the Poynting vector.

From (B.3) we can interpret $\frac{\mathbf{E}^2 \varepsilon_0}{2}$ and $\frac{\mathbf{B}^2}{2\mu_0}$ as energy in the electric field and in the magnetic field respectively. Moreover we can interpret \mathbf{S} as the flux density of energy.

By integrating (B.3) over a fixed volume V we obtain

$$\frac{d}{dt} \int_V \left(\frac{\mathbf{E}^2 \varepsilon_0}{2} + \frac{\mathbf{B}^2}{2\mu_0} \right) dV = - \int_{\partial V} \mathbf{S} \cdot \hat{\mathbf{n}} dS - \int_V \mathbf{E} \cdot \mathbf{J} dV , \quad (\text{B.4})$$

where $\hat{\mathbf{n}}$ is the normal to ∂V pointing outside.

It is important to remark that Poynting vector is defined modulo a divergenceless field. When also media are present, the stored energy is given by

$$\mathbf{H} \frac{\partial \mathbf{B}}{\partial t} + \mathbf{E} \frac{\partial \mathbf{D}}{\partial t} = \frac{\partial}{\partial t} \left(\frac{\mathbf{E}^2 \varepsilon_0}{2} + \frac{\mathbf{B}^2}{2\mu_0} \right) + \mu_0 \mathbf{H} \cdot \frac{\partial \mathbf{M}}{\partial t} + \varepsilon_0 \mathbf{E} \cdot \frac{\partial \mathbf{P}}{\partial t} . \quad (\text{B.5})$$

The last two terms are interpreted as the work done by magnetic field and electric field respectively on the media.

Appendix C

Nonlinear Dynamics

To analyze nonlinear systems we need to define some topological properties of the system.

We say that two systems are topologically equivalent if there exists an homeomorphism between the state spaces that commutes with the time evolution operator. Given two systems

$$\dot{\mathbf{x}} = \mathbf{f}(\mathbf{x}) \quad \text{and} \quad \dot{\mathbf{y}} = \mathbf{g}(\mathbf{y})$$

the time evolution operators φ_t and ϕ_s are defined by

$$\mathbf{x}(t) = \varphi_t \mathbf{x}(0) \quad \text{and} \quad \mathbf{y}(s) = \phi_s \mathbf{y}(0) . \quad (\text{C.1})$$

The two system are equivalent if there exists Φ such that

$$\phi_s \Phi(\mathbf{x}) = \Phi(\varphi_t \mathbf{x}) \quad (\text{C.2})$$

for every point in the state space.

In two dimensions spaces, equivalent dynamic systems have the same number of equilibrium points and limit cycles with the same type of stability; in higher dimensions spaces there might exist other types of attractors such as tori.

A bifurcation is a qualitative change of the phase portrait topology due to the variation of some parameters. This means that the number or the stability of the equilibrium points and limit cycles is altered.

C.1 Saddle node bifurcation

The simplest type of bifurcation is the saddle-node bifurcation: it occurs when two equilibria collide and consequently disappear as in figure C.1.

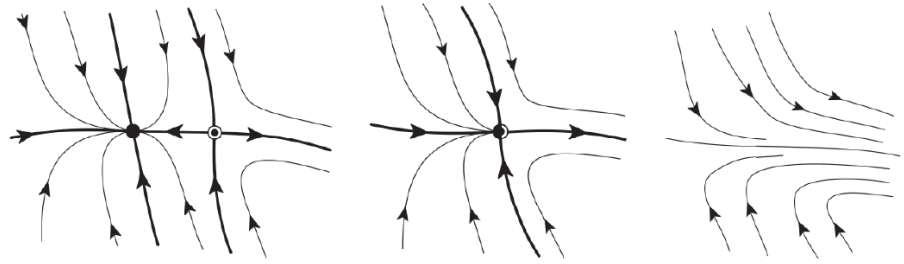


Figure C.1: Qualitative representation of a saddle node bifurcation: on the left a stable node and a saddle, in the middle the two equilibria collide and they become a semistable node, on the right, after the bifurcation, equilibria are no longer present

The limit condition, in the central panel of the figure, can be detected by analyzing the linearized system in the two equilibria: a semistable equilibrium is impossible in linear systems, hence this effect is due to the nonlinear part of the system. In this condition one eigenvalue of the linearized system takes value zero.

In two dimensional systems this condition can be easily detected by checking the determinant of the linearized system in the equilibrium.

C.2 Hopf bifurcation

Hopf bifurcation occurs when an equilibrium point and a limit cycle collide, or equivalently when a limit cycle spawns from an equilibrium point as represented in figure C.2.

Let us consider a stable limit point in a two dimensional system. The linearized system has two eigenvalues with negative real part in this point. If they are complex and conjugate, a Hopf bifurcation may occur.

If some parameters of the system change and the complex conjugate eigenvalues cross the imaginary axis, the equilibrium point becomes unstable. If its basin of attraction is not instantly destroyed, there must be a new attractor, i.e. a limit cycle surrounding the point.

An analogous logic can be applied also to unstable equilibrium points. In this case the limit cycle will be stable, saddle cannot have Hopf bifurcation because the eigenvalues of the linearized system cannot be complex conjugate.

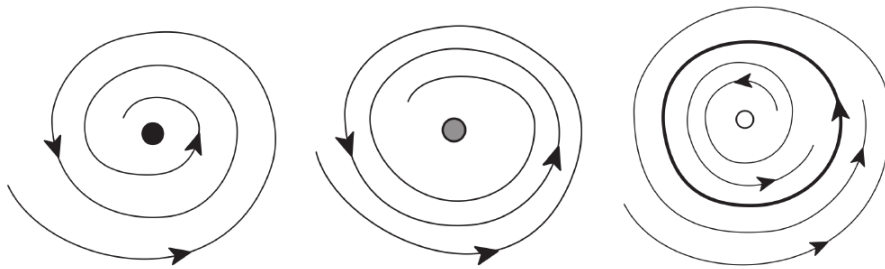


Figure C.2: Qualitative representation of a Hopf bifurcation: on the left a stable focus, in the middle the focus eigenvalues cross the real axis, on the right a limit cycle appears and the focus becomes unstable.

C.3 Homoclinic bifurcation

Let us consider a saddle equilibrium with a stable trajectory coming from an unstable equilibrium (see figure C.3). By changing some system parameters, the stable trajectory may get close to an unstable trajectory and they may eventually match. When stable and unstable trajectories intersect, a closed trajectory passing for the saddle appears. This condition corresponds to the homoclinic bifurcation. If there is a further change in the parameter the unstable trajectory gets surrounded by the stable one, so that it cannot end in the unstable equilibrium point. Hence, for topological reasons, a limit cycle must appear between the unstable trajectory starting from the saddle and the unstable equilibrium.

Unlike the other bifurcations, a homoclinic bifurcation is not local and it cannot be detected by using a linearized system.

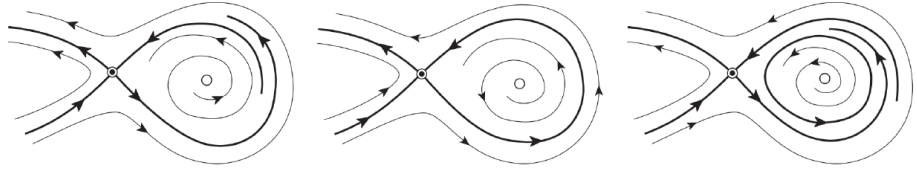


Figure C.3: Qualitative representation of a homoclinic bifurcation: on the left a trajectory pointing to the saddle starts from the unstable focus, in the middle a trajectory pointing to the saddle matches exactly with a trajectory starting from the saddle and a closed trajectory is generated, on the right the closed trajectory leaves the saddle and surrounds the unstable focus.

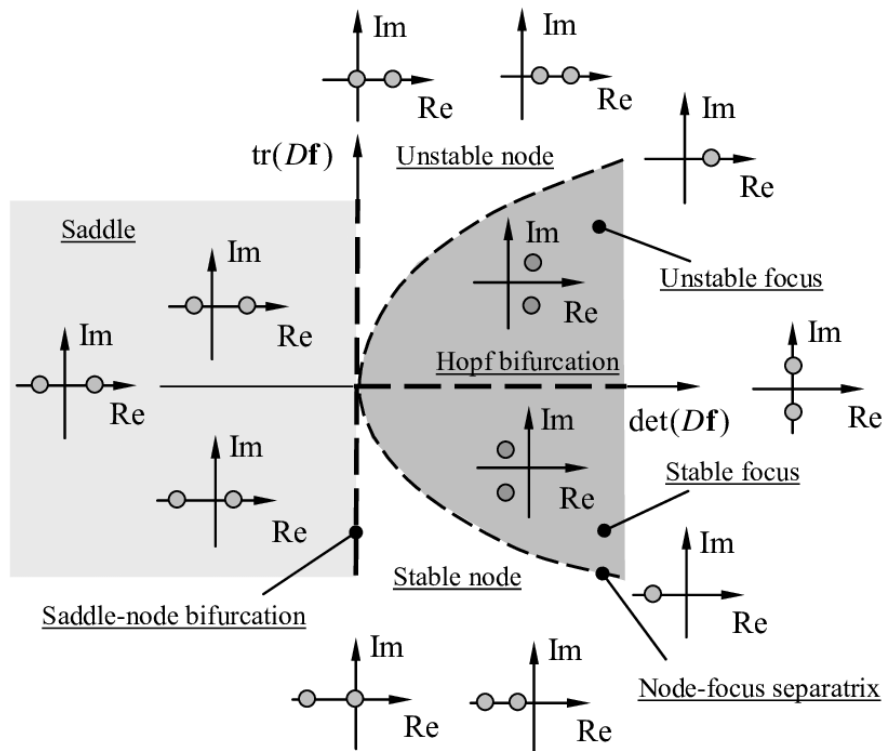


Figure C.4: Classification of the behavior of the equilibrium points in two dimensions depending on the determinant and on the trace of the dynamical matrix of the linearized system. Signs of the eigenvalues in each region are also indicated.

Appendix D

Magnetostatic field in thin films

This section shows in detail how the magnetostatic field for a sinusoidal magnetization distribution is computed. Let us assume that the magnetization is given by

$$\mathbf{M}(x, y, z) = \text{Re} \left[(\hat{\mathbf{e}}_x M_x + \hat{\mathbf{e}}_y M_y + \hat{\mathbf{e}}_z M_z) e^{jkx} \right] \chi_d(z), \quad (\text{D.1})$$

where $M_x, M_y, M_z \in \mathbb{C}$ and χ is a characteristic function which takes into account the geometry. The magnetic field is given by the sum of two contributes, one due to the volume charges and one due to the surface charges

$$\mathbf{H}_M(\mathbf{r}) = -\frac{1}{4\pi} \nabla \left(\int_{\Omega} \frac{\nabla \cdot \mathbf{M}(\mathbf{r}')}{\|\mathbf{r} - \mathbf{r}'\|} d\mathbf{r}' - \int_{\partial\Omega} \frac{\hat{\mathbf{n}} \cdot \mathbf{M}(\mathbf{r}')}{\|\mathbf{r} - \mathbf{r}'\|} d\mathbf{r}' \right), \quad (\text{D.2})$$

where $\Omega = \mathbb{R} \times \mathbb{R} \times [-d/2; +d/2]$.

Each type of charge is generated by a different component of the magnetization:

- the component M_x generates the volume charges: $\nabla \cdot \mathbf{M} = \text{Re} [jk M_x e^{jkx}]$,
- the component M_z generates the surface charges: $\mathbf{M} \cdot \hat{\mathbf{n}} = \text{Re} [M_z e^{jkx}]$,
- the component M_y does not generate any demagnetizing field.

The two contributions can be computed separately, but they have some important features in common. The analytical expression for the demagnetizing field

is

$$\begin{aligned} \mathbf{H}_M(x, y, z) = \text{Re}[-\nabla\varphi_M] = \\ -\text{Re} \left[\frac{1}{4\pi} \nabla \left(jkM_x \int_{\Omega} \frac{e^{jk(x'-x)}}{\sqrt{(x'-x)^2 + (y'-y)^2 + (z'-z)^2}} dx'dy'dz \right. \right. \\ \left. \left. - M_z \int_{\partial\Omega} \frac{e^{jk(x'-x)}}{\sqrt{(x'-x)^2 + (y'-y)^2 + (z'-z)^2}} dx'dy \right) \right]. \end{aligned} \quad (\text{D.3})$$

Because of the translation symmetry of the system along the x -axis, we expect (D.3) to have a solution of the type $\varphi(x, y, z) = f(z)e^{jk(x-x_0)}$. This can also be proved by applying the substitution $x'' = x' - x$ in (D.3) which allows to move x outside the integral.

Once the x dependence is known, it is useful to investigate the possible solutions of the Laplace equation which will be used to satisfy the boundary condition. The Laplace equation is

$$\begin{aligned} (\partial_x^2 + \partial_z^2) \varphi_M^0 = -k^2 f(z)e^{jkx} + f''(z)e^{jkx} = 0 \implies \\ f(z) = e^{\pm kz} \implies \varphi_M^0 = e^{jkx \pm kz} \end{aligned} \quad (\text{D.4})$$

where the sign can be chosen by imposing the field to be finite at $z \rightarrow \pm\infty$.

D.1 Field Generated by Surface Charges

For the magnetic field the following set of equations need to be solved

$$\nabla^2 \varphi_M = \begin{cases} 0 & \text{for } z > +d/2 \\ 0 & \text{for } -d/2 > z > d/2 \\ 0 & \text{for } z < -d/2 \end{cases}, \quad (\text{D.5})$$

with the extra condition of periodicity in x and the interface conditions at $z = d/2$ and $z = -d/2$. The interface conditions are applied on the tangent and the normal component of \mathbf{H}_M right before and right after the interface (subscripts “+” and “-” are used for different media)

$$\begin{aligned} (\mathbf{H}_{M+} - \mathbf{H}_{M-}) \times \hat{\mathbf{n}} = 0 & \implies \varphi_M \text{ is continuous across the surfaces,} \\ (\mathbf{H}_{M+} - \mathbf{H}_{M-}) \cdot \hat{\mathbf{n}} = +M_z e^{jkx} & \text{ in } z = +d/2, \\ (\mathbf{H}_{M+} - \mathbf{H}_{M-}) \cdot \hat{\mathbf{n}} = -M_z e^{jkx} & \text{ in } z = -d/2. \end{aligned} \quad (\text{D.6})$$

Despite the trivial solution seems to be correct inside the media, it does not satisfy boundary conditions in case of surface charge. Hence solutions of the Laplace equation must be added

$$\varphi_M = \begin{cases} Ae^{-kz} e^{jkx} & \text{for } z > +d/2 \\ (B_1 e^{-kz} + B_2 e^{+kz}) e^{jkx} & \text{for } -d/2 > z > d/2 \\ Ce^{+kz} e^{jkx} & \text{for } z < -d/2 \end{cases} \quad (D.7)$$

The four constants must satisfy the boundary conditions

$$\begin{bmatrix} +1 & -1 & -e^{kd} & 0 \\ -1 & +1 & -e^{kd} & 0 \\ 0 & e^{kd} & +1 & -1 \\ 0 & e^{kd} & -1 & +1 \end{bmatrix} \begin{bmatrix} A \\ B_1 \\ B_2 \\ C \end{bmatrix} = \frac{M_z e^{kd/2}}{k} \begin{bmatrix} 0 \\ 1 \\ 0 \\ 1 \end{bmatrix}, \quad (D.8)$$

hence

$$\begin{bmatrix} A \\ B_1 \\ B_2 \\ C \end{bmatrix} = \frac{M_z}{2k} \begin{bmatrix} -2 \sinh(kd/2) \\ +e^{-kd/2} \\ -e^{-kd/2} \\ +2 \sinh(kd/2) \end{bmatrix}. \quad (D.9)$$

The scalar potential of the demagnetizing field is then given by

$$\varphi_M = \begin{cases} -M_z k^{-1} \sinh(kd/2) e^{-kz} e^{jkx} & \text{for } z > +d/2 \\ -M_z k^{-1} \sinh(kz) e^{-kd/2} e^{jkx} & \text{for } -d/2 > z > d/2 \\ +M_z k^{-1} \sinh(kd/2) e^{+kz} e^{jkx} & \text{for } z < -d/2 \end{cases} \quad (D.10)$$

If it is needed the average magnetic field inside the thin film, integration of (D.10) over the thickness yields

$$\mathbf{H}_M = -M_z \frac{\sinh(kd/2)}{kd/2} e^{-\frac{kd}{2}} e^{jkx} \hat{\mathbf{e}}_z = -M_z \frac{1 - e^{-kd}}{kd} e^{jkx} \hat{\mathbf{e}}_z = -M_z S_{\mathbf{k}} e^{jkx} \hat{\mathbf{e}}_z \quad (D.11)$$

where $S_{\mathbf{k}} = (1 - \exp(-kd))/(kd)$.

D.2 Field Generated by Volume Charges

The field generated by the volume charges is composed by a particular solution which satisfies the Poisson equation on the whole space and by a homogeneous

solution which satisfies the boundary conditions.

The magnetostatic problem is defined by the following equations

$$\nabla^2 \varphi_M = \begin{cases} 0 & \text{for } z > d/2 \\ jkM_x e^{jkx} & \text{for } -d/2 > z > d/2 \\ 0 & \text{for } z < -d/2 \end{cases} \quad (\text{D.12})$$

with particular solution

$$\varphi_M = \begin{cases} 0 & \text{for } z > +d/2 \\ -jk^{-1}M_x e^{jkx} & \text{for } -d/2 > z > d/2 \\ 0 & \text{for } z < -d/2 \end{cases} \quad (\text{D.13})$$

As in the previous section we use the ansatz for the homogeneous solution and we impose the boundary conditions. In the current case the linear systems reads

$$\begin{bmatrix} +1 & -1 & -e^{kd} & 0 \\ -1 & +1 & -e^{kd} & 0 \\ 0 & e^{kd} & +1 & -1 \\ 0 & e^{kd} & -1 & +1 \end{bmatrix} \begin{bmatrix} A \\ B_1 \\ B_2 \\ C \end{bmatrix} = j \frac{M_x e^{kd/2}}{k} \begin{bmatrix} -1 \\ 0 \\ +1 \\ 0 \end{bmatrix} \quad (\text{D.14})$$

with solution

$$\begin{bmatrix} A \\ B_1 \\ B_2 \\ C \end{bmatrix} = \frac{M_x}{2k} \begin{bmatrix} -2 \sinh(kd/2) \\ e^{-kd/2} \\ e^{-kd/2} \\ -2 \sinh(kd/2) \end{bmatrix} \quad (\text{D.15})$$

The scalar potential for the demagnetizing field is

$$\varphi_M = \begin{cases} -jM_x k^{-1} \sinh(kd/2) e^{-kz} e^{jkx} & \text{for } z > +d/2 \\ +jM_x k^{-1} (\cosh(kz) e^{-kd/2} - 1) e^{jkx} & \text{for } -d/2 > z > d/2 \\ -jM_x k^{-1} \sinh(kd/2) e^{+kz} e^{jkx} & \text{for } z < -d/2 \end{cases} \quad (\text{D.16})$$

As before we consider the averaged field inside the ferromagnetic material

$$\mathbf{H}_M = -M_x \left(1 - \frac{\sinh(kd/2)}{kd/2} e^{-\frac{kd}{2}} \right) e^{jkx} \hat{\mathbf{e}}_x = -M_x (1 - S_{\mathbf{k}}) e^{jkx} \hat{\mathbf{e}}_x \quad (\text{D.17})$$

where $S_{\mathbf{k}} = (1 - \exp(-kd))/(kd)$.

Appendix E

Formal definition of the noise

The gaussian white-noise process can be formally defined as the derivative of the isotropic vector Wiener process (or vector Brownian motion) [50, 51, 43, 44]

$$\mathbf{h}_N(t) = \frac{d\mathbf{W}}{dt} , \quad (\text{E.1})$$

where the cartesian components $W_k(t)$ of $\mathbf{W}(t)$ are statistically independent scalar Wiener processes.

By definition, the scalar Wiener process must satisfy the following three properties

$$W(0) = 0 \quad (\text{E.2})$$

$$\langle [W(t) - W(s)]^2 \rangle = t - s \quad \text{with } t > s \geq 0 \quad (\text{E.3})$$

$$\langle [W(t_1) - W(s_1)][W(t_2) - W(s_2)] \rangle = 0 \quad \text{with } 0 \leq s_2 < t_2 \leq s_1 < t_1 \quad (\text{E.4})$$

where the brackets $\langle \cdot \rangle$ denote statistical average.

A particular property of the Wiener process is that it has continuous trajectories which are not differentiable in any instant of time. The second property implies

$$\lim_{t \rightarrow s} \frac{\langle [W(t) - W(s)]^2 \rangle}{(t - s)^2} = +\infty . \quad (\text{E.5})$$

Indeed, while for differentiable functions of time the differential is first order in dt , in this case we have

$$\langle (dW)^2 \rangle = dt . \quad (\text{E.6})$$

As consequence of equation (E.6), Riemann-Stieltjes is no more properly defined. By definition it is given by

$$\int_{t_i}^{t_f} G(t) dW(t) = \lim_{n \rightarrow \infty} \sum_{i=1}^n g(\tau_i) (W(t_i) - W(t_{i-1})) , \quad (\text{E.7})$$

where $t_i = t_0 < t_1 < \dots < t_n = t_f$ are a mesh of the interval $[t_0, t]$ and $t_{i-1} < \tau_i < t_i$. Let us consider the case $G(t) = W(t)$, the expected value of the integral in equation (E.7) is

$$\begin{aligned} \left\langle \int_{t_i}^{t_f} W(t) dW \right\rangle &= \lim_{n \rightarrow \infty} \sum_{i=1}^n \langle W(\tau_i) W(t_i) \rangle - \langle W(\tau_i) W(t_{i+1}) \rangle = \\ &= \lim_{n \rightarrow \infty} \sum_{i=1}^n (t_{i-1} - \tau_i) . \end{aligned} \quad (\text{E.8})$$

Equation (E.8) has the unpleasant feature of depending on the choice of the points τ_i . For this reason a default choice of the τ_i 's has to be made so that the integral is univocally defined. The two choices are the Ito integral

$$\int_{t_i}^{t_f} G(t) dW(t) = \lim_{n \rightarrow \infty} \sum_{i=1}^n g(t_{i-1}) (W(t_i) - W(t_{i-1})) \quad (\text{E.9})$$

and the Stratonovich integral

$$\int_{t_i}^{t_f} G(t) dW(t) = \lim_{n \rightarrow \infty} \sum_{i=1}^n g\left(\frac{t_i + t_{i-1}}{2}\right) (W(t_i) - W(t_{i-1})) . \quad (\text{E.10})$$

In the present thesis we consider always the Stratonovich integral because the usual integration rules hold for it and hence it keeps the magnetization module fixed.

Bibliography

- [1] I. Tagawa, M. Shiimoto, M. Matsubara, S. Nosaki, Y. Urakami, J. Aoyama, *Advantage of MAMR Read-Write Performance*, IEEE Transaction on Magnetics, Vol. 52, No. 9 (2016)
- [2] M. Mallary, K. Srinivasan, G. Bertero, D. Wolf, C. Kaiser, M. Chaplin, C. Elliott, M. Pakala, Q. Leng, F. Liu, Y. Wang, T.J. Silva, J.M. Shaw, H.T. Nembach, *Head and Media Challenges for 3 Tb/in² Microwave-Assisted Magnetic Recording*, IEEE Transaction on Magnetics, Vol. 50, No. 7 (2014)
- [3] S. Okamoto, N. Kikuchi, M. Furuta, O. Kitakami, T. Shimatsu, *Microwave assisted magnetic recording technologies and related physics*, J. Phys. D: Appl. Phys. 48 353001 (2015)
- [4] W. Kang, Y. Zhang, Z. Wang, J.O. Klein, C. Chappert, D. Ravelosona, G. Wang, Y. Zhang, W. Zhao, *Spintronics: Emerging Ultra-Low-Power Circuits and Systems beyond MOS Technology*, Journal of emerging Technologies in Computing Systems, Vol. 12 No. 2 (2015)
- [5] <https://blog.seagate.com/craftsman-ship/hamr-next-leap-forward-now/>
- [6] Seagate Storage Update *LOC Designing Storage Architecture for Digital Collections* (2018)
- [7] Seagate Technology Paper, *HAMR technology* (2017)
- [8] Western Digital, Technology Brief *Next-Generation Technologies for a New Decade of Big Data* (2017)
- [9] G. Varvaro, F. Casoli, *Ultra-High-Density Magnetic Recording: Storage Materials and Media Designs*, CRC Press (2016)

-
- [10] G.Bertotti, *Hysteresis in Magnetism*, Academic Press, San Diego (1998)
 - [11] D.D. Stancil, A. Prabhakar, *Spin Waves*, Springer Science (2009)
 - [12] W.F. Brown Jr, *Magnetostatic Principles in Ferromagnetism*, North-Holland Publishing Company (1962).
 - [13] W.F. Brown Jr, *Micromagnetics*, Interscience Publishers (1963)
 - [14] L. Peliti, *Statistical mechanics in a nutshell* , Princeton University Press, Princeton 2011
 - [15] H. B. Callen, *Thermodynamics*, John Wiley & sons (1960)
 - [16] H. Reiss, *Mathods of Thermodynamics*, Blaisdell Publishing Company (1965)
 - [17] S.R. De Groot, P. Mazur, *Non-equilibrium Thermodynamics*, Dover Publication inc, New York
 - [18] S. Tandon, M. Beleggiab, Y. Zhub, M. De Graef, *On the computation of the demagnetization tensor for uniformly magnetized particles of arbitrary shape. Part I: Analytical approach*, Journal of Magnetism and Magnetic Materials 271, pp. 9-26 (2004)
 - [19] M. Beleggia, M. De Graef, Y.T. Millev, D.A. Goode, G. Rowlands, *Demagnetization factors for elliptic cylinders*, J. Phys. D: Appl. Phys. 38, pp. 3333-3342 (2005)
 - [20] Stoner, E.C. and Wohlfarth, *A mechanism of magnetic hysteresis in heterogeneous alloys*, Philosophical Transactions of the Royal Society, Series A, 240, p.599-642 (1948)
 - [21] H. Hancock, *Elliptic integrals*, Wiley, New York (1917).
 - [22] C. Serpico, G. Bertotti, I.D. Mayergoyz, M. d'Aquino, *Nonlinear Magnetization dynamics in Nanomagnets*, Handbook of Magnetism and Advanced Magnetic Materials, Joh Wiley & sons (2007)
 - [23] H.D. Hubbard, B.H. West, *Differential Equation: A Dynamical System Approach (ordinary differential equation)*, Springer (1991)
 - [24] H.D. Hubbard, B.H. West, *Differential Equation: A Dynamical System Approach (Higher dimensional systems)*, Springer (1991)

-
- [25] L.D. Landau, E.M. Lifshitz, *Theory of the dispersion of magnetic permeability in ferromagnetic bodies*, Phys. Z. Sowietunion 8, 153 (1935)
- [26] L.D. Landau, E.M. Lifshitz, *Statistical Physics*, Pergamon (1980)
- [27] T.L. Gilbert, *A Phenomenological Theory of Damping in Ferromagnetic Materials*, Physical Review, 100 (1955), p. 1243.
- [28] G. Bertotti, I. Mayergoyz, C. Serpico, *Nonlinear magnetization dynamics in nanosystems*, Elsevier (2009)
- [29] S.M. Thompson, *The discovery, development and future of GMR: The Nobel Prize 2007*, J. Phys. D: Appl. Phys., 41, 093001 (2008)
- [30] I. Firastrau, L.D. Buda-Prejbeanu, B. Dieny, U. Ebels, *Spin-torque nano-oscillator based on a synthetic antiferromagnet free layer and perpendicular to plane polarizer*, Journal of Applied Physics, 113 (2013)
- [31] B. Lacoste, B.D. Buda-Prejbeanu, U. Ebels, B. Dieny, *Magnetization dynamics of an in-plane magnetized synthetic ferrimagnetic free layer submitted to spin-transfer torques and applied field*, Physical Review B, 89 (2014)
- [32] J. C. Slonczewski, *Currents, torques, and polarization factors in magnetic tunnel junctions*, Physical Review B, 71, 024411 (2005)
- [33] J. C. Slonczewski, *Current-driven excitation of magnetic multilayers*, J. Magn. Magn. Mater., 159, L1, 1996
- [34] H. Suhl, *the Theory of Ferromagnetic Resonance at High Signals Power*, Phys. Chem. Solid, Pergamon Press, Vol. 1, pp. 209-227 (1957)
- [35] G. Bertotti, I.D. Mayergoyz, C. Serpico, *Spin-Wave Instabilities in Large-Scale Nonlinear Magnetization Dynamics*, Physical Review Letter (2001)
- [36] S.H. Strogatz, *Nonlinear Dynamics and Chaos*, CRC Press (2014)
- [37] Y.A. Kuznetsov, *Elements of Applied Bifurcation Theory*, Springer-Verlag New York (1995)
- [38] M. d'Aquino, C. Serpico, G. Miano, *Geometrical Integration of Landau-Lifshitz-Gilbert equation based on the mid-point rule*, Journal of Computational Physics, 209 (2005) 730-753

-
- [39] C. Kittel, *on the theory of Ferromagnetic Resonance Absorption*, Phys. Rev. 73, 155 (1948)
 - [40] N. N. Bogoliubov and Yu. A. Mitropolskii, *Asymptotic Methods in the Theory of Nonlinear Oscillations*, New York: Gordon and Breach (1961)
 - [41] M. d'Aquino, A. Quercia, V. Scalera, S. Perna, G. Bertotti, I.D. Mayergoyz, C. Serpico, *Analytical Treatment of Nonlinear Ferromagnetic Resonance in Ferromagnets*, IEEE transaction on Magnetics (2017)
 - [42] A. Quercia, M. d'Aquino, V. Scalera, S. Perna, C. Serpico, *Normal form of nonlinear oscillator model relevant to spin-torque nano-oscillator theory*, Physica B: Condensed Matter 549, pp. 87-90 (2018)
 - [43] C.W. Gardiner, *Handbook of stochastic methods*, Springer-Verlag (1985)
 - [44] H. Risken, *The Fokker-Planck Equation*, Springer-Verlag (1989)
 - [45] J.C. Mallinson, *On damped gyromagnetic precession*, IEEE Transactions on Magnetics, 23, p. 2003 (1987).
 - [46] W.F. Brown, *Thermal fluctuation of a single-domain particle*, Physical Review, Vol. 130, Num. 5 (1963)
 - [47] M. d'Aquino, S. Perna, A. Quercia, V. Scalera, C. Serpico, *Current-driven hysteretic synchronization in vortex nanopillar spin-transfer oscillators*, IEEE Magnetics Letters 8,3504005 (2017)
 - [48] M. d'Aquino, S. Perna, A. Quercia, V. Scalera, C. Serpico, *Effect of Temperature in Hysteretic Synchronization of Magnetic Vortex Spin-Torque Nano-Oscillators*, IEEE Transactions on Magnetics 53(11),7922618 (2017)
 - [49] M. d'Aquino, V. Scalera, C.Serpico, *Analysis of switching times statistical distributions for perpendicular magnetic memories*, Journal of Magnetism and Magnetic Materials 475, pp. 652-661 (2019)
 - [50] A. Einstein, *On the motion of small particles suspended in liquids at rest required the Molecular Kinetic theory of heat*, Annalen der Physik, 17, 549-560 (1905)
 - [51] P. Langevin, *On the theory of Brownian motion*, Comptes. Rendues 146, 530A908)

-
- [52] L.N. Trefethen, *Spectral Methods in MATLAB*, Philadelphia, Society for Industrial and Applied Mathematics (2000)
- [53] B. Fornberg, *A practical Guide to Pseudospectral Methods*, Cambridge monographs on applied and computational mathematics (1996)
- [54] E. Beaurepaire, J.C. Merle, A. Daunois, J.Y. Bigot, *Ultrafast spin dynamics in ferromagnetic nickel*, Physical Review Letters 76, 4250 (1996)
- [55] M.C. Ciornei, J. Rub , J.E. Wegrowe, *Magnetization dynamics in the inertial regime: Nutation predicted at short time scales*, Physical Review B 83, 020410 (2011)
- [56] J.E. Wegrowe, M.C. Ciornei, *Magnetization dynamics, gyromagnetic relation, and inertial effects*, American Journal of Physics 80, 607-611 (2012)
- [57] E. Olive, Y. Lansac, and J.E. Wegrowe, *Beyond ferromagnetic resonance: The inertial regime of the magnetization*, Applied Physics Letters 100 (2012)
- [58] E. Olive, Y. Lansac, M. Meyer, M. Hayoun, J.E. Wegrowe, *Deviation from the Landau-Lifshitz-Gilbert equation in the inertial regime of the magnetization*, Journal of Applied Physics 117 (2015)
- [59] J.X. Zhu, Z. Nussinov, A. Shnirman, A.V. Balatsky, *Novel spin dynamics in a Josephson junction*, Physical Review Letters 92 (2004).
- [60] A. Kimel, et al, *Inertia-driven spin switching in antiferromagnets*, Nature Physics 5, 727 (2009).
- [61] M. Faraday, Diary, 13 September 1845, Vol. 4, p. 7504
- [62] Z.Q. Qiu, S.D. Bader, *Surface Magneto-Optic Kerr Effect*, Review of Scientific Instruments Vol. 71 (2000)
- [63] B. Koopmans, M. Van Kampen, J.T. Kohlhepp, W.J.M. De Jonge, *Ultrafast magneto-optics in nickel: magnetism or optics?*, Physical Review Letters 85, 844 (2000).
- [64] B. Koopmans, M. Van Kampen, W. De Jonge, *Experimental access to femtosecond spin dynamics*, Journal of Physics: Condensed Matter 15, S723 (2003).

-
- [65] B. Koopmans, J. Ruigrok, F. Dalla Longa, W. De Jonge, *Unifying ultrafast magnetization dynamics*, Physical Review Letters 95, 267207 (2005).
- [66] A. Kirilyuk, A.V. Kimel, T. Rasing, *Ultrafast optical manipulation of magnetic order*, Reviews of Modern Physics 82, 2731 (2010).
- [67] M. Battiato, K. Carva, P.M. Oppeneer, *Superdiffusive spin transport as a mechanism of ultrafast demagnetization*, Physical Review Letters 105, 027203 (2010).
- [68] 18. Mathias, S. et al. Probing the timescale of the exchange interaction in a ferromagnetic alloy. Proceedings of the National Academy of Sciences 109, 4792-4797 (2012).
- [69] I. Radu et al, *Transient ferromagnetic-like state mediating ultrafast reversal of antiferromagnetically coupled spins*, Nature 472, 205 (2011).
- [70] C. Stamm et al, *Femtosecond modification of electron localization and transfer of angular momentum in nickel*, Nature Materials 6, 740 (2007).
- [71] B. Koopmans et al, *Explaining the paradoxical diversity of ultrafast laser-induced demagnetization*, Nature Materials 9, 259 (2010).
- [72] C. Boeglin et al, *Distinguishing the ultrafast dynamics of spin and orbital moments in solids*, Nature 465, 458 (2010).
- [73] E. Carpene et al, *Dynamics of electron-magnon interaction and ultrafast demagnetization in thin iron films*, Physical Review B 78, 174422 (2008).
- [74] F. Dalla Longa, J. Kohlhepp, W. De Jonge, B. Koopmans, *Influence of photon angular momentum on ultrafast demagnetization in nickel*, Physical Review B 75, 224431 (2007).
- [75] C.H. Lambert et al, *All-optical control of ferromagnetic thin films and nanostructures*, Science 345, 1337-1340 (2014).
- [76] K. Carva, M. Battiato, D. Legut, P.M. Oppeneer, *Ab initio theory of electron-phonon mediated ultrafast spin relaxation of laser-excited hot electrons in transition-metal ferromagnets*, Physical Review B 87, 184425 (2013).
- [77] M.C. Hoffmann, J.A. Fulop, *Intense ultrashort terahertz pulses: generation and applications*, Journal of Physics D: Applied Physics 44, 083001 (2011)

-
- [78] D. Polley et al. *THz-driven demagnetization with perpendicular magnetic anisotropy: towards ultrafast ballistic switching*, Journal of Physics D: Applied Physics 51, 084001 (2018)
- [79] S. Kovalev et al, *Probing ultra-fast processes with high dynamic range at 4th-generation light sources: Arrival time and intensity binning at unprecedented repetition rates*, Structural Dynamics 4, 024301 (2017)
- [80] M. Hudl, M. d'Aquino, M. Pancaldi, S.H. Yang, M.G. Samant, S.S.P. Parkin, H.A. Durr, C. Serpico, M.C. Hoffmann, S. Bonetti, *Nonlinear magnetization dynamics driven by strong terahertz fields*, Phys. Rev. Lett. 123, 197204 (2019)
- [81] N. Kumar, N. Awari, S. Kovalev, D. Polley, N.Z. Hagstrom, S.S.P.K. Arekapudi, A. Semisalova, K. Lenz, B. Green, J.C. Deinert, I. Ilyakov, M. Chen, M. Bowatna, V. Scalera, M d'Aquino, C. Serpico, O. Hellwig, J.E. Wegrowe, M. Gensch, S. Bonetti, *Experimental evidence of inertial dynamics in ferromagnets*, arXiv:1910.11284
- [82] M. Hudl, M. d'Aquino, M. Pancaldi, S.H. Yang, M.G. Samant, S.S.P. Parkin, C. Serpico, H.A. Durr, M.C. Hoffmann, S. Bonetti, *Non-linear magnetization dynamics driven by strong terahertz fields*, Physical Review Letters 123, 197204 (2019)